Thesis

Role of Interchain Coupling in Magnetic Properties of Pseudo-One-Dimensional Quantum Spin Systems

Satoshi Kokado

Division of Materials Physics
Department of Physical Science
Graduate School of Engineering Science
OSAKA UNIVERSITY
Toyonaka Osaka

January 1999

Abstract

Theoretical study on magnetic properties of pseudo-one-dimensional (pseudo-1D) quantum spin systems is made by developing new useful theoretical methods. Particular attention is paid to magnetic phenomena in which interchain coupling plays an important role.

1. Magnetic Properties of Pseudo-1D Exchange-Alternating Systems

The pair dynamical correlated-effective-field approximation (Pair-DCEFA) is formulated by extending the DCEFA developed originally by Suzuki. This Pair-DCEFA is suitable for treating exchange-alternating systems such as antiferromagnetic-ferromagnetic (AF–F) alternating chains, and also has advantages of being able to calculate easily the q- and ω-dependent susceptibility and its temperature dependence. Magnetic phase transitions of pseudo-1D S=1/2 AF–F alternating systems under zero and non-zero magnetic fields are investigated by the combined method of the Pair-DCEFA and the usual mean-field approximation (MFA). Interchain exchange couplings of a couple of pseudo-1D S=1/2 AF–F alternating systems are successfully evaluated.

The q-dependent staggered susceptibilities at finite temperatures of S=1/2 exchange-alternating chains are calculated for the first time by using the exact diagonalization method (EDM) for finite chains. It is shown that interchain couplings of pseudo-1D S=1/2 exchange-alternating systems can be evaluated more quantitatively with use of the staggered susceptibilities obtained by the EDM and by applying the MFA to interchain interaction.

Intensities of inelastic neutron scattering of pure-1D S=1/2 AF–F alternating chains are calculated by numerical method based on the EDM, and several interesting natures of the magnetic excitations are predicted: (1) the so-called second gap exists always, (2) the lowest energy in the continuum region above the second gap takes the maximum value at $q = \pi/2$, (3) the magnitude of the second gap at q=0 decreases with increasing the magnitude of the ferromagnetic coupling, (4) the continuum states above the second gap may be observable at large q, and (5) the intensity due to the lowest triplet states takes the maximum value at $q = \pi/2$ in the whole range of the exchange ratio.

2. Magnetic Resonance in Spin Peierls System $CuGeO_3$

The interchain exchange integral J' along the b-axis of $CuGeO_3$ has been evaluated by analyzing the exchange splitting of EPR spectra observed at T=300 K under ultra-high

magnetic fields on the basis of the mean-field random-phase approximation (MF–RPA). The two peak structure of the observed EPR spectra and its dependence on the field direction are explained successfully, and by solving the equation of motion for the spins it is clarified that the observed two peaks correspond to the ferromagnetic and antiferromagnetic resonance, respectively.

Origins of two kinds of ESR lines (2 meV and 5 meV) in the spin Peierls phase of $CuGeO_3$ are clarified or proposed. By assuming the Dzyaloshinsky-Moriya interaction and the different g values for spin pairs of the Cu dimer, which can be expected reasonably from the supposed crystal structure, it is shown that the 2 meV line is ascribed to the transition to the lowest triplet state with q=0 from the singlet ground state. As the origin for the 5 meV line, transition to two triplet excited states above the second gap is proposed. This model can explain well the configuration dependence of the observed ESR spectra and also the recent experimental findings such as observation under zero magnetic field.

Acknowledgments

The author would like to express his sincere thanks to Professor N. Suzuki for continuous guidance and encouragement, helpful comments and discussions and critical reading of this thesis.

Thanks are also due to Professor M. Shirai not only for lending his insight about the physics to the author but also for helpful advice on numerical calculations. He is also grateful to all of the members of Suzuki laboratory for providing him with the useful discussions.

Finally, he would like to thank Dr. M. Hagiwara of RIKEN, Professor H. Nojiri of Tohoku University, Dr. H. Manaka of Chiba University and Professor T. Kubo of Nara University of Education for useful discussions and showing him their experimental data prior to publication.

Contents

Chapter 1

Introduction

The low-dimensional quantum spin systems have been attracting much attention as typical examples which manifest remarkable quantum effect. In particular, the magnetic properties of the quantum spin gap systems which have a spin singlet ground state with a finite gap to the lowest excited state are the most interesting problem among them. Examples are the exchange-alternating chains [1, 2, 3] inclusive of spin Peierls [4] systems, Haldane systems [5] and S=1/2 double spin chain systems [6] and so on. These systems have been studied extensively both experimentally and theoretically, and many interesting results have been reported so far. Theoretically purely one-dimensional exchange-alternating chain systems have been extensively studied mostly on the basis of the exact diagonalization method (EDM) for finite chains [7, 8, 9]. However, it is the present status that there are few theoretical works about role of interchain coupling in pseudo one-dimensional systems. To be important, the real systems are pseudo-one-dimensional and there are many phenomena in which interchain coupling can not be neglected. In fact, the magnetic phase transitions have been observed experimentally in a couple of pseudo one-dimensional systems [1, 2, 10], which show clearly the importance of the interchain coupling. By focusing our attention on the effect of interchain coupling, we have developed quite useful methods which can take into account interchain coupling quantitatively and performed theoretical analyses of magnetic properties of a couple of pseudo-one-dimensional quantum spin systems.

Magnetic properties of S=1/2 exchange-alternating chains

Recently, interesting one-dimensional exchange-alternating chain systems such as antiferromagnetic-ferromagnetic (AF–F) alternating chains have been synthesized and the magnetic properties of these systems are activatively investigated. Quite recently three

dimensional magnetic order has been observed in pseudo-one-dimensional AF–F alternating systems such as $Cu(TIM)CuCl_4$, $(4\text{-}BzpipdH)CuCl_3$ [1] and MeNN [2]. However there were few effective methods to discuss these phenomenon, and it is desired to develop a practically useful method which can take account properly the interchain coupling. So, as one of such methods we propose the following combined method: the intrachain and interchain couplings are treated by the pair dynamical correlated-effective-field approximation (Pair-DCEFA) and the mean field approximation (MFA), respectively. This Pair-DCEFA has advantages of being able to calculate easily the q- and ω-dependent susceptibility and its temperature dependence and also being applicable to three dimensional systems without difficulty. By using this combined method, the magnetic phase transitions of pseudo-one-dimensional S=1/2 exchange-alternating chains are investigated, and the exchange couplings in real S=1/2 AF–F alternating systems are evaluated. Further, the same phenomena are studied also by another combined method in which the intrachain and interchain couplings are treated by the exact diagonalizaion method (EDM) for finite chains and the MFA, respectively.

By specific heat measurements H. Manaka *et al.* have observed magnetic phase transitions [10] under magnetic fields in a pseudo-one-dimensional S=1/2 AF–F alternating chain $(CH_3)_2CHNH_3CuCl_3$ [3] which does not order in zero field. So, we have extended the combined method of Pair-DCEFA and MFA to the case under magnetic fields, and investigated the magnetic phase transition observed in $(CH_3)_2CHNH_3CuCl_3$. Also we have analyzed by Pair-DCEFA the temperature dependence of nuclear spin-lattice relaxation time T_1 of this system, which has been measured by T. Kubo *et al.* [11].

Finally, as an theoretical propose, the intensity of neutron scattering is calculated for the one dimensional AF–F alternating chain by using EDM for finite chain. In particular, we focus ourselves on whether the excited states above the second gap is observable or not.

Magnetic Resonance in spin Peierls System $CuGeO_3$

Since Hase, Terasaki and Uchinokura [4] reported the first example of spin-Peierls system (T_{sp}=14 K) in an inorganic linear Cu^{2+} (S=1/2) chain compound, $CuGeO_3$, a large number of experimental studies of various types have been carried out. The neutron scattering experiments [12] confirmed a finite gap between the singlet ground state and the triplet excited states, and also showed clearly that the interchain coupling, particularly along the b-axis, is quite large compared with other spin Peierls systems. Existence of significant interchain coupling has been also indicated from high field EPR measurements

[13]. These experimental evidences for large interchain coupling challenge the view that one-dimensional nature is very important for spin-Peierls system. The neutron scattering experiments [14] discovered also the existence of the second gap above the lowest triplet excited states, which is characteristic to the exchange alternating systems.

Another quite interesting experimental result is the two kinds of transition from the singlet ground state to the triplet excited states in the spin-Peierls phase, which were observed by ESR measurements [13, 15]. The transition between the singlet ant the triplet states is usually forbidden in the Heisenberg model, and the origin of these ESR lines is still open to question.

Exchange splitting of high field EPR

Recently, the exchange splitting of the high field EPR spectra has been observed due to the differences between the principal axes of the g-values of two adjacent Cu^{2+} ions, named respectively as sublattices 1 and 2 [13]. It should be noted that interchain exchange coupling has a great influence on this phenomenon. However, there were no useful methods to discuss quantitatively this phenomenon. In practice, though we have analyzed by using Hamano-Shibata theory [16], the reasonable results have not been obtained. So, we have analyzed the observed exchange splitting of EPR spectra by the Mean-Field Random-Phase-Approximation (MF–RPA), and estimated the interchain exchange integrals. Further, the origin of respective peaks is discussed by solving the equation of motion for the spins with use of the MF–RPA's Hamiltonian. It is shown that the spins at sublattices 1 and 2 perform the motion coupled each other and the obtained mode correspond to those of the ferromagnetic or antiferromagnetic resonance.

ESR spectra in SP phase

For the ESR spectra of $CuGeO_3$ in the spin-Peierls phase, we focus our attention on the mechanism of the direct transitions from the singlet ground state to the triplet excited states lying respectively at 2 meV [13] and 5 meV [15, 17], which are essentialy forbidden. In order to investigate the possibility of the transitions, we have calculated the intensity of ESR spectra at T=0 K. The used Hamiltonian is the isotropic Heisenberg model plus the Dzyaloshinsky-Moriya interaction and the Zeeman interaction with different g values in the Cu dimer, and the triplet excited states are treated by the singlet-triplet dimer model, whose framework is described simply as follows: the singlet ground state consists of the direct products of singlet pairs and the triplet excited states are described as a triplet pair

traveling in the background of the direct products of singlet pairs. This picture is thought to be favorable for the respective states in the SP phase. It is noted that the calculated results can explain well the transition to 2 meV states. On the other hand, the transitions to 5 meV have been investigated on the basis of the following two cases; in one model the 5 meV transition is ascribed to the transition to the zone folded states originated from the staggered field induced along the direction of interchain, and in the other model it is ascribed to that to the excited states above the second gap. To describe the states above the second gap, we have taken into account a situation that two triplet pairs are traveling in the singlet background. By considering a couple of new experimental results [17, 18], we find that the latter model is suitable for explaining the transition to 5 meV states.

Chapter 2

Magnetic Properties of Pseudo-One-Dimensional Exchange-Alternating System

2.1 Pair Dynamical Correlated-Effective-Field Approximation

There are many spin systems which can be regarded as assembly of exchange-coupled spin pairs. Examples are exchange-alternating systems such as antiferromagnetic (AF) alternating chains and antiferromagnetic-ferromagnetic (AF-F) alternating chains. Theoretically purely one-dimensional exchange-alternating systems have been extensively studied mostly on the basis of the exact diagonalization method (EDM) for finite chains [7, 8, 9]. Experimentally, on the other hand, there have been few exchange-alternating spin systems, but the examples are increasing recently. To be important, the real exchange-alternating chain systems are pseudo-one-dimensional, and there are many cases in which interchain coupling cannot be neglected. In fact, quite recently three dimensional magnetic order has been observed in pseudo-one-dimensional AF-F alternating systems such as Cu(TIM)$CuCl_4$, (4-BzpipdH)$CuCl_3$ [1] and MeNN [2]. Therefore it is desired to develop a practically useful method which can take into account the interchain coupling. As one of such methods we propose in this paper the pair dynamical correlated-effective-field approximation (Pair-DCEFA) in which the spin-pair is solved exactly and the interaction between the pairs is treated by the DCEFA [19]. The original DCEFA developed by Suzuki has shown sufficiently its effectiveness through its previous successful application to the paramagnetic state and the magnetic ordered state in various magnetic systems [20, 21, 22, 23, 24, 25].

As examples, Pair-DCEFA is applied to calculate magnetic excitation and uniform static susceptibility of S=1/2 AF alternating chains and also of S=1/2 AF-F alternating chains, and the results are compared with those obtained by the EDM for finite spins [7, 9]. Finally, the exchange integrals in Cu(TIM)$CuCl_4$, (4-BzpipdH)$CuCl_3$ [1] and MeNN [2] are estimated by combining Pair-DCEFA for intrachain coupling and the mean field approximation (MFA) for interchain coupling.

2.1.1 Formalism

We consider a spin system whose Hamiltonian is expressed as follows:

$$\mathcal{H} \;=\; -\sum_i J\vec{S}_{i1}\cdot\vec{S}_{i2} \;-\; \frac{1}{2}\sum_{i\neq j}\sum_{\mu\nu} J_{i\mu,j\nu}\vec{S}_{i\mu}\cdot\vec{S}_{j\nu}, \tag{2.1}$$

where $\vec{S}_{i\mu}$ ($\vec{S}_{j\nu}$) denotes the spin μ (spin ν) in the unit cell i (unit cell j) with μ (ν) being 1 or 2. The first term represents the Hamiltonian of isolated spin-pairs in each of which two spins are interacting through J, and the second term denotes the interaction between the pairs. In the following we first solve exactly the spin-pair Hamiltonian $-J\vec{S}_{i1}\cdot\vec{S}_{i2}$, and then treat the interaction between the pairs by the DCEFA, *i.e.* the following decoupling is adopted for the second term of eq. (2.1):

$$J_{i\mu,j\nu}\vec{S}_{i\mu}\cdot\vec{S}_{j\nu} \rightarrow J_{i\mu,j\nu}[\vec{S}_{i\mu}\cdot(\langle\vec{S}_{j\nu}\rangle - \alpha\langle\vec{S}_{i\mu}\rangle) + \vec{S}_{j\nu}\cdot(\langle\vec{S}_{i\mu}\rangle - \alpha\langle\vec{S}_{j\nu}\rangle)] \;, \tag{2.2}$$

where $\langle\vec{S}\rangle$ denotes the spontaneous or the field-induced spin moment and α represents a parameter which should be determined self-consistently. The parameter α is a quantity reflecting the correlation between neighboring spins, and in the original DCEFA it has been shown that α corresponds exactly to the nearest-neighbor (n.n.) spin correlation in the case of the paramagnetic state of an isotropic Heisenberg system [19]. The effective spin-pair Hamiltonian for the unit cell i is now given by

$$\mathcal{H}_i^{\rm eff} = -J\vec{S}_{i1}\cdot\vec{S}_{i2} - \sum_{j(\neq i)}\sum_{\mu\nu} J_{i\mu,j\nu}\vec{S}_{i\mu}\cdot(\langle\vec{S}_{j\nu}\rangle - \alpha\langle\vec{S}_{i\mu}\rangle). \tag{2.3}$$

Here $\langle\vec{S}_{j\nu}\rangle$ denotes the spontaneous moment, and hence the second term of the above equation vanishes in the paramagnetic state. From now on we confine ourselves to the paramagnetic state and calculate the transverse susceptibility tensor $\tilde{\chi}^{+-}(\vec{q},\omega)$ in the spirit of the DCEFA. For this purpose we apply fictitious rotating magnetic fields for the respective sublattice as follows:

$$\text{sublattice 1}: \quad h^+_{\vec{q},1}\mathrm{e}^{\mathrm{i}(\vec{q}\cdot\vec{R}_{i1}-\omega t)}, \tag{2.4}$$

$$\text{sublattice 2}: \quad h^+_{\vec{q},2}\mathrm{e}^{\mathrm{i}(\vec{q}\cdot\vec{R}_{i2}-\omega t)}, \tag{2.5}$$

with $\vec{R}_{i\mu} = \vec{R}_i + \vec{r}_\mu$, where $\vec{R}_i$ denotes the position vector of the unit cell i and $\vec{r}_\mu$ the position vector of the spin μ in a unit cell. By taking into account the field-induced spin moments of the other unit cells, the effective Zeeman interaction for the i-th unit cell is expressed in the DCEFA as follows:

$$\mathcal{H}^{\rm eff}_{i,\rm Zeeman} \;=\; -F_{i1}S^-_{i1} \;- F_{i2}S^-_{i2}, \tag{2.6}$$

where

$$F_{i1} \;=\; h^+_{\vec{q},1}{\rm e}^{{\rm i}(\vec{q}\cdot\vec{R}_{i1}-\omega t)} + \sum_{j(\neq i)}\sum_{\nu}\frac{J_{i1,j\nu}}{2}(\langle S^+_{j\nu}\rangle - \alpha\langle S^+_{i1}\rangle), \tag{2.7}$$

$$F_{i2} \;=\; h^+_{\vec{q},2}{\rm e}^{{\rm i}(\vec{q}\cdot\vec{R}_{i2}-\omega t)} + \sum_{j(\neq i)}\sum_{\nu}\frac{J_{i2,j\nu}}{2}(\langle S^+_{j\nu}\rangle - \alpha\langle S^+_{i2}\rangle). \tag{2.8}$$

Now, within the linear response approximation we get the following relations:

$$\langle S^+_{i1}\rangle \;=\; \phi^{+-}_{11}(\omega)F_{i1} \;+\; \phi^{+-}_{12}(\omega)F_{i2}, \tag{2.9}$$

$$\langle S^+_{i2}\rangle \;=\; \phi^{+-}_{21}(\omega)F_{i1} \;+\; \phi^{+-}_{22}(\omega)F_{i2}. \tag{2.10}$$

Here $\phi^{+-}_{\mu\nu}(\omega)$ (μ,ν=1 or 2) denotes the spin-pair susceptibility calculated on the basis of the effective spin-pair Hamiltonian eq. (2.3) and is obtained generally from

$$\phi^{+-}_{\mu\nu}(\omega) = \sum_{m,n}\frac{(\rho_n-\rho_m)\langle m|S^+_\mu|n\rangle\langle n|S^-_\nu|m\rangle}{\omega+E_m-E_n}, \tag{2.11}$$

where E_m and $|m\rangle$ denote the eigenvalue and the eigenstate of eq. (2.3), respectively, and $\rho_n \equiv \exp(-\beta E_n)/\sum_m \exp(-\beta E_m)$ with $\beta = 1/k_{\rm B}T$. Performing the spatial Fourier transformation of eq. (2.9) and (2.10), and then solving the resultant equations we obtain

$$\begin{aligned}
\begin{pmatrix} \langle S^+_{\vec{q},1}\rangle \\ \langle S^+_{\vec{q},2}\rangle \end{pmatrix} \;&=\; (hh^* - kk^*)^{-1}\times \\
&\begin{pmatrix} h^*\phi^{+-}_{11} - k\phi^{+-}_{12}{\rm e}^{{\rm i}\vec{q}\cdot\vec{r}_{12}} & h^*\phi^{+-}_{12}{\rm e}^{-{\rm i}\vec{q}\cdot\vec{r}_{12}} - k\phi^{+-}_{11} \\ -k^*\phi^{+-}_{11} + h\phi^{+-}_{12}{\rm e}^{{\rm i}\vec{q}\cdot\vec{r}_{12}} & -k^*\phi^{+-}_{12}{\rm e}^{-{\rm i}\vec{q}\cdot\vec{r}_{12}} + h\phi^{+-}_{11} \end{pmatrix}\begin{pmatrix} h^+_{\vec{q},1}{\rm e}^{-{\rm i}\omega t} \\ h^+_{\vec{q},2}{\rm e}^{-{\rm i}\omega t}\end{pmatrix} \\
&\equiv \begin{pmatrix} \chi^{+-}_{11}(\vec{q},\omega) & \chi^{+-}_{12}(\vec{q},\omega) \\ \chi^{+-}_{21}(\vec{q},\omega) & \chi^{+-}_{22}(\vec{q},\omega)\end{pmatrix}\begin{pmatrix} h^+_{\vec{q},1}{\rm e}^{-{\rm i}\omega t} \\ h^+_{\vec{q},2}{\rm e}^{-{\rm i}\omega t}\end{pmatrix},
\end{aligned} \tag{2.12}$$

where

$$\begin{aligned}
h \;&=\; 1 + \frac{1}{2}\phi^{+-}_{11}\{J_{11}(\vec{q}) - \alpha[J_{11}(0)+J_{12}(0)]\} - \frac{1}{2}\phi^{+-}_{12}J_{21}(\vec{q}){\rm e}^{-{\rm i}\vec{q}\cdot\vec{r}_{12}}, \\
k \;&=\; -\frac{1}{2}\phi^{+-}_{12}\{J_{22}(\vec{q}) - \alpha[J_{22}(0)+J_{21}(0)]\}{\rm e}^{-{\rm i}\vec{q}\cdot\vec{r}_{12}} - \frac{1}{2}\phi^{+-}_{11}J_{12}(\vec{q}),
\end{aligned} \tag{2.13}$$

with

$$\vec{r}_{12} = \vec{r}_1 - \vec{r}_2.$$

Here the Fourier transforms of spin moments and exchange couplings are defined by

$$\langle S^+_{\vec{q},\mu}\rangle = \frac{1}{N}\sum_i \langle S^+_{i\mu}\rangle \mathrm{e}^{-\mathrm{i}\vec{q}\cdot\vec{R}_{i\mu}}, \quad J_{\nu\mu}(\vec{q}) = \sum_j J_{i\mu,j\nu}\mathrm{e}^{\mathrm{i}\vec{q}\cdot(\vec{R}_{i\mu}-\vec{R}_{j\nu})}. \tag{2.14}$$

Now, we impose the following self-consistency condition to determine the correlation parameter α:

$$\langle\{S^+_1, S^-_1\}\rangle = \frac{1}{N}\sum_{\vec{q}}\frac{1}{\pi}\int_{-\infty}^{\infty}\mathrm{d}\omega \coth(\frac{\beta\omega}{2})\ \mathrm{Im}\chi^{+-}_{11}(\vec{q},\omega+\mathrm{i}s). \tag{2.15}$$

Here $\langle\{S^+_1, S^-_1\}\rangle = \langle S^+_1 S^-_1 + S^-_1 S^+_1\rangle$ represents the on-site spin correlation calculated by using the effective spin-pair Hamiltonian eq. (2.3), and in the paramagnetic state we have $\langle\{S^+_1, S^-_1\}\rangle = \frac{4}{3}S(S+1)$. The implication of the above self-consistency condition is that the on-site spin correlation calculated from the dynamical susceptibility (the right-hand side of eq. (2.15)) should be equal to that calculated from the effective spin-pair Hamiltonian. It is noted that the self-consistency equation constructed by using $\chi^{+-}_{22}(\vec{q},\omega)$ gives the same results.

Once the correlation parameter α is determined self-consistently, the form of the dynamical susceptibility tensor $\tilde{\chi}^{+-}(\vec{q},\omega)$ of the paramagnetic state is fixed and then we calculate physical quantities from $\tilde{\chi}^{+-}(\vec{q},\omega)$. First, the energy of magnetic excitation $\omega(\vec{q})$ is obtained from the pole of the dynamical susceptibility $\chi^{+-}_{\mu\nu}(\vec{q},\omega)$. Secondly, the uniform static susceptibility per unit cell $\chi(T)$ is obtained as follows:

$$\chi(T) = \frac{(g\mu_{\mathrm{B}})^2}{2}[\chi^{+-}_{11}(0,0) + \chi^{+-}_{12}(0,0) + \chi^{+-}_{21}(0,0) + \chi^{+-}_{22}(0,0)]. \tag{2.16}$$

Also, the intensity of neutron scattering $S(q,\omega(q))$ is calculated from,

$$S(q,\omega(q)) \propto \frac{1}{1-\mathrm{e}^{-\beta\omega(q)}}\mathrm{Im}[\chi^{+-}_{11}(q,\omega(q)) + \chi^{+-}_{12}(q,\omega(q)) + \chi^{+-}_{21}(q,\omega(q)) + \chi^{+-}_{22}(q,\omega(q))]. \tag{2.17}$$

2.1.2 Application to Purely-One-Dimensional Systems

To see the effectiveness of Pair-DCEFA we apply it to S=1/2 exchange-alternating chains and compare the results with those obtained by the EDM [7, 9]. The relevant Hamiltonian is expressed as

$$\mathcal{H} \ = \ -\sum_i (J_1\vec{S}_{i,1}\cdot\vec{S}_{i,2} + J_2\vec{S}_{i-1,2}\cdot\vec{S}_{i,1}). \tag{2.18}$$

Here we assume $J_1 < 0$. The system is an AF alternating chain if $J_2 < 0$, and an AF-F alternating chain if $J_2 > 0$. Since we are considering the paramagnetic state, the effective spin-pair Hamiltonian for the unit cell i is given simply by

$$\mathcal{H}_i^{\rm eff} \;=\; -J_1 \vec{S}_{i,1} \cdot \vec{S}_{i,2}, \tag{2.19}$$

and the expressions of h and k defined by eq. (2.36) are given explicitly by

$$h = 1 + \frac{J_2}{2}[\alpha\phi_{11}^{+-} - \phi_{12}^{+-}\mathrm{e}^{\mathrm{i}q(c+c')}], \quad k = \frac{J_2}{2}(-\phi_{11}^{+-}\mathrm{e}^{-\mathrm{i}qc'} + \alpha\phi_{12}^{+-}\mathrm{e}^{\mathrm{i}qc}), \tag{2.20}$$

with

$$\begin{aligned}
\phi_{11}^{+-} &= \beta\rho_2\delta_{\omega,0} + J_1(\rho_1 - \rho_2)\frac{1}{\omega^2 - J_1^2}, \\
\phi_{12}^{+-} &= \beta\rho_2\delta_{\omega,0} - J_1(\rho_1 - \rho_2)\frac{1}{\omega^2 - J_1^2}, \\
c &= \mid R_{i,2} - R_{i,1} \mid, \quad c' = \mid R_{i+1,1} - R_{i,2} \mid,
\end{aligned} \tag{2.21}$$

where

$$\rho_1 = \frac{1}{1 + 3\mathrm{e}^{\beta J_1}}, \quad \rho_2 = \frac{\mathrm{e}^{\beta J_1}}{1 + 3\mathrm{e}^{\beta J_1}}. \tag{2.22}$$

It is noted here that $\phi_{11}^{+-} = \phi_{22}^{+-}$ and $\phi_{12}^{+-} = \phi_{21}^{+-}$. Now, the energy of magnetic excitation $\omega(q)$ and the uniform static susceptibility $\chi(T)$ are given as follows:

$$\omega(q) \;=\; |J_1| \sqrt{1 + \frac{J_2}{J_1}(\rho_2 - \rho_1)[\alpha + \cos q(c + c')]}, \tag{2.23}$$

$$\chi(T) = \frac{(g\mu_{\rm B})^2}{k_{\rm B}T[3 + \exp(\frac{\mid J_1 \mid}{k_{\rm B}T})] + J_2(\alpha - 1)}. \tag{2.24}$$

We have performed numerical calculations by varying the values of $a \equiv J_2/J_1$. Since we are considering the case of $J_1 < 0$, $a > 0$ corresponds to an AF alternating chain and $a < 0$ to an AF-F alternating chain. In Fig. 2.1 we show the temperature dependence of the correlation parameter α for several values of a determined from the self-consistency condition eq. (2.15). The value of α exhibits a characteristic temperature dependence. First, α is negative for AF alternating chains ($J_2 < 0$) and positive for AF-F alternating chains ($J_2 > 0$). Secondly, the magnitude of α approaches zero when $T \to \infty$. With decreasing temperature from high temperatures, it increases monotonously, takes a maximum around the temperature corresponding to about $0.3|J_1|$, and then approaches to some finite value toward T=0 K. Thirdly, the smaller the value of $\mid a \mid$ or $\mid J_2 \mid$ takes, the

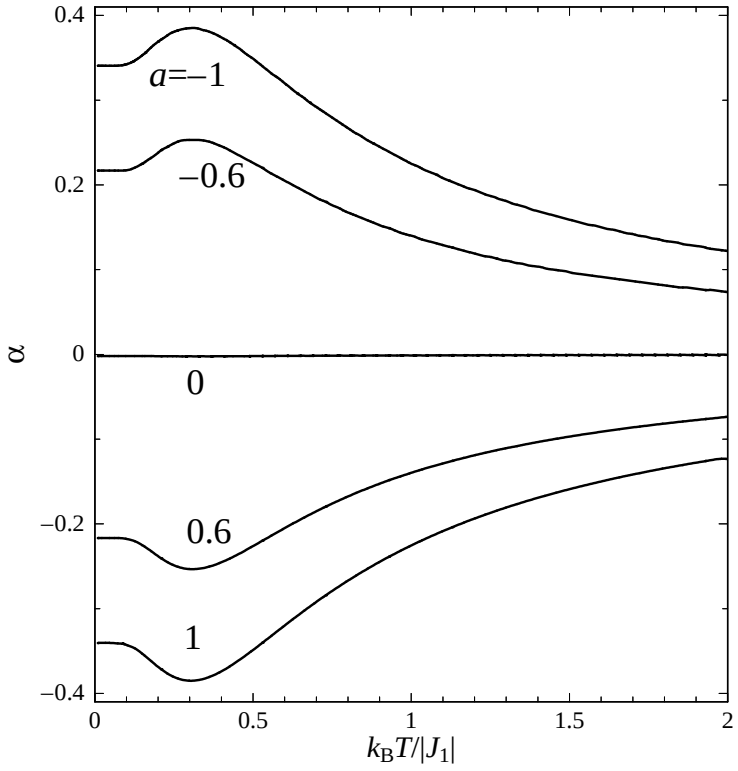

Figure 2.1: The temperature dependence of the correlation parameter α for a=–1, –0.6, 0, 0.6, 1.

smaller the magnitude of α becomes. These characteristic behaviors can be understood essentially by considering that α is related to the spin correlation between the neighboring spin pairs. But the physical origin of the maximum of $|\alpha|$ as a function of temperature is not clear. In Fig. 2.2 the dispersion curves of $\omega(q)$ at T=0 K calculated for a=–1, –0.6, 0, 0.6 by Pair-DCEFA are shown by the thick solid lines. It should be noted that $\omega(q)$ has a minimum value at q=0, π in AF alternating chains and at q=$\pm\pi/2$ in AF-F alternating chains. This magnetic excitation may be regarded as a kind of Frenkel exciton in the sense that the excitation from the ground state to the triplet excited state within a spin pair propagates in the crystal through the inter-pair exchange interaction J_2. In the isolated spin-pair (a=0), $\omega(q)$ of Pair-DCEFA naturally gives a exact result. Further, $\omega(q)$ in an AF alternating chain with a=0.6 agrees fairly well with that of the EDM for 10 spins [7] shown by the dotted curve. The agreement is better in the high energy region ($q\sim\pi/2$) than in the low energy region ($q\sim$0 or π). When Pair-DCEFA is applied formally to an AF uniform chain (a=1), the obtained $\omega(q)$ shown by the thin solid curve deviates considerably from the exact result [26] shown by the dot–dashed curve. In

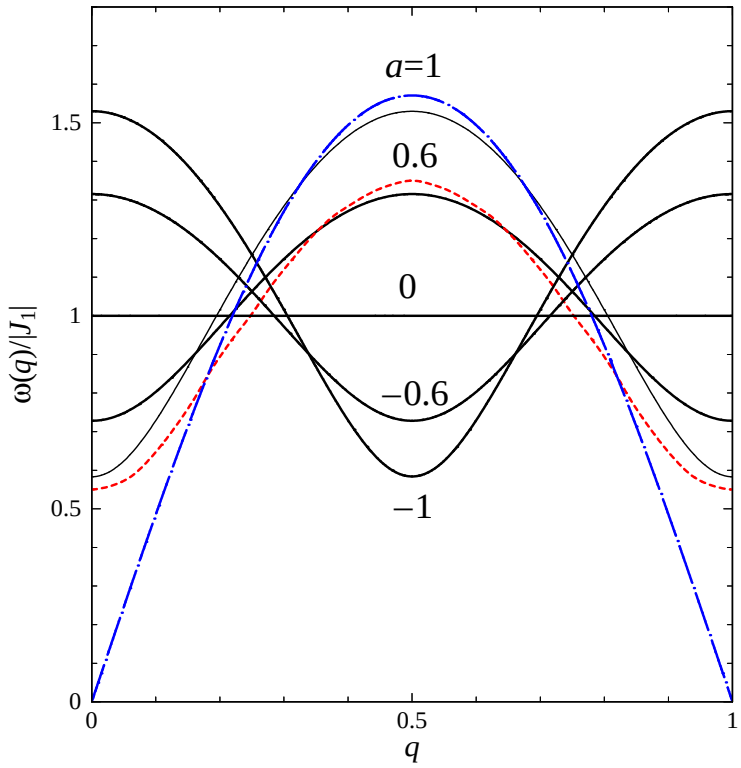

Figure 2.2: The magnetic excitation $\omega(q)$ at T=0 K for a=–1, –0.6, 0, 0.6, 1. The solid curves represent the results calculated by Pair-DCEFA. The dotted curve of a=0.6 denotes $\omega(q)$ obtained by the EDM for 10 spins [7]. The dot–dashed curve of a=1 is the des Cloizeaux and Pearson curve [26]. The unit of q is $2\pi/(c+c')$.

particular Pair-DCEFA gives a finite gap at q=0, π which contradicts even qualitatively with the gapless behavior of the exact result. This large discrepancy implies that the local singlet nature is too stressed in Pair-DCEFA. It is noted, however, that $\omega(q)$ of Pair-DCEFA agrees fairly well with that of the exact results in the high energy region ($q\sim\pi/2$) even in case of AF uniform chains.

Also, such magnetic excitation can be observed practically by inelastic neutron scattering measurements. Its scattering intensity $S(q,\omega(q))$ is now obtained as,

$$S(q,\omega(q)) \propto \frac{1}{1-\mathrm{e}^{-\beta\omega(q)}}\frac{|J_1|(\rho_1-\rho_2)}{\omega(q)}[1-\cos(qc)]. \tag{2.25}$$

The concrete calculational results will be touched upon later.

In Fig. 2.3 the full curve represents the gap energy Δ (*i.e.* the minimum value of $\omega(q)$) calculated for $-\infty < a \leq 1$ by Pair-DCEFA, and the open circles denote the gap energy between the singlet ground state and the triplet excited states which was

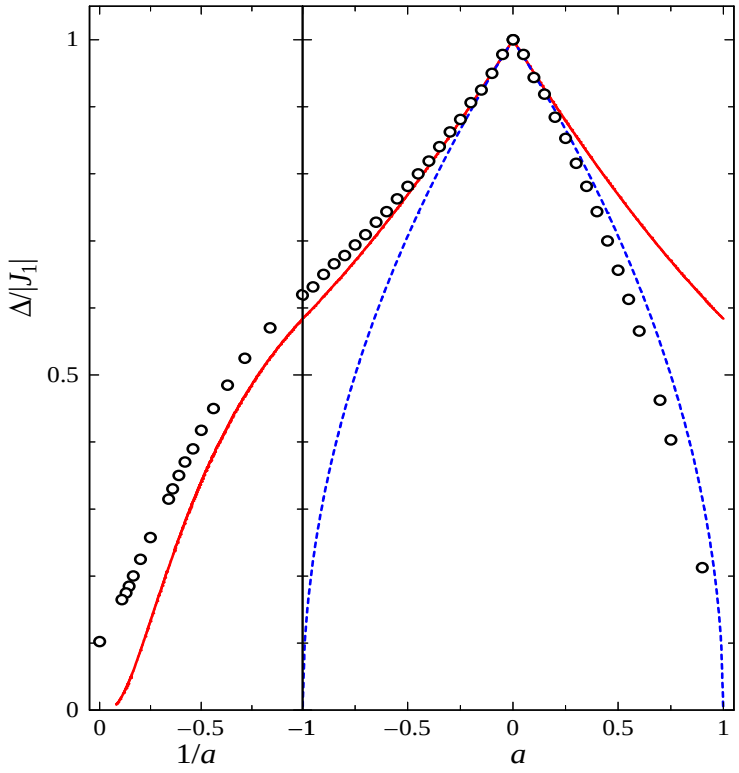

Figure 2.3: The gap energy Δ as a function of $a = J_2/J_1$. The full curves are the results of Pair-DCEFA and the open circles those of EDM [8]. The dotted curve represents the results of Pair-MFA.

extrapolated from the results of EDM calculations for finite spins. In this figure the plot is made as a function of $1/a$ for $-\infty < a \leq -1$. According to the EDM results the gap exists always except for the case of a=1, and the gap at $a = -\infty$ ($1/a$=0) can be regarded as the Haldane gap [8]. By comparing the gap energy of Pair-DCEFA with that of EDM we can point out the two important points. First, for $0 < a \leq 1$ the gap energy of Pair-DCEFA is overestimated, and it is finite for a=1 which contradicts qualitatively with the EDM result as mentioned previously. Secondly, for $a < 0$ the gap energy of Pair-DCEFA is underestimated, and it vanishes at $a \simeq -10$ ($1/a \simeq -0.1$). For $a \leq -10$ we cannot obtain a self-consistent solution of α at T=0 K. These results imply that the effective-field theory like Pair-DCEFA is not appropriate for treating the Haldane gap behavior ($a = -\infty$) or the quantum liquid behavior of a uniform AF chain (a=1) which are truly of quantum nature. But, judging from this figure, we can emphasize that Pair-DCEFA will be practically useful for a fairly wide range of a, particularly for $a < 0$. In case of $a < -1$, namely when the magnitude of the F coupling is larger than that of the AF coupling,

we may expect to obtain better results by solving the F pairs exactly and treating the AF coupling in terms of DCEFA. We have actually performed such calculations, but the results have never been improved in the sense no gap is obtained for the whole range of $a < -1$, reflecting the degenerate ground state of the pair.

In Fig. 2.4 the temperature dependence of the uniform static susceptibility $\chi(T)$ of

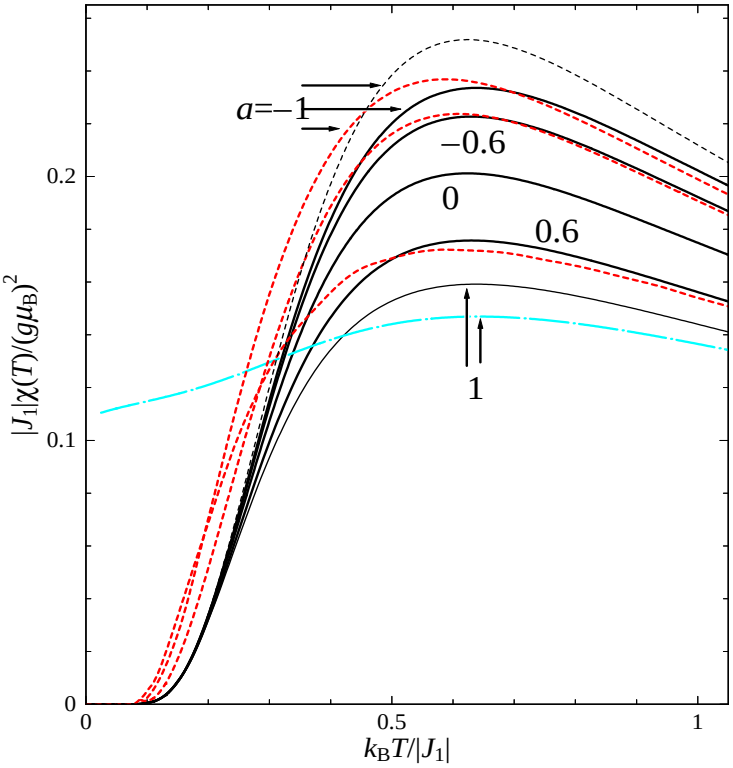

Figure 2.4: The uniform static susceptibility $\chi(T)$ for a=–1, –0.6, 0, 0.6, 1. The full curves are the results of by Pair-DCEFA. The dotted curves for a=–1, –0.6 and 0.6 are those of EDM for 14 spins [9] and 10 spins [7], respectively. The dot–dashed curve of a=1 is that obtained from the Bethe ansatz [27]. The thin dotted curve of $a = -1$ is that obtained by Pair-MFA.

Pair-DCEFA is shown by the full curve. In the vicinity of T=0 K $\chi(T)$ behaves as $\chi(T) \propto \frac{(g\mu_B)^2}{k_BT} \exp(-\frac{|J_1|}{k_BT})$ and hence $\chi(T)$ vanishes at T=0 K. With increasing temperature it increases rapidly, shows a broad maximum around a temperature corresponding to T_{max}=0.6∼0.7$|J_1|$, and finally approaches to zero towards $T = \infty$. Compared with the results of EDM calculations for a=–1, –0.6 and 0.6 [7, 9] (thick dotted curves in Fig. 2.4) the susceptibilities of Pair-DCEFA agree well with the EDM results at temperatures higher than T_{max}. On going toward 0 K from T_{max}, however, $\chi(T)$ of Pair-DCEFA decreases more

rapidly than that of EDM. We consider that this large deviation of Pair-DCEFA $\chi(T)$ from EDM $\chi(T)$ at low temperatures originates from that the singlet-ground-state nature of the individual spin-pair is too stressed in Pair-DCEFA. In an AF uniform chain (a=1) the behavior of $\chi(T)$ of Pair-DCEFA at low temperatures differs even qualitatively from the highly accurate result [27] shown by the dot–dashed curve in Fig. 2.4.

2.1.3 Effect of Interchain Coupling

One of the advantages of Pair-DCEFA is that it can calculate easily the q-dependent susceptibility and its temperature dependence. As an example we show in Fig. 2.5 the q-dependence of the susceptibility $\chi_+(q,T) \equiv \chi_{11}^{+-}(q) + \mid \chi_{12}^{+-}(q) \mid$ of exchange-alternating chains for several temperatures in case of a=–0.6 and 0.6. As a function of q, $\chi_+(q,T)$

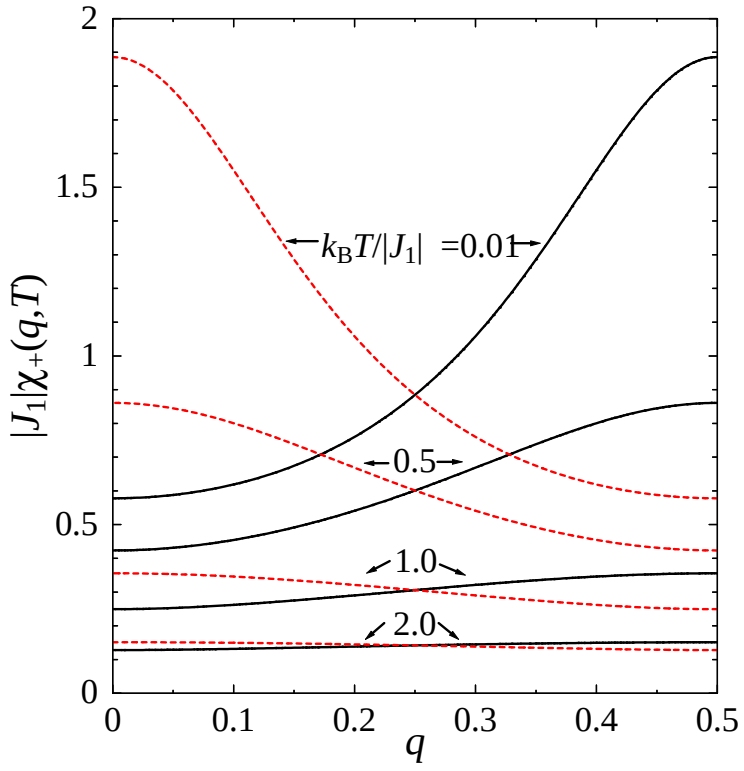

Figure 2.5: The q-dependence of the staggered susceptibility $\chi_+(q,T)$ calculated for several temperatures in case of a=–0.6 and 0.6 are shown by the full curves and the dotted curves, respectively. The unit of q is $2\pi/(c+c')$.

of a=–0.6 and 0.6 takes the maximum at q=$\pi/2$ and q=0, respectively, and the maximum value increases with decreasing temperature. Here, it is noted that $\chi_\pm(q_z)$ are in proportion to the two eigenvalues of the transverse susceptibility tensor $\chi_{ij}^{+-}(q_z)$, and

$\chi_+(q_z)$ $[\chi_-(q_z)]$ represents susceptibility when magnetic fields at sublattices 1 and 2 are antiparallel [parallel]. In particular, $\chi_-(0,T)$ corresponds to the uniform static susceptibility. If the interchain interaction is switched on to the assembly of exchange-alternating chains, three-dimensional magnetic order may be realized at low temperatures. For simplicity we treat the interchain coupling by the MFA, and then within the linear response approximation we can easily get the following relations:

$$\frac{1}{N_z}\sum_k \langle S^+_{ijk1}\rangle \mathrm{e}^{-\mathrm{i}q_z z_{k1}} = \chi^{+-}_{11} G^0_1(1) + \chi^{+-}_{12} G^1_2(1), \tag{2.26}$$

$$\frac{1}{N_z}\sum_k \langle S^+_{ijk2}\rangle \mathrm{e}^{-\mathrm{i}q_z z_{k2}} = \chi^{+-}_{21} G^{-1}_1(2) + \chi^{+-}_{22} G^0_2(2), \tag{2.27}$$

where

$$G^v_u(\mathrm{w}) = h^+_{\vec{q},u}\mathrm{e}^{\mathrm{i}(q_x x_i + q_y y_j + q_z c\times v - \omega t)} + \frac{1}{N_z}\sum_{i'j'k'} J'_{ij,i'j'}\langle S^+_{i'j'k'u}\rangle \mathrm{e}^{-\mathrm{i}q_z z_{k'\mathrm{w}}}. \tag{2.28}$$

Here the chains are formed along z-axis and $J'_{ij,i'j'}$ denotes the interchain exchange integral in x, y plane. By performing spatial Fourier transformation in x, y direction, q-dependent susceptibility tensor is finally obtained as follows:

$$\frac{1}{HH^* - KK^*}\begin{pmatrix} H^*\chi^{+-}_{11} - K\chi^{+-}_{12}\mathrm{e}^{\mathrm{i}q_z c} & H^*\chi^{+-}_{12}\mathrm{e}^{-\mathrm{i}q_z c} - K\chi^{+-}_{11} \\ -K^*\chi^{+-}_{11} + H\chi^{+-}_{12}\mathrm{e}^{\mathrm{i}q_z c} & -K^*\chi^{+-}_{12}\mathrm{e}^{-\mathrm{i}q_z c} + H\chi^{+-}_{11} \end{pmatrix}, \tag{2.29}$$

where

$$\begin{aligned} H &= 1 - \chi^{+-}_{11}(q_z,\omega)(J'_{q_x,q_y} - \alpha J'_0)/2, \\ K &= \chi^{+-}_{12}(q_z,\omega)(J'_{q_x,q_y}\mathrm{e}^{\mathrm{i}q_z c} - \alpha J'_0)/2, \\ J'_{q_x,q_y} &= \sum_{i'j'} J'_{ij,i'j'}\mathrm{e}^{\mathrm{i}[q_x(x_i - x_{i'}) + q_y(y_j - y_{j'})]}. \end{aligned} \tag{2.30}$$

The expression obtained on condition that the q-dependent susceptibility tensor diverges is written as:

$$HH^* - KK^* = [(2/J'_{q_x,q_y}) - \chi_+(q_z,T)][(2/J'_{q_x,q_y}) - \chi_-(q_z,T)] = 0. \tag{2.31}$$

If we assume four n.n. chains, the transition temperature is determined from $1/\mid 2J'\mid = \chi_+(\pi/2,T)$ for $a<0$ and $1/\mid 2J'\mid = \chi_+(0,T)$ for $a>0$, respectively. Here J' denotes the n.n. interchain exchange integral.

Quite recently the measurements of uniform static susceptibility have been done in detail for $Cu(TIM)CuCl_4$, $(4\text{-}BzpipdH)CuCl_3$ and MeNN, which are S=1/2 AF-F alternating chains, and a phase transition has been observed at about 1 K, 2 K [1] and

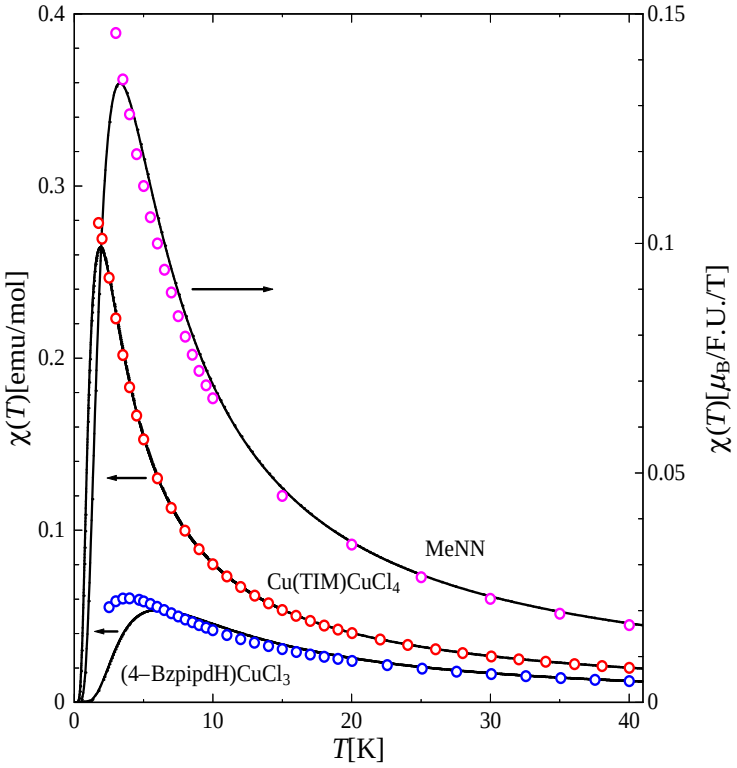

Figure 2.6: The uniform static susceptibilities $\chi(T)$ of Cu(TIM)$CuCl_4$, (4-BzpipdH)$CuCl_3$ and MeNN. The solid curves show the results obtained by Pair-DCEFA and the experimental data [1, 2] are shown by the open circles.

1.3 K [2], respectively. The uniform susceptibility observed in these three compounds [1, 2] are shown by the open circles in Fig. 2.6. We have evaluated the values of J_1 and J_2 in these systems by fitting the Pair-DCEFA susceptibility to the observed data. In the fitting procedure we have tried to reproduce the data particularly well at higher temperatures. The determined values of J_1 and J_2 are given in Table 2.1, and the full curves in Fig. 2.6 show the theoretical uniform susceptibilities of the AF-F alternating chains calculated by Pair-DCEFA with use of those intrachain exchange integrals. Then, we have estimated the magnitude of the interchain exchange integral $|J'|$ so as to reproduce the observed transition temperature $T_{\rm N}$ on the basis of the above combined method of Pair-DCEFA and MFA. Explicitly speaking, $|J'|$ has been determined from the condition $1/\mid 2J' \mid = \chi_+(\pi/2, T_{\rm N})$. As examples of the temperature dependence of the staggered susceptibility Fig. 2.7 shows $\chi_+(\pi/2, T)$ and $T_{\rm N}$ of Cu(TIM)$CuCl_4$ and MeNN. The values of $|J'|$ determined in this way are also shown in Table 2.1.

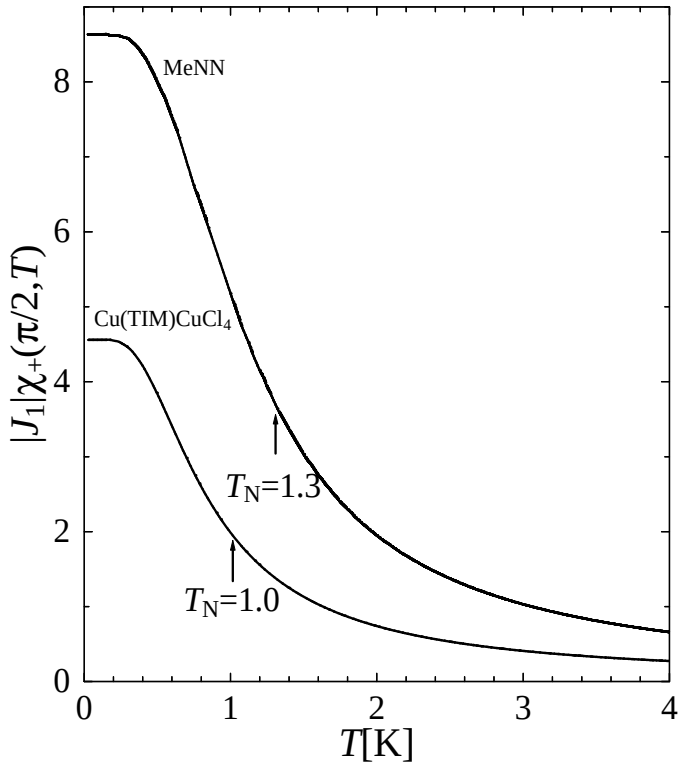

Figure 2.7: The temperature dependence of the staggered susceptibility $\chi_+(\pi/2, T)$ of $Cu(TIM)CuCl_4$ and MeNN.

2.1.4 Discussion and Conclusion

First we compare the results of Pair-DCEFA with those of Pair-MFA in which the exchange interaction between the spin pairs is treated by MFA instead of DCEFA. As easily understood, the results of Pair-MFA can be obtained by putting α=0 in those of Pair-DCEFA. In Fig. 2.3 the dot–dashed curve denotes the gap energy obtained by Pair-MFA for an S=1/2 exchange-alternating chain. For $a > 0$ the gap of Pair-MFA apparently agrees better with EDM result in comparison with that of Pair-DCEFA. In particular, it vanishes at a=1 as required from the exact theory. However, this does not necessarily mean that Pair-MFA gives reasonable results also for other physical quantities or it is superior to Pair-DCEFA. For example, with decreasing a from zero for $a < 0$ the gap of Pair-MFA deviates significantly from the EDM, and it vanishes only at a=–1 (note that the gap of Pair-DCEFA vanishes at $a \simeq -10$). Further, the low temperature behavior of $\chi(T)$ obtained by Pair-MFA is essentially the same as that obtained by Pair-DCEFA. As an example, $\chi(T)$ of Pair-MFA for a=–1 is shown by the thin dotted curve in Fig. 2.4.

Table 2.1: The intrachain exchange integrals (J_1 and J_2) and the interchain exchange integral (J') evaluated for three pseudo-one-dimensional AF-F alternating systems, Cu(TIM)$CuCl_4$, (4-BzpipdH)$CuCl_3$ and MeNN. The unit of the exchange integral is K and $a = J_2/J_1$.

compound	J_1/k_B	J_2/k_B	a	$\lvert J'/k_B\rvert$	$\lvert J'/J_1\rvert$
Cu(TIM)$CuCl_4$	-2.92	4.09	-1.40	0.38	0.130
(4-BzpipdH)$CuCl_3$	-8.74	38.46	-4.40	0.22	0.025
MeNN	-5.00	10.00	-2.00	0.34	0.068

In general, at temperatures higher than $T_{\max}$ $\chi(T)$ of Pair-DCEFA is closer to the EDM result than that of Pair-MFA.

Secondly, we discuss the temperature dependence of the staggered susceptibility $\chi_+(\pi/2, T)$ of S=1/2 exchange-alternating chains. The characteristic behavior that $\chi_+(\pi/2, T)$ of Pair-DCEFA takes the finite maximum value at T=0 K and decreases monotonously as a function of T is expected to be unchanged even if we obtain the exact solution of $\chi_+(\pi/2, T)$. In fact, this has been confirmed from our preliminary results of EDM calculations of $\chi_+(\pi/2, T)$ for finite chains up to twelve spins. Our preliminary results also show that $\chi_+(\pi/2, T)$ of Pair-DCEFA is larger (smaller) than that of EDM for $a < 0$ ($a > 0$), which is reasonably understood from the fact that Pair-DCEFA underestimates (overestimates) the gap energy. Therefore, the values of $|J'|$ determined for Cu(TIM)$CuCl_4$, (4-BzpipdH)$CuCl_3$ and MeNN are expected to be underestimated.

In conclusion, we have developed a new method called Pair-DCEFA by extending DCEFA originally proposed by Suzuki to the pair-approximation. By applying Pair-DCEFA to S=1/2 exchange-alternating chains it has been shown that Pair-DCEFA is practically useful for a fairly wide range of a, particularly for $a < 0$, with $a = J_2/J_1$ and $J_1 < 0$. It has been also shown that Pair-DCEFA cannot treat the Haldane gap behavior or the quantum liquid behavior of a uniform AF chain. Pair-DCEFA has an advantage of being able to calculate the q-dependent susceptibility and its temperature dependence without difficulty. Because of this advantage the effect of interchain coupling in pseudo-one-dimensional S=1/2 exchange-alternating systems can be easily investigated by using the combined method of Pair-DCEFA and MFA. The method has been applied to estimate the intrachain and the interchain exchange integrals of real pseudo-one-dimensional AF-F exchange-alternating systems, Cu(TIM)$CuCl_4$, (4-BzpipdH)$CuCl_3$ and MeNN. We

are also calculating the staggered susceptibility of S=1/2 exchange-alternating chains by performing detailed EDM calculations for finite spins. The results will be reported in the following section.

2.2 Pair-DCEFA under Magnetic Fields

Quite recently, by specific heat measurements Manaka *et al.* [10] have observed magnetic phase transitions under magnetic fields in a pseudo-1D S=1/2 AF–F alternating chain $(CH_3)_2CHNH_3CuCl_3$ [3] which does not order in zero field. In this section, we extend the combined method of Pair-DCEFA and MFA to the case under magnetic fields, and investigate the magnetic phase transition observed in $(CH_3)_2CHNH_3CuCl_3$. We also analyze by Pair-DCEFA the temperature dependence of nuclear spin-lattice relaxation time T_1 of this system, which has been measured by T. Kubo *et al.* [11].

2.2.1 Formalism

We first consider a single S=1/2 AF–F alternating chain under magnetic fields along the z-axis. The relevant Hamiltonian is expressed as,

$$\mathcal{H} = -\sum_i \left[J_1 \vec{S}_{i,1} \cdot \vec{S}_{i,2} + J_2 \vec{S}_{i-1,2} \cdot \vec{S}_{i,1} - g\mu_{\rm B} H (S^z_{i,1} + S^z_{i,2}) \right]. \tag{2.32}$$

Here we have assumed the nearest neighbor (n.n.) exchange couplings J_1 (< 0) and J_2 (> 0). H represents the strength of the magnetic field and $\vec{S}_{i,\mu}$ denotes the spin μ in the unit cell i with μ being 1 or 2. Within the framework of Pair-DCEFA the first and the third terms in eq. (2.32), *i.e.* the antiferromagnetic coupling spin-pair, is treated exactly, and for the second term $J_2 \vec{S}_{i-1,2} \cdot \vec{S}_{i,1}$ in eq. (2.32), *i.e.* the interaction between the pairs, the following decoupling is adopted:

$$J_2 \left[\vec{S}_{i-1,2} \cdot (\langle \vec{S}_{i,1} \rangle - \alpha \langle \vec{S}_{i-1,2} \rangle) + \vec{S}_{i,1} \cdot (\langle \vec{S}_{i-1,2} \rangle - \alpha \langle \vec{S}_{i,1} \rangle) \right], \tag{2.33}$$

where $\langle \vec{S} \rangle$ denotes the field-induced spin moment and α represents a correlation parameter which should be determined self-consistently.

The effective spin-pair Hamiltonian for the unit cell i is now given by

$$\mathcal{H}^{\rm eff}_i = -J_1 \vec{S}_{i,1} \cdot \vec{S}_{i,2} + H'(S^z_{i,1} + S^z_{i,2}), \tag{2.34}$$

with

$$H' = g\mu_{\rm B} H - J_2 \langle S^z \rangle (1 - \alpha),$$

where $\langle S^z \rangle$ ($\equiv \langle S^z_{i,1} \rangle = \langle S^z_{i,2} \rangle$) denotes the site-independent spin moment induced by the uniform external filed. By using the eigenvalues and eigenstates of the above effective Hamiltonian and in the spirit of the DCEFA we can calculate the transverse susceptibility tensor $\tilde{\chi}^{+-}(q,\omega)$ of the whole system. The final expression of $\tilde{\chi}^{+-}(q,\omega)$ is written as follows:

$$\begin{pmatrix} \chi^{+-}_{11}(q,\omega) & \chi^{+-}_{12}(q,\omega) \\ \chi^{+-}_{21}(q,\omega) & \chi^{+-}_{22}(q,\omega) \end{pmatrix} = (hh^* - kk^*)^{-1} \times \begin{pmatrix} h^*\phi^{+-}_{11} - k\phi^{+-}_{12}\mathrm{e}^{-\mathrm{i}qc} & h^*\phi^{+-}_{12}\mathrm{e}^{\mathrm{i}qc} - k\phi^{+-}_{11} \\ -k^*\phi^{+-}_{11} + h\phi^{+-}_{12}\mathrm{e}^{-\mathrm{i}qc} & -k^*\phi^{+-}_{12}\mathrm{e}^{\mathrm{i}qc} + h\phi^{+-}_{11} \end{pmatrix}, \tag{2.35}$$

with

$$\begin{aligned} h &= 1 + \frac{1}{2}J_2\left(\alpha\phi^{+-}_{11} - \phi^{+-}_{12}\mathrm{e}^{\mathrm{i}q(c+c')}\right), \\ k &= -\frac{1}{2}J_2\left(\phi^{+-}_{11}\mathrm{e}^{-\mathrm{i}qc'} - \alpha\phi^{+-}_{12}\mathrm{e}^{\mathrm{i}qc}\right), \\ \phi^{+-}_{11} &= \frac{1}{2}\left(\frac{\rho_\mathrm{s} - \rho_{\mathrm{t},1}}{\omega - J_1 + H'} + \frac{\rho_{\mathrm{t},-1} - \rho_\mathrm{s}}{\omega + J_1 + H'} + \frac{\rho_{\mathrm{t},-1} - \rho_{\mathrm{t},1}}{\omega + H'}\right), \\ \phi^{+-}_{12} &= \frac{1}{2}\left(\frac{\rho_{\mathrm{t},1} - \rho_\mathrm{s}}{\omega - J_1 + H'} + \frac{\rho_\mathrm{s} - \rho_{\mathrm{t},-1}}{\omega + J_1 + H'} + \frac{\rho_{\mathrm{t},-1} - \rho_{\mathrm{t},1}}{\omega + H'}\right), \end{aligned}$$

where c and c' represent the bond length for AF and F interactions, respectively, and $\rho_\mathrm{s} = \mathrm{e}^{-\beta J_1}/Z$ and $\rho_{\mathrm{t},m} = \mathrm{e}^{-\beta H' m}/Z$ (m=−1, 0, 1) with $Z = \mathrm{e}^{-\beta J_1} + \mathrm{e}^{\beta H'} + 1 + \mathrm{e}^{-\beta H'}$ and $\beta = 1/k_\mathrm{B}T$.

In order to determine $\langle S^z \rangle$ and α simultaneously, we impose the following self-consistency conditions:

$$\langle S^z \rangle = \mathrm{Tr}[S^z_{i1}\exp(-\beta\mathcal{H}^{\mathrm{eff}}_i)]/\mathrm{Tr}[\exp(-\beta\mathcal{H}^{\mathrm{eff}}_i)], \tag{2.36}$$

$$\langle\{S^+_1, S^-_1\}\rangle = \frac{2}{N}\sum_q \frac{1}{\pi}\int_{-\infty}^{\infty}\mathrm{d}\omega\coth(\frac{\beta\omega}{2})\ \mathrm{Im}\chi^{+-}_{11}(q,\omega+\mathrm{i}s), \tag{2.37}$$

where N denotes the total number of spins and $\langle\{S^+_1, S^-_1\}\rangle \equiv \langle S^+_1 S^-_1 + S^-_1 S^+_1\rangle = 2\{S(S+1) - \langle(S^z)^2\rangle\}$ represents the on-site spin correlation calculated by using the effective spin-pair Hamiltonian eq. (2.34). Equation (2.36) represents the usual self-consistency condition for $\langle S^z \rangle$. Equation (2.37) is required from the fluctuation-dissipation theorem, and its implication is that the on-site spin correlation calculated from the dynamical susceptibility (the right-hand side of eq. (2.37)) should be equal to that calculated from the effective spin-pair Hamiltonian.

Equation (2.36) is expressed more explicitly as

$$\langle S^z \rangle = \frac{1}{2}(\rho_{\mathrm{t},1} - \rho_{\mathrm{t},-1}). \tag{2.38}$$

The actual calculational procedure of the right-hand side of eq. (2.37) is as follows. We first solve $hh^* - kk^*$=0 to obtain poles $\omega_i(q)$ (i=1$\sim$3) of $\chi_{11}^{+-}(q,\omega)$. Then, by using these $\omega_i(q)$, $\chi_{11}^{+-}(q,\omega)$ is transformed as

$$\chi_{11}^{+-}(q,\omega) = \sum_{i=1}^{3} \frac{\gamma_i(q)}{\omega - \omega_i(q)}, \tag{2.39}$$

with

$$\gamma_l(q) = G(q,\omega_l(q)) \prod_{i=1}^{3} (\omega_l(q) + x_i) / \prod_{\substack{m,n=1 \\ (m\neq n)}}^{3} (\omega_m(q) - \omega_n(q)), \tag{2.40}$$

where

$$G(q,\omega) = h^* \phi_{11}^{+-} - k\phi_{12}^{+-} \mathrm{e}^{-\mathrm{i}qc},$$
$$x_1 = -J_1 + H', \quad x_2 = J_1 + H', \quad x_3 = H'.$$

Inserting eq. (2.39) into the righthand side of eq. (2.37) we can rewrite eq. (2.37) in the following form:

$$\langle (S^z)^2 \rangle - \frac{3}{4} = \frac{1}{N} \sum_q \left[\sum_{i=1}^{3} \gamma_i(q) \coth(\beta\omega_i(q)/2) \right]. \tag{2.41}$$

From eq. (2.38) and eq. (2.41), $\langle S^z \rangle$ and α are determined self-consistently.

In Figs. 2.8(A) and (B) we show examples of temperature and magnetic-field dependencies of α. As seen from Fig. 2.8(A), with decreasing temperature from high temperatures, α increases monotonously, takes a maximum around the temperature corresponding to about $0.3|J_1|$, and then approaches to a finite value toward T=0 K. Further, α becomes large when H increases. Figure 2.8(B) shows that the smaller the value of $J_2/|J_1|$ takes, the smaller α becomes. Most of these characteristic behaviors of α can be understood by considering that spin correlation between the spin pairs become strong for large J_2 and also they develop with decreasing temperature or increasing magnetic fields. However, the physical origin of the maximum of α as a function of temperature is not clear at present. As to the temperature and magnetic-field dependencies of $\langle S^z \rangle$ we simply note that it takes rather small values in the whole temperature range for magnetic fields smaller than the gap energy. Once $\langle S^z \rangle$ and α are determined, the dynamical susceptibility tensor $\tilde{\chi}^{+-}(q,\omega)$ is fixed and we can calculate various physical quantities from $\tilde{\chi}^{+-}(q,\omega)$.

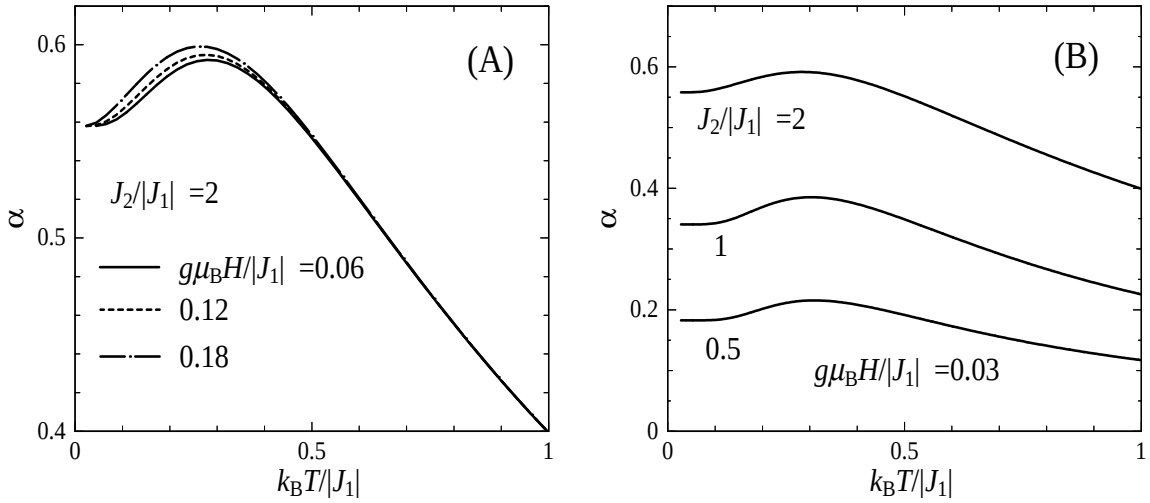

Figure 2.8: (A) The temperature dependence of the correlation parameter α for $g\mu_{\rm B}H/|J_1|$=0.06, 0.12, 0.18 and $J_2/|J_1|$=2. (B) The temperature dependence of the correlation parameter α for $J_2/|J_1|$=0.5, 1, 2 and $g\mu_{\rm B}H/|J_1|$=0.03.

2.2.2 Effect of Interchain Coupling

Recently, magnetic phase transitions under magnetic fields have been observed in an organic pseudo-1D S=1/2 AF–F exchange alternating chain $(CH_3)_2CHNH_3CuCl_3$ [10] which does not order at zero field. Motivated by this experimental results, we have investigated the effect of interchain coupling on the magnetic phase transition under magnetic fields. For this purpose we have adopted the combined method of Pair-DCEFA and the mean-field approximation (MFA), that is, we use Pair-DCEFA for intrachain coupling and MFA for interchain coupling. According to this method the generalized susceptibility for the whole three dimensional system can be obtained in terms of the interchain coupling and the susceptibility of a single chain obtained by Pair-DCEFA. Occurrence of phase transitions is generally determined from the condition of divergence of the generalized susceptibility and in the present case the condition is expressed as,

$$[(1/|2J'|) - \chi_+(q,H,T)][(1/|2J'|) - \chi_-(q,H,T)] = 0, \tag{2.42}$$

where J' denotes the n.n. interchain exchange integral (the number of n.n. spins is assumed to be four), and $\chi_\pm(q,H,T)$ denote $\chi_{11}^{+-}(q,0) \pm |\chi_{12}^{+-}(q,0)|$ which are the two eigenvalues of the static susceptibility tensor $\tilde{\chi}^{+-}(q,0)$ of a single chain. It is noted here that $\chi_-(0,0,T)$ corresponds to the uniform static susceptibility of a single chain. In Fig. 2.9, we show as an example q- and temperature dependence of $\chi_+(q,H,T)$ for

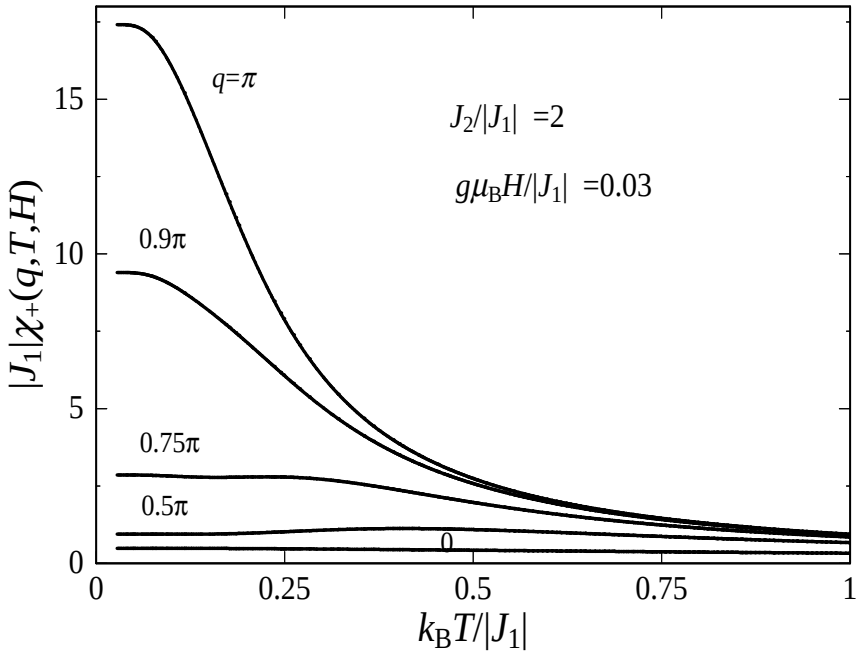

Figure 2.9: The temperature dependence of $\chi_+(q, H, T)$ calculated for several values of q by fixing $J_2/|J_1|$ and $g\mu_{\rm B}H/|J_1|$ to 2 and 0.03, respectively. The unit of q is $1/(c + c')$.

$J_2/|J_1| = 2$ and $g\mu_{\rm B}H/|J_1|$=0.03. To be important, for AF–F chains $\chi_+(q, H, T)$ is larger than $\chi_-(q, H, T)$ for any value of q. Furthermore, at each temperature for a given field $\chi_+(q, H, T)$ takes the maximum value at $q = \pi$ as a function of q, and this behavior can be explained by considering that the gap has the minimum value at q=π. It should be also noted that for a given temperature the value of $\chi_+(q, H, T)$ increases with increasing H.

The actual transition temperature (Néel temperature $T_{\rm N}$) is defined as the highest temperature which satisfies the condition (2.42). Hence, by taking into consideration the characteristic behaviors of $\chi_\pm(q, H, T)$ mentioned above the equation to determine $T_{\rm N}$ is expressed simply as

$$1/|2J'| - \chi_+(\pi, H, T) = 0. \tag{2.43}$$

It is easily recognized that $T_{\rm N}$ is practically determined from the crossing between the curve of $\chi_+(\pi, H, T)$ as a function of T and the straight line corresponding to $1/|2J'|$. Since $\chi_+(\pi, H, T)$ is a decreasing function of T, if $1/|2J'| > \chi_+(\pi, H, 0)$ is satisfied, no crossing point is obtained, *i.e.* phase transition does not occur. In particular, if $1/|2J'| > \chi_+(\pi, 0, 0)$, it means that the system does not order at zero field. Even in

that case, the phase transition is expected to occur for finite fields because $\chi_+(\pi, H, 0)$ increases with increasing H and hence $1/|2J'| < \chi_+(\pi, H, 0)$ may be fulfilled for H larger than some critical value.

In applying the above method to $(CH_3)_2CHNH_3CuCl_3$ we first analyzed by Pair-DCEFA the observed uniform static susceptibility [3] at temperatures higher than T_N and estimated the intrachain exchange integrals as J_1=−47.0 K and J_2=94.0 K. The observed

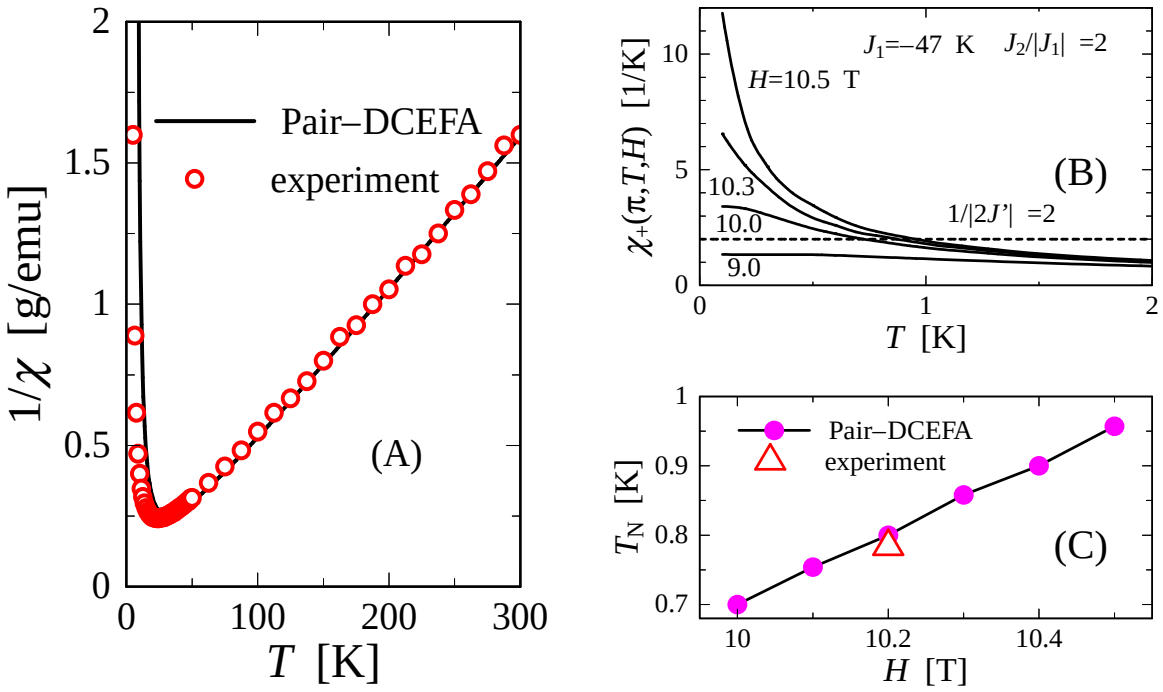

Figure 2.10: (A) The temperature dependence of inverse of the uniform susceptibility of $(CH_3)_2CHNH_3CuCl_3$. The circles denote the experimental data [?] and the full curve represents the theoretical results for a single AF–F chain obtained by Pair-DCEFA with use of J_1=−47.0 K and J_2=94.0 K. (B) The temperature dependence of $\chi_+(\pi, T, H)$ of $(CH_3)_2CHNH_3CuCl_3$ calculated for several values of H. The horizontal dotted line represents $1/|2J'| = 2$. (C) The magnetic-field dependence of T_N. The open triangles denote the experimental data [10] and the closed circles the theoretical results.

and the calculated uniform static susceptibilities as functions of temperature are shown in Fig. 2.10(A). Next, by making use of $\chi_+(\pi, T, H)$ calculated with use of g=2.26 [10] and the determined J_1 and J_2 we have estimated the magnitude of J' so as to reproduce the observed Néel temperature at H=10.2 T (see Figs. 2.10(B) and (C)). The magnitude of interchain exchange coupling determined in this way is $|J'|$=0.125 K.

2.2.3 Nuclear Spin-Lattice Relaxation Rate

Quite recently, T. Kubo *et al.* [11] have measured proton spin-lattice relaxation rate $1/T_1$ of $(CH_3)_2CHNH_3CuCl_3$ under magnetic fields. According to their results $1/T_1$ shows at a low temperature region a behavior of activate energy type expressed as $\exp[-(\Delta - g\mu_{\rm B}H)/k_{\rm B}T]$, but its origin is not clear. Hence, in this section we try to understand this behavior of $1/T_1$ by performing analysis with use of the susceptibility under magnetic fields obtained by Pair-DCEFA. First of all, it should be noted that there are no methods of analysis for this phenomena, and in such a sense the challenge of using susceptibility of Pair-DCEFA is quite significant.

Now, the nuclear spin-lattice relaxation rate $1/T_1$ [28] in this system is written as,

$$1/T_1 \propto \int {\rm d}t {\rm e}^{{\rm i}\omega_0 t} \sum_q \sum_{m,n=1}^{2} \left[\frac{1}{4} A^{\perp}_{mn}(q) \langle\{S^+_q(t), S^-_{-q}(0)\}\rangle + A^{//}_{mn}(q) \langle\{S^z_q(t), S^z_{-q}(0)\}\rangle \right], \quad (2.44)$$

where ω_0 denotes the resonance energy and is thought to be about one thousands of $\omega_i(q)$ in eq. (2.39), that is, the energy of the spin system. Further $A^l_{mn}(q)$ (m, n=1 or 2, l=$\perp$ or //) are the coefficients of hyperfine structure which are defined as the Fourier component of the product of two dipole-dipole interaction between electric spin S_i and nuclear spin [29]. Explicitly $A^l_{mn}(q)$ are given as follows:

$$A^{\perp}_{mn}(q) = \sum_{i,j} \frac{(1-3\cos^2\theta_{p,im})(1-3\cos^2\theta_{p,jn}) + 9\sin^2\theta_{p,im}\sin^2\theta_{p,jn}}{r^3_{p,im} r^3_{p,jn}} \times {\rm e}^{{\rm i}q(r_{im}-r_{jn})}, \quad (2.45)$$

$$A^{//}_{mn}(q) = \sum_{i,j} \frac{9\sin\theta_{p,im}\cos\theta_{p,im}\sin\theta_{p,jn}\cos\theta_{p,jn}}{r^3_{p,im} r^3_{p,jn}} {\rm e}^{{\rm i}q(r_{im}-r_{jn})}, \quad (2.46)$$

where r_{im} (r_{jn}) represents m (n) site in ith (jth) unit cell with m (n) being 1 or 2, and $r_{p,im}$ ($r_{p,jn}$) denotes the distance between proton site and r_{im} (r_{jn}). Further, the $\theta_{p,im}$ ($\theta_{p,jn}$) is defined as the angle between the direction of electric spin at r_{im} (r_{jn}) and that of proton spin.

By using the fluctuation dissipation theorem (2.15) and the condition $T \gg \omega_0$, the above expression is given as,

$$1/T_1 \propto T \sum_q \sum_{m,n=1}^{2} \left[\frac{1}{4} A^{\perp}_{mn}(q) \frac{{\rm Im}\chi^{+-}_{mn}(q,\omega_0)}{\omega_0} + A^{//}_{mn}(q) \frac{{\rm Im}\chi^{zz}_{mn}(q,\omega_0)}{\omega_0} \right]. \quad (2.47)$$

Within the Pair-DCEFA, we can certainly investigate the temperature dependence of ${\rm Im}\chi(q,\omega_i(q))$. Unfortunately, however, in the Pair-DCEFA the damping effect is not taken into account, and as the result ${\rm Im}\chi(q,\omega_0)$ does not have finite values at all. In the

present study, we try to calculate $1/T_1$ on the basis of the q-dependent static susceptibility of Pair-DCEFA. Then we assume the following standard form [30, 31]:

$$\mathrm{Im}\chi^{ij}_{mn}(q,\omega_0) = \chi^{ij}_{mn}(q)\frac{\omega_0\Gamma_q}{\omega_0^2+\Gamma_q^2}, \tag{2.48}$$

where Γ_q is damping constant [31], and ij denote $+-$ or zz. Further under condition $\Gamma_q > \omega_0$, we obtain

$$\frac{\mathrm{Im}\chi^{ij}_{mn}(q,\omega_0)}{\omega_0} \sim \frac{\chi^{ij}_{mn}(q)}{\Gamma_q}. \tag{2.49}$$

In actual calculation of $A^l_{mn}(q)$ we have taken into account the proton and copper

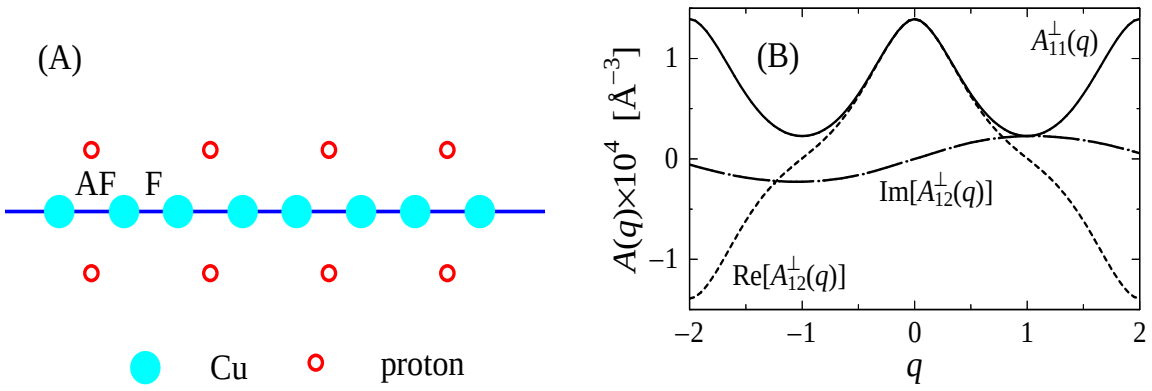

Figure 2.11: (A) The positions of protons in the vicinity of Cu ions in $(CH_3)_2CHNH_3CuCl_3$. (B) The q-dependencies of $A^{\perp}_{11}(q)$, $\mathrm{Re}[A^{\perp}_{12}(q)]$ and $\mathrm{Im}[A^{\perp}_{12}(q)]$ in $(CH_3)_2CHNH_3CuCl_3$ are shown by the solid, dotted and dot-dashed curves, respectively. The unit of q is $\pi/(c+c')$.

positions as shown in Fig. 2.11(A) and the following distances are used: Cu-Cu [short] =3.417 Å, Cu-Cu [long] =3.506 Å [32], and distance between proton and Cu chain $\sim$ 6.0 Å. In Fig. 2.11(B), q-dependencies of $A^{\perp}_{11}(q)$, $\mathrm{Re}[A^{\perp}_{12}(q)]$ and $\mathrm{Im}[A^{\perp}_{12}(q)]$ are shown by the solid, dotted and dot-dashed curves, respectively. As seen from Fig. 2.11(B) $A^{\perp}_{11}(q)$ and $|\mathrm{Re}[A^{\perp}_{12}(q)]|$ have large values around q=0 and 2π, but they are small around q=π. Further the magnitude of $\mathrm{Im}[A^{\perp}_{12}(q)]$ is rather small compared with those of $A^{\perp}_{11}(q)$ and $\mathrm{Re}[A^{\perp}_{12}(q)]$, and it should be noted also that $A^{//}_{mn}(q)$ (m, n=1 or 2) have quite small magnitude for any value of q. Considering all of these characteristic features of $A^l_{mn}(q)$ we adopt the following drastic approximation, namely we take into account only $A^{\perp}_{11}(q)$ and $\mathrm{Re}[A^{\perp}_{12}(q)]$ for q=0 and 2π and neglect all of other $A^l_{mn}(q)$. Furtheremore, for simplicity we assume

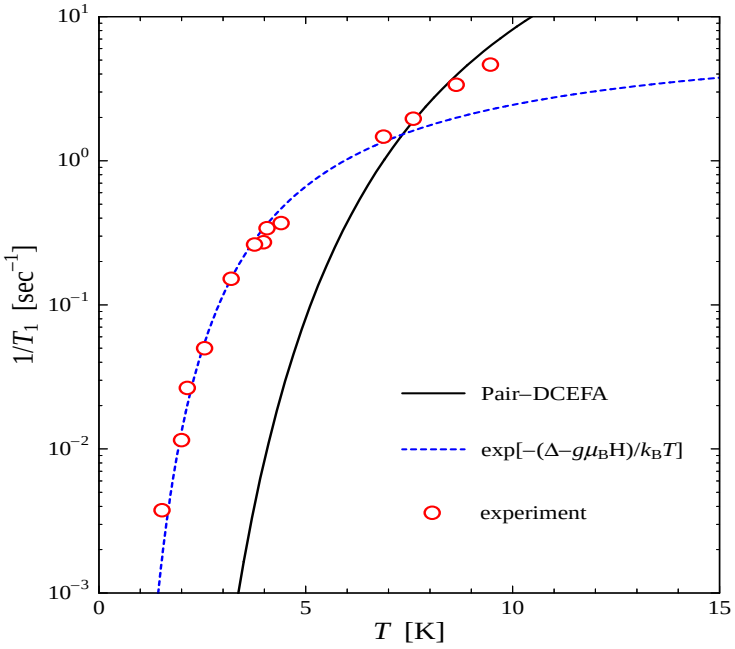

Figure 2.12: The temperature dependence of $1/T_1$ of $(CH_3)_2CHNH_3CuCl_3$ at H=3.5 T. The solid and dotted curves represent the results obtained by using Pair-DCEFA and by assuming the activate energy type, respectively. The circles denote the experimental data [11].

that $\Gamma_{q=0}$ is equal to $\Gamma_{q=2\pi}$ and they are independent of temperature. As the results, $1/T_1$ can be represented by $A(q)$ and $\chi^{ij}_{mn}(q)$. Then the resultant $1/T_1$ is expressed simply as,

$$1/T_1 \propto T\{A^{\perp}_{11}(0)\chi^{+-}_{11}(0) + \mathrm{Re}[A^{\perp}_{12}(0)]\mathrm{Re}[\chi^{+-}_{12}(0)] + A^{\perp}_{11}(2\pi)\chi^{+-}_{11}(2\pi) + \mathrm{Re}[A^{\perp}_{12}(2\pi)]\mathrm{Re}[\chi^{+-}_{12}(2\pi)]\}. \quad (2.50)$$

From this equation we have calculated the temperature dependence of $1/T_1$ at H=3.5 T by using $\chi^{+-}_{11}(q)$ and $\mathrm{Re}[\chi^{+-}_{12}(q)]$ (q=0, 2π) obtained in the previous section. The results are shown in Fig. 2.12 by the full curve. The agreement is better in the high temperature region than in the low temperature region. The large discrepancy at low temperature region may imply the necessity of taking account of the effects which are not included in the expression of $1/T_1$ (2.50). For example, it may be necessary to consider temperature and wave-vector dependences of Γ_q

2.3 Staggered Susceptibility by Exact Diagonalization Method

In the previous sections the magnetic phase transitions of pseudo-one-dimensional S=1/2 exchange alternating chains have been investigated by a combined method in which the intrachain and interchain couplings are treated by Pair-DCEFA and mean field approximation (MFA), respectively. However, it is sometimes insufficient for truly quantitative discussion. In this section we calculate the q-dependent staggered susceptibilities of S=1/2 exchange alternating chains by using the EDM for finite chains and estimate interchain coupling of real pseudo-one-dimensional S=1/2 exchange alternating chains by combining with MFA.

We express the Hamiltonian of an S=1/2 exchange alternating chain as follows:

$$\mathcal{H} \ = \ -\sum_i (J_1 \vec{S}_{i,1} \cdot \vec{S}_{i,2} + J_2 \vec{S}_{i-1,2} \cdot \vec{S}_{i,1}), \tag{2.51}$$

where $\vec{S}_{i,1}$ ($\vec{S}_{i,2}$) denotes the spin 1 (spin 2) in the unit cell i. J_1 and J_2 are the exchange integrals. Further we define a=J_2/J_1. The base of Hamiltonian is writen as

$$|m_1, m_2, m_3, \cdots, m_i, \cdots, m_N\rangle, \tag{2.52}$$

where m_i represents the up spin $\uparrow$ or down spin $\downarrow$ at i site. Using the above base, new bases indexed by K are written as follows:

$$\Phi_K = \frac{1}{\sqrt{N}} \sum_{n=0}^{\infty} \mathrm{e}^{\mathrm{i}Kn} T_n |m_1, m_2, m_3, \cdots, m_i, \cdots, m_N\rangle. \tag{2.53}$$

Here T_n denotes the translation operator, K is the wave vector. This bases apparently satisfy the Bloch theorem,

$$T_m \Phi_K = \mathrm{e}^{\mathrm{i}Km} \Phi_K. \tag{2.54}$$

By using such bases, we obtain the Hamiltonian blocked with each index K. Further the size of matrix being diagonalized is reduced by classifying with use of $S_z^{\mathrm{total}} = \sum_i (S_{i1}^z + S_{i2}^z)$.

By using all the eigenvalues and eigenstates obtained by EDM we can calculate the transverse susceptibility tensor $\chi_{ij}^{+-}(q_z)$, where i, j=1 or 2 specify the sublattice. We define the generalized susceptibility as follows:

$$\chi_{\pm}(q_z) = \chi_{11}^{+-}(q_z) \pm |\chi_{12}^{+-}(q_z)|, \tag{2.55}$$

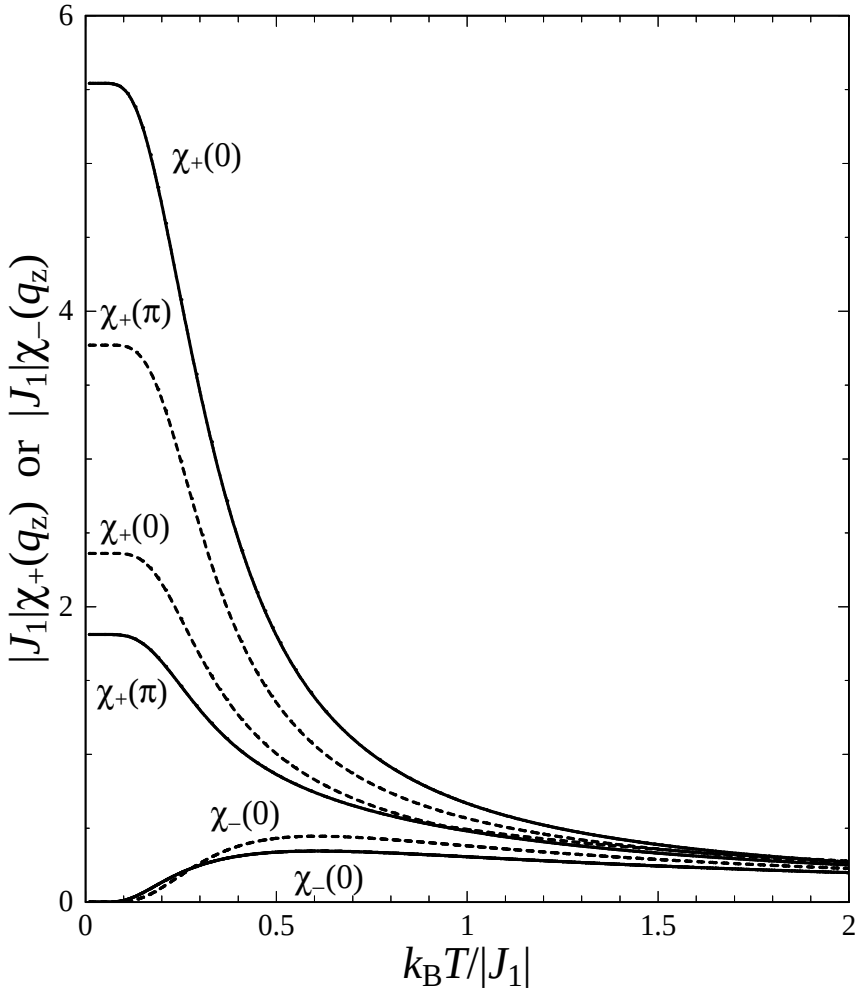

Figure 2.13: The temperature dependence of $\chi_+(q_z)$ ($q_z = 0, \pi$) and $\chi_-(0)$ for a=±0.6 calculated by EDM. The solid and dotted lines represent the results for a=0.6 and –0.6, respectively.

where $\chi_\pm(q_z)$ are in proportion to the two eigenvalues of the transverse susceptibility tensor $\chi_{ij}^{+-}(q_z)$, and $\chi_+(q_z)$ [$\chi_-(q_z)$] represents susceptibility when magnetic fields at sublattices 1 and 2 are antiparallel [parallel]. From now on we call $\chi_+(q_z)$ the staggered susceptibility.

As a function of temperature, $\chi_\pm(q_z)$ show characteristic behaviors. As examples we show in Fig. 2.13 the temperature dependence of the staggered susceptibilities $\chi_+(0)$ and $\chi_+(\pi)$ and the uniform susceptibility $\chi_-(0)$ calculated by EDM for a 12 site chain with $a = \pm\ 0.6$. The uniform susceptibility $\chi_-(0)$ vanishes at T=0 K reflecting the existence of a gap between the singlet ground state and the excited states. The value of $\chi_+(q_z)$

increases with decreasing temperature for any q_z, and finally becomes the maximum at T=0 K. To be important, $\chi_+(0)$ and $\chi_+(\pi)$ takes the largest value at each temperature for the AF and AF–F alternating chains, respectively. These behaviors can be understood essentially by considering respective ordering vectors within a chain. Further we compare

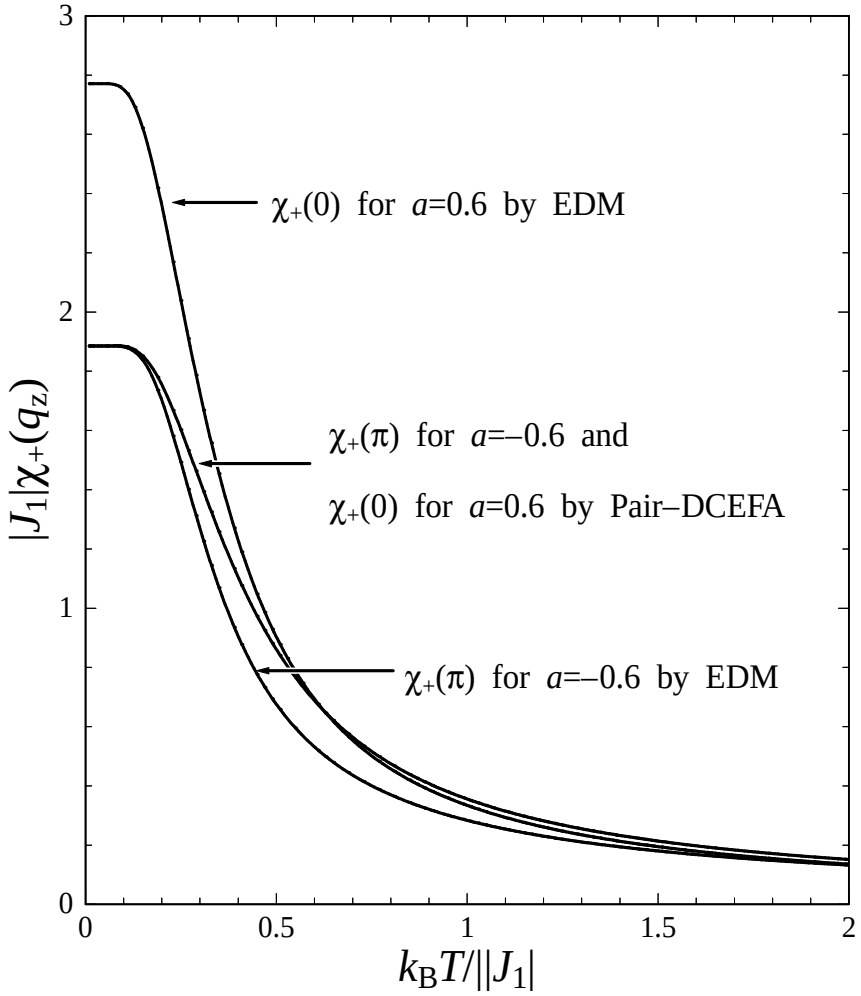

Figure 2.14: The comparison of the staggered susceptibility of EDM and that of Pair-DCEFA, for the system of a=±0.6.

the temperature dependence of $\chi(q)$ by EDM with that by Pair-DCEFA. In Fig. 2.14, we show the temperature dependence of $\chi(q)$ for AF–AF alternating chain a=0.6 and AF–F alternating chain a=–0.6. Though the agreement between them is not sufficient for a=0.6, it is fairly well for a=–0.6. This is under the influence of different magnitude of gap between both the method.

If the interchain couplings are switched on to this system, three-dimensional mag-

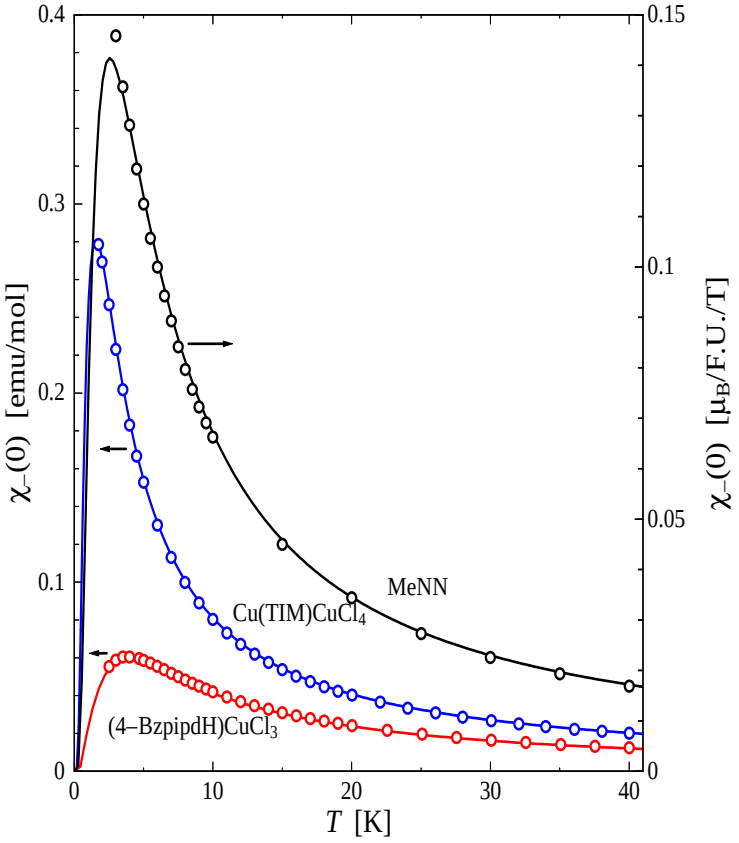

Figure 2.15: The temperature dependence of uniform static susceptibility for $Cu(TIM)CuCl_4$, (4-BzpipdH)$CuCl_3$ [1] and MeNN [2]. The circles and lines denote the experimental data and the susceptibility calculated by EDM.

netic order may be realized at low temperatures. We treat the interchain couplings by MFA, and then within the linear response approximation we can easily get the 2×2 susceptibility tensor $\tilde{\chi}(\vec{q})$ for the pseudo-one-dimensional exchange alternating chain. This tensor is certainly the same as eq. (2.29). The transition temperature of magnetic order is usually determined from the condition that the static susceptibility diverges, that is, eq. (2.31). As noted previously, $\chi_+(0)$ and $\chi_+(\pi)$ are the largest at each temperature for AF and AF–F alternating chains, respectively, and hence the actual transition temperature $T_{\rm N}$ is determined from $1/|2J'| = \chi_+(0)$ for AF alternating chain and $1/|2J'| = \chi_+(\pi)$ for AF–F alternating chain. Here we take into account only the n.n. interchain exchange integral J' and the number of the n.n. chains is assumed to be four.

The method has been applied to three real pseudo-one-dimensional S=1/2 AF–F alternating chains $Cu(TIM)CuCl_3$, (4-BzpipdH)$CuCl_3$ [1] and MeNN [2], whose magnetic

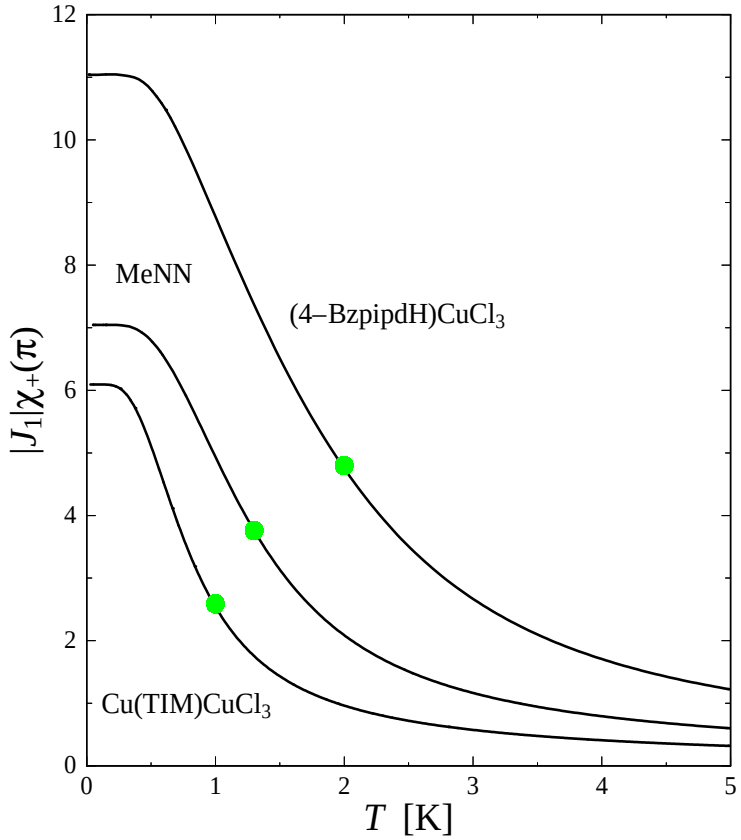

Figure 2.16: The temperature dependence of $\chi_+(\pi)$ of Cu(TIM)$CuCl_4$, (4-BzpipdH)$CuCl_3$ [1] and MeNN [2] calculated by EDM. Each T_N is shown by the circle.

phase transitions have been observed at about 1 K, 2 K and 1.3 K, respectively. As shown in Fig. 2.15, we first analyzed by EDM the observed uniform static susceptibility at temperatures higher than T_N and estimated the intrachain exchange integrals J_1 and J_2. Secondly, by making use of $\chi_+(\pi)$ calculated with use of the determined J_1 and J_2 (see Fig. 2.16) we have estimated the magnitude of J' so as to reproduce the observed Néel temperature. The values of J_1, J_2 and $|J'|$ determined in this way are given in Table 1. As seen from Table 1 the magnitude of J' determined by our present calculations is larger than that estimated by a combined method of Pair-DCEFA and MFA. This difference originates from that Pair-DCEFA underestimates the gap energies of AF–F alternating chain and hence $\chi_+(\pi)$ of Pair-DCEFA is larger than that of EDM.

Table 2.2: The exchange integrals determined for three real pseudo-one-dimensional S=1/2 AF–F alternating chains. The values in ( ) denote those estimated by using the combined method of Pair-DCEFA and MFA. The unit of the exchange integrals is K.

compound	J_1	J_2	$\|J'\|$	$a(=J_2/J_1)$
$Cu(TIM)CuCl_4$	–2.90	4.70	0.55	1.60
	(–2.92)	(4.09)	(0.38)	(1.40)
$(4\text{-}BzpipdH)CuCl_3$	–8.80	38.80	0.88	4.40
	(–8.74)	(38.46)	(0.22)	(4.40)
MeNN	–5.00	10.00	0.65	2.00
	(–5.00)	(10.00)	(0.34)	(2.00)

2.4 Intensity of Neutron Scattering by Numerical Calculation

Recently, many experimental and theoretical studies for the S=1/2 AF–AF alternating chain are performed for the purpose of investigating the excited states in detail. Among them, the second gap and continuum states have been newly observed in the dimerized spin Peierls system $CuGeO_3$, and a few explanations for these excited states are reported. For S=1/2 AF–F alternating chain K. Hida [33] has previously reported the magnon dispersions obtained by using EDM for finite spin chain, but there are no experimental and theoretical reports about the intensity of neutron scattering. Since the neutron scattering experiment are planned for the AF–F alternating chain system $(CH_3)_2CHNH_3CuCl_3$ ($J_2/|J_1|$=2, J_1: antiferromagnetic exchange, J_2: ferromagnetic exchange) [3] which was treated in the previous section, theoretical studies are desired urgently. In particular, the second gap and the continuum states have been attracting considerable interesting. Therefore, in order to investigate whether they are observable or not, we tried to calculate the intensity of neutron scattering by means of the numerical calculation (NC) based on the exact diagonalization method.

We use eq. (2.51) as the Hamiltonian $\mathcal{H}$, and calculate the intensity of neutron scattering from

$$S(q,\omega) \propto \lim_{\eta\to+0} \mathrm{Im}[\langle \mathrm{GS}|S^z_{-q}(\omega - i\eta + E_{\mathrm{GS}} - \mathcal{H})^{-1}S^z_q|\mathrm{GS}\rangle],$$

where E_{GS} and $|\mathrm{GS}\rangle$ denote the eignvalue and the eigenvector of the ground state, respectively. Further, since the system with two sublattices is now kept in mind, S^z_q is defined

as

$$S_q^z = N^{-1/2}\sum_n \mathrm{e}^{\mathrm{i}qr_n}(S_{n,1}^z + \mathrm{e}^{\mathrm{i}qc}S_{n,2}^z), \tag{2.56}$$

where c is distance between sublattice 1 and 2.

The actual procedure of NC is as follows: The $|\mathrm{GS}\rangle$ is first obtained by using EDM. Once the ground state is obtained, then $S(q,\omega)$ can be calculated by using the continued fraction expansion for the expression in the tridiagonal basis of the Hamiltonian with the initial state $S_q^z|\mathrm{GS}\rangle$. Here, the tridiagonal expansion of the Hamiltonian is performed with use of the Lanczos algorithm. It is known that this method is useful for the low energy region.

In Figs. 2.17 $\sim$ 2.22, we show the magnon dispersions and their intensities of neutron scattering for the S=1/2 AF–F alternating chains with the alternating parameter a = $J_2/|J_1|$ = 0.5, 1.0, 2.0, respectively. The obtained dispersions give almost the same results as Hida's. As seen from these figures the second gap is clearly seen. Further, the dispersions above the second gap show the characteristic behavior. In particular, the lowest energy in the continuum region takes maximum value at $q = \pi/2$, and the magnitude of the second gap at q=0 decrease with increasing a. The Haldane gap system, which corresponds to the system of $a \to \infty$, does not have the second gap at q=0 while the second gap exists around $q = \pi/2$. From this fact, it is predicted that these behaviors represent the peculiar character of S=1/2 AF–F alternating chains. The intensity at $q = 0$ certainly takes zero reflecting the singlet ground state for any a. And, for each q the intensity has the maximum value at the first excited states and decays as the energy ω becomes higher. To be remarkable, the intensities take the maximum value at $q = \pi/2$ for the whole range of a, and also the intensity for each q increase with increasing a.

Now, in order to understand such q dependencies of neutron scattering intensity, we perform the consideration with use of the intensity of Pair-DCEFA. The used expression of Pair-DCEFA is eq. (2.25) at T=0 K. In Fig. 2.23 we show the q-dependence of intensity for the transition to the triplet excited states obtained by using NC and Pair-DCEFA. The full curves and the points represent the intensities of Pair-DCEFA and NC, respectively. To be noted, as regards Pair-DCEFA's intensities we have plotted the values multiplied by different constant values for respective cases, $J_2/|J_1|$=0.5, 1.0, 2.0. Therefore, the absolute magnitude of Pair-DCEFA's intensities is not in agreemen with that of EDM intensities. It should be noted, however, that the results of Pair-DCEFA simulate well the the q-dependence of the EDM intensities. Pair-DCEFA's intensity is in proportion inversely to the magnon energy which becomes maximum at q=0 and π and minimum at

q=$\pi/2$, and hence the intensities take the maximum value at $q = \pi/2$.

Finally, it should be also noted that for the whole range of q the intensities of transition to the excited states above the second gap are weaker than those to the excited states above first gap. However, the intensities at larger q are relatively strong in comparison with those at other q, and therefore the spectra at large q may be observable.

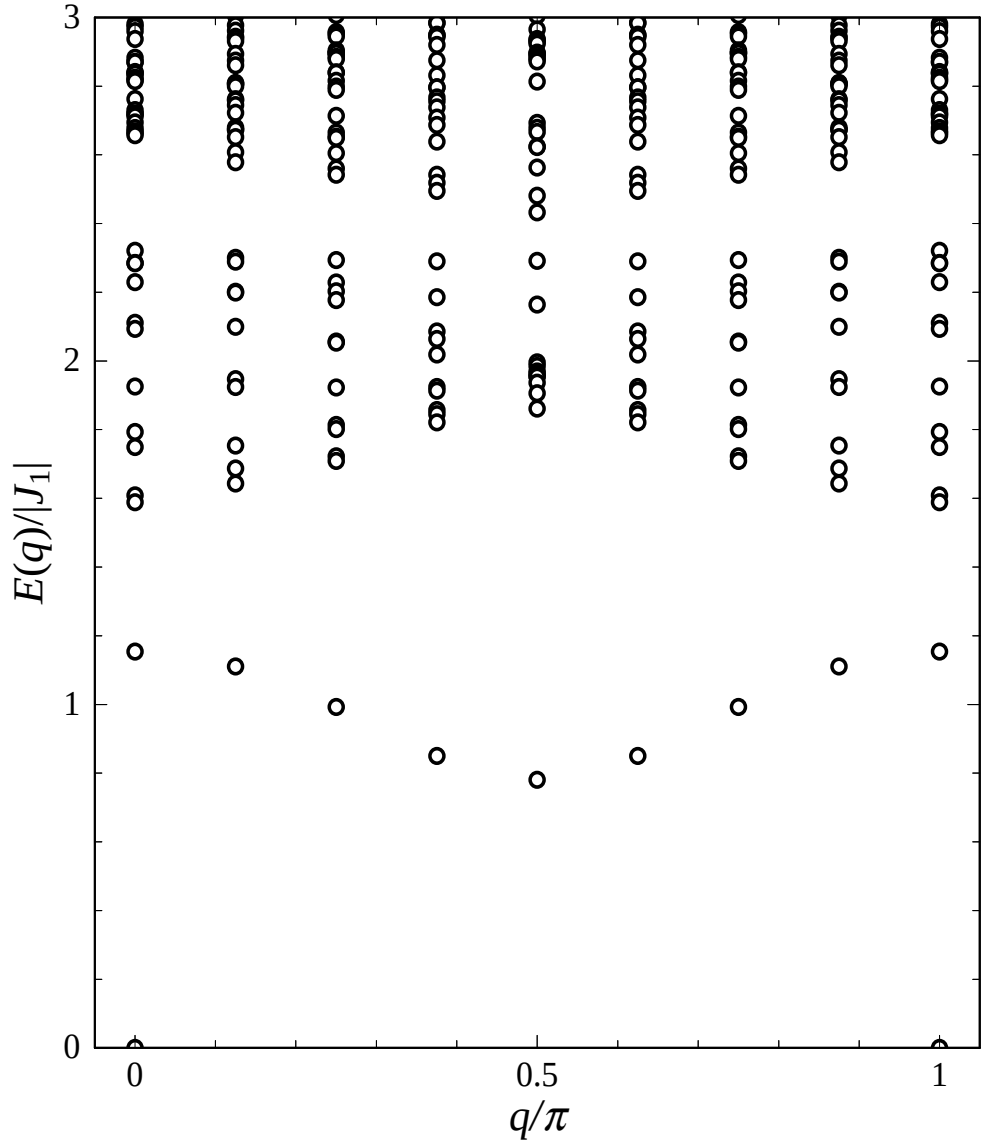

Figure 2.17: The magnon dispersion for the system of $J_2/|J_1|$=0.5 obtained by using EDM for 16 sites chain.

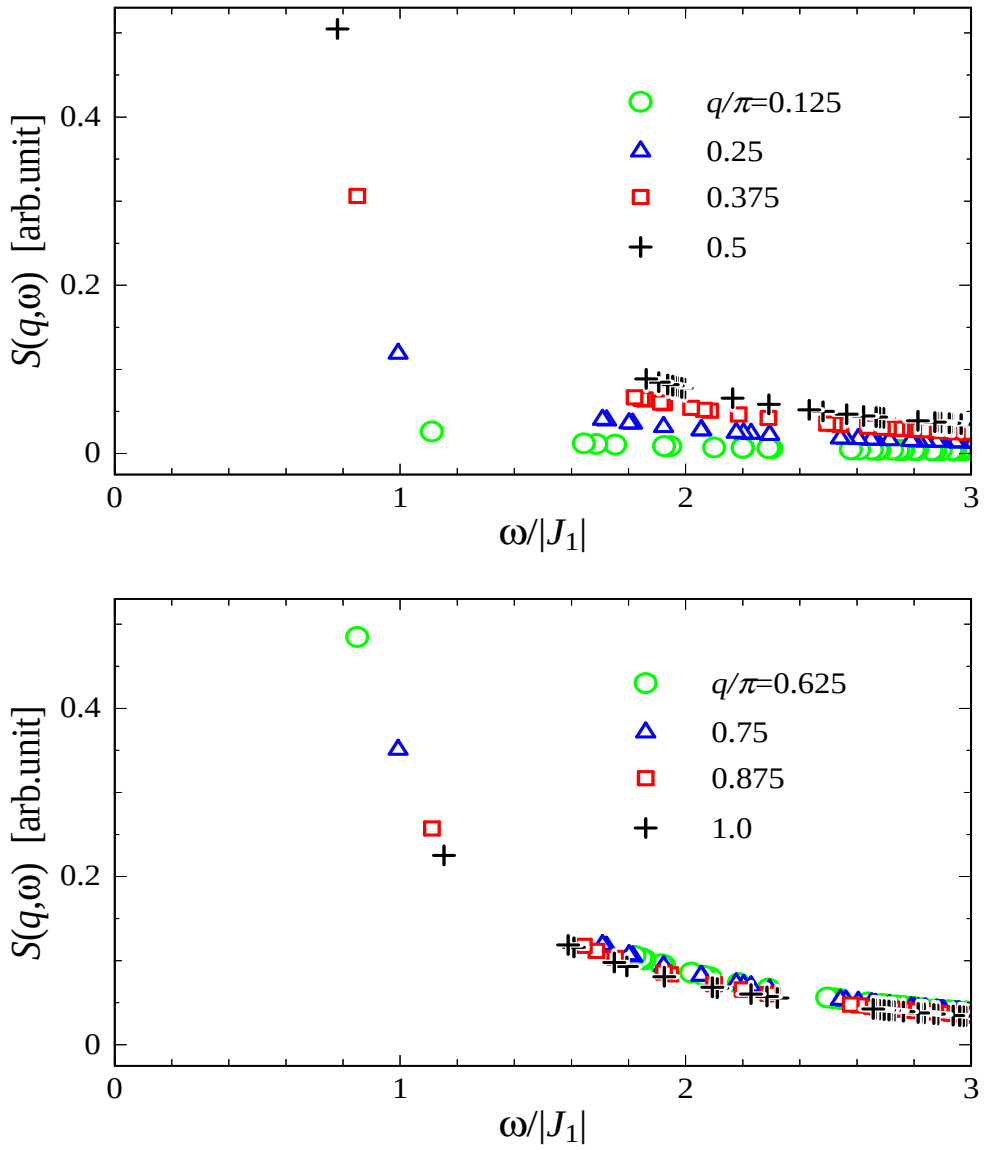

Figure 2.18: The intensity of neutron scattering for the system of $J_2/|J_1|$=0.5 obtained by using Lanczos algorithm. The upper and lower figures show the intensity in the region of $0 < q \leq 0.5$ and $0.5 < q \leq 1$, respectively. The intensities for respective q are designated by points as shown in figures.

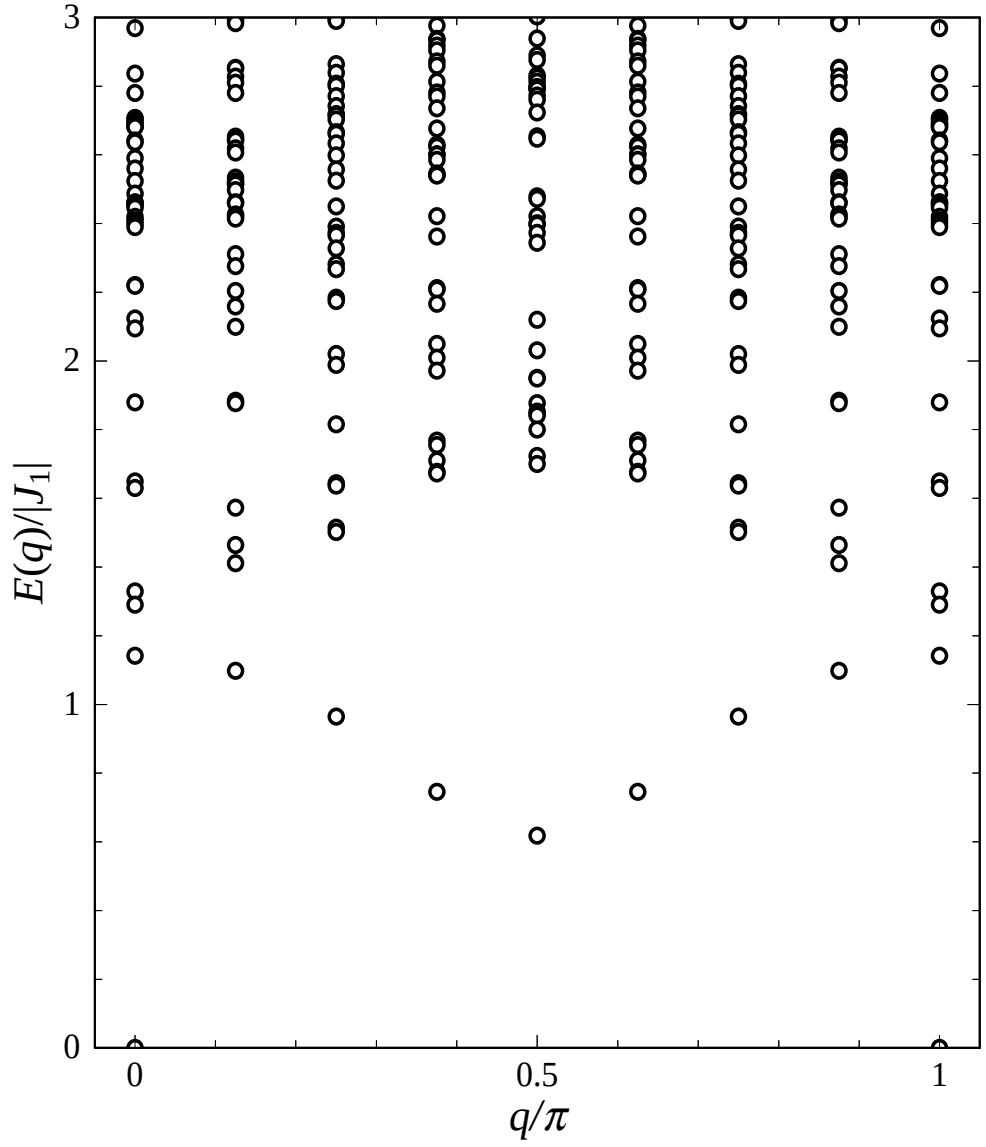

Figure 2.19: The magnon dispersion for the system of $J_2/|J_1|$=1.0 obtained by using EDM for 16 sites chain.

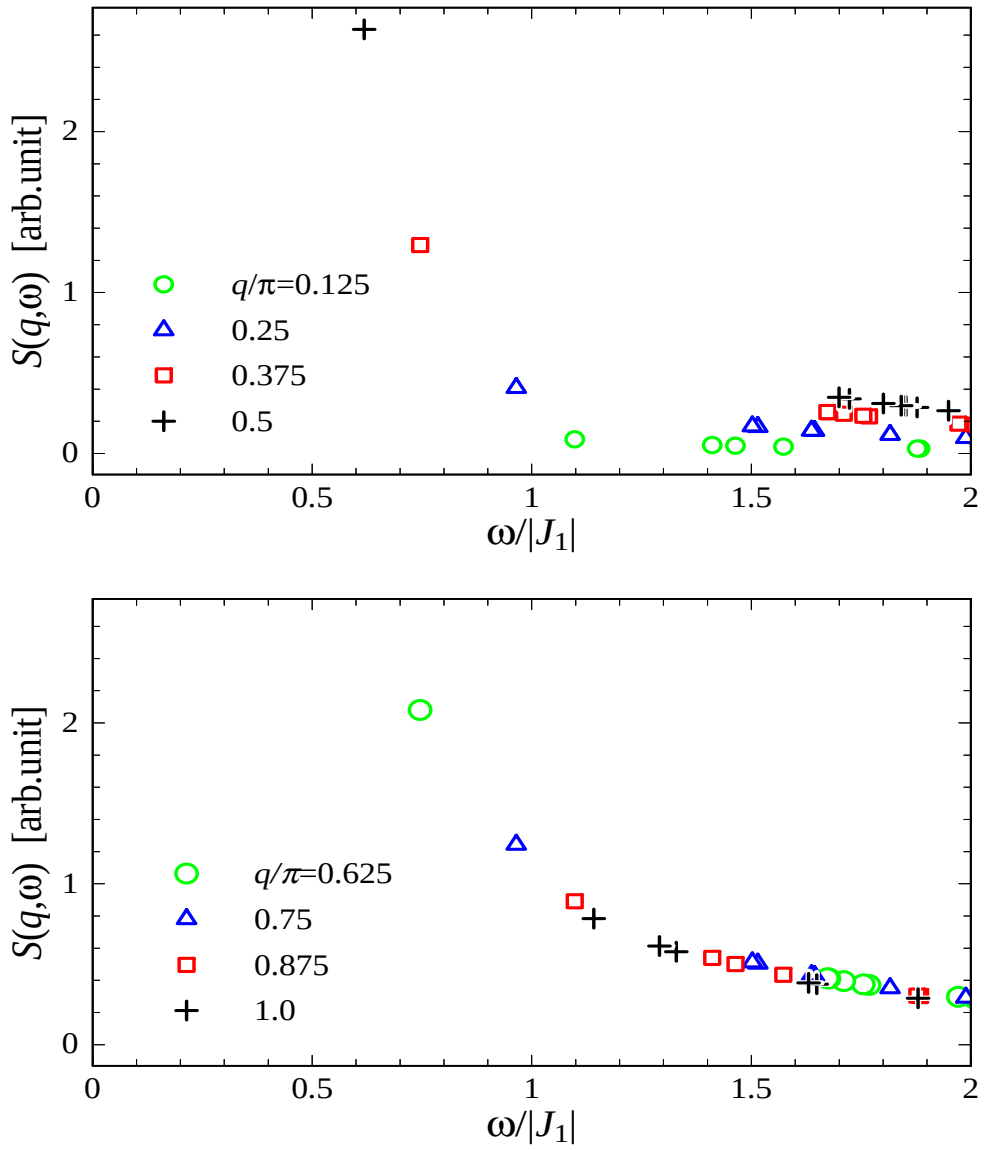

Figure 2.20: The intensity of neutron scattering for the system of $J_2/|J_1|$=1.0 obtained by using Lanczos algorithm. The upper and lower figures show the intensity in the region of $0 < q \leq 0.5$ and $0.5 < q \leq 1$, respectively. The intensities for respective q are designated by points as shown in figures.

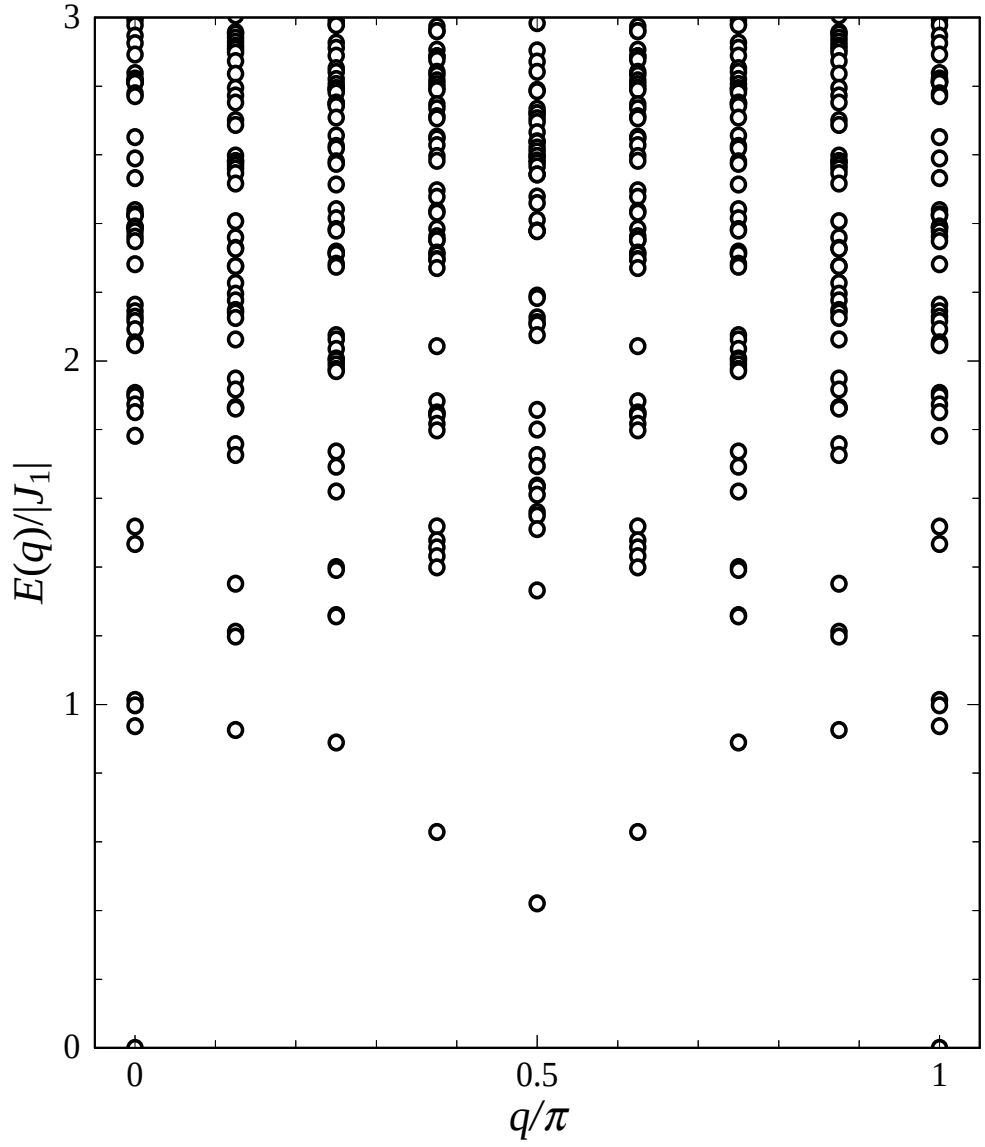

Figure 2.21: The magnon dispersion for the system of $J_2/|J_1|$=2.0 obtained by using EDM for 16 sites chain.

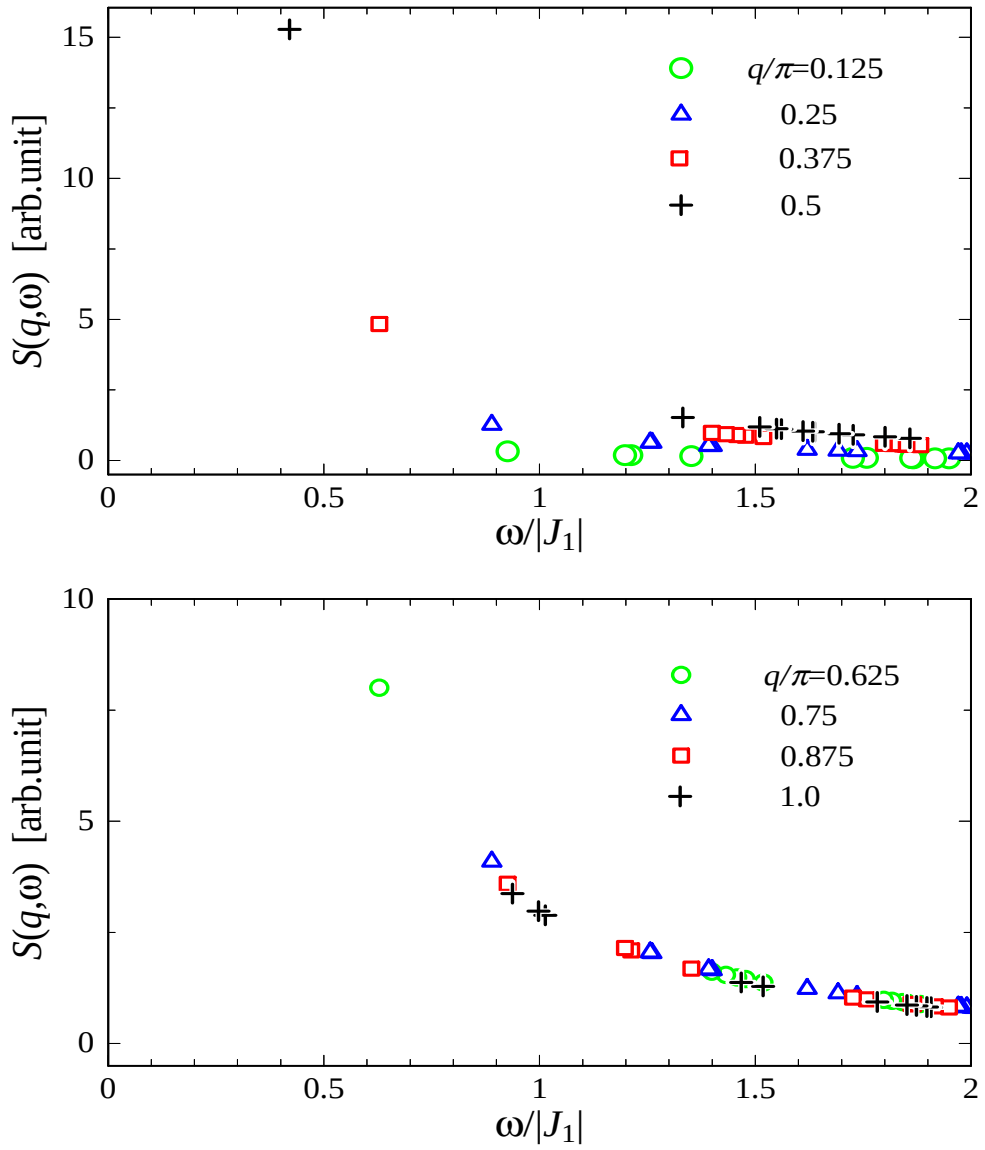

Figure 2.22: The intensity of neutron scattering for the system of $J_2/|J_1|$=2.0 obtained by using Lanczos algorithm. The upper and lower figures show the intensity in the region of $0 < q \leq 0.5$ and $0.5 < q \leq 1$, respectively. The intensities for respective q are designated by points as shown in figures.

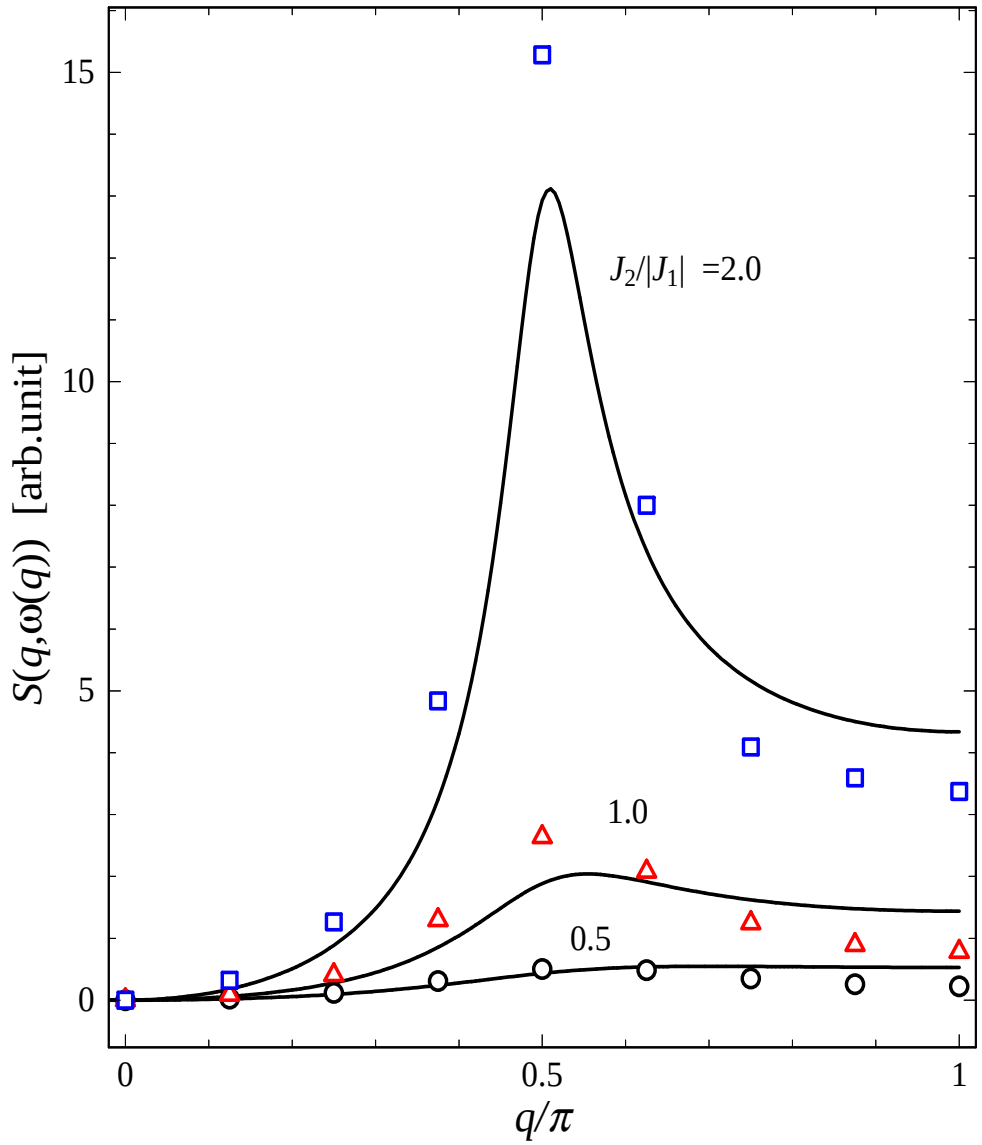

Figure 2.23: The q-dependencies of intensity for transition to the triplet excited states. The circles, triangles and squares denote the intensity obtained by using NC for systems with $J_2/|J_1|$=0.5, 1.0, 2.0, respectively. The full curves represent the Pair-DCEFA's intensity.

Chapter 3

Magnetic Resonance in Spin Peierls System $CuGeO_3$

The spin-Peierls system $CuGeO_3$ has recently attracted much attention. This compoud is found to form pseudo-one-dimensional S=1/2 antiferromagnetic chain along the c-aaxis, and turn into the spin-Peierls state below T_{sp}=14 K. Many studies on this compound have been performed so far. Among them, as the remarkable point it is reported that the magnitude of interchain coupling is much larger than that of other spin Peierls systems. In this thesis we have performed a couple of theoretical studies with paying particular attention to the left problems such as the role of interchain coupling in $CuGeO_3$.

In the first subsection, the fundamental data inclusive of the crystal structure are shown. In the next subsection, we investigate the role of interchain coupling in the exchange splitting of EPR spectra observed under high magnetic fields in the uniform phase of $CuGeO_3$. In particular, the intensity, the peak positions and the nature of the respective resonance mode in the EPR spectra are discussed within the mean field random phase approximation. In the third subsection, we focus on the transitions from the singlet ground state to the triplet excited state in the spin Peierls phase observed by ESR measurements, and then mechanisms of the transitions are discussed in detail by using two proposed models.

3.1 Experimental Background of $CuGeO_3$

Since Hase, Terasaki and Uchinokura [4] reported the first example of spin-Peierls system (T_{sp}=14 K) in an inorganic linear Cu^{2+} (S=1/2) chain compound, $CuGeO_3$, a large number of experimental studies of various types have been carried out. As regards the arrangement of Cu ions in the bc-plane, a schematic representation as shown in Fig. 3.1

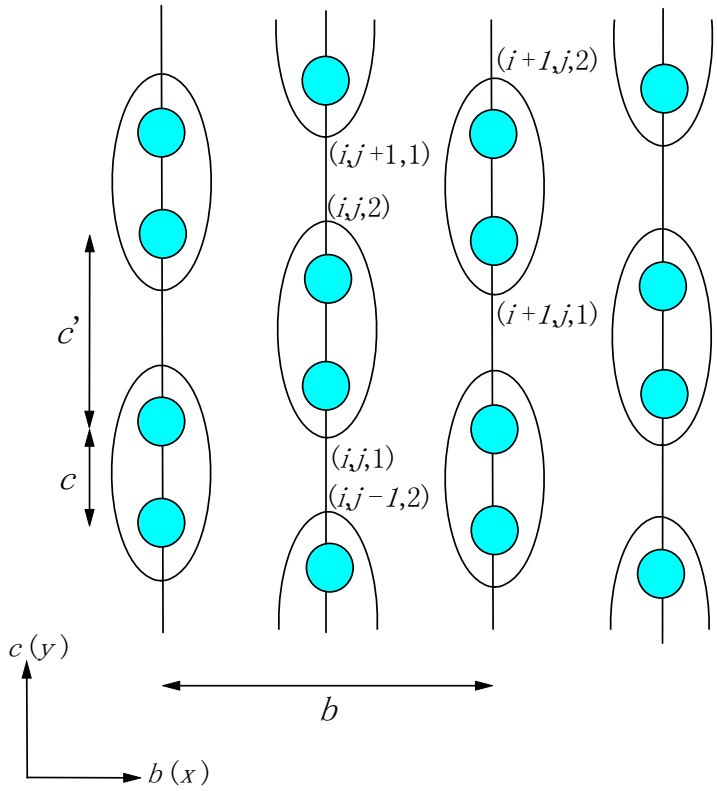

Figure 3.1: The arrangement of Cu ions in the bc-plane of $CuGeO_3$ in the SP phase. Here c and c' denote the distance between two Cu ions of intra-dimer and inter-dimer along the c-axis, respectively, and b is the lattice constant along the b-axis.

is obtained for the spin Peierls phase by analyzing the neutron diffraction experimental results [34]. In the ab-plane, on the other hand, CuO_6 octahedron form the zigzag chain along the b-axis as shown schematically in Fig. 3.2 in both the SP and the uniform phases. From the analysis of x-ray diffraction experiments at room temperature it is suggested that the zigzag chains of CuO_6 octahedron take a slightly different structure in adjacent ab-planes [35]. Figure 3 illustrates one of the possible arrangements of CuO_6 octahedron in adjacent ab-planes. These characteristic features of the crystal structure can gives rise to Dzyaloshinsky-Moriya interaction and different g-values for intra-dimer Cu pairs along the c-axis.

As for the low lying magnetic excitations, the existence of a finite gap of 2.1 meV between the singlet ground state and the triplet excited states has been confirmed by the neutron scattering experiment [12, 36]. Further the dispersions of triplet excited states along the a, b and c directions have been observed as shown in left figure of Fig. 3.3

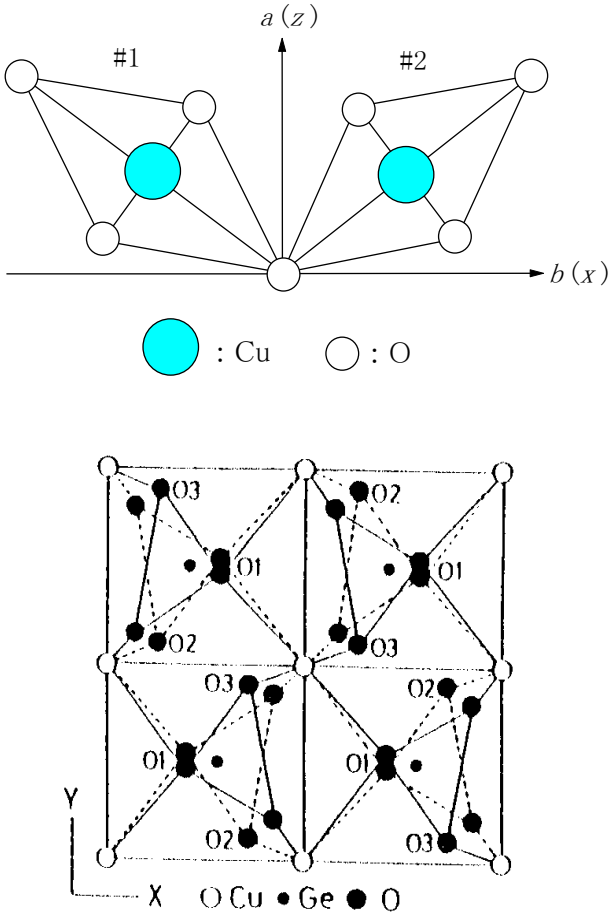

Figure 3.2: The upper figure shows the zigzag structure of $CuGeO_3$ in the ab-plane. The two adjacent Cu ions along the b-axis belong to the sublattices #1 and #2, respectively. In lower figure, the possible model for the structure of $CuGeO_3$ in adjacent ab-planes suggested by M. Hidaka *et al.* [35]. It is shown that there is a slight differences between two adjacent CuO_6 octahedron along the c-axis.

[12]. We have previously analyzed these dispersions on the basis of the Pair-DCEFA and estimated the value of J_b/J_c to be J_b/J_c=0.08, where J_c and J_b represent the exchange integral of intrachain coupling along the c-axis and interchain coupling along the b-axis, respectively. Thus, the experimental results of magnetic excitations informs us that the magnitude of interchain coupling in the b direction is not quite small, namely one-dimensionality is not so good compared with the other spin-Peierls systems.

Another interesting point in the magnetic excitations in the SP phase of $CuGeO_3$ is the existence of the second gap [14]. In a uniform AF chain continuum of excited states exist continuously above the lowest triplet excited states. On the other hand, in the SP

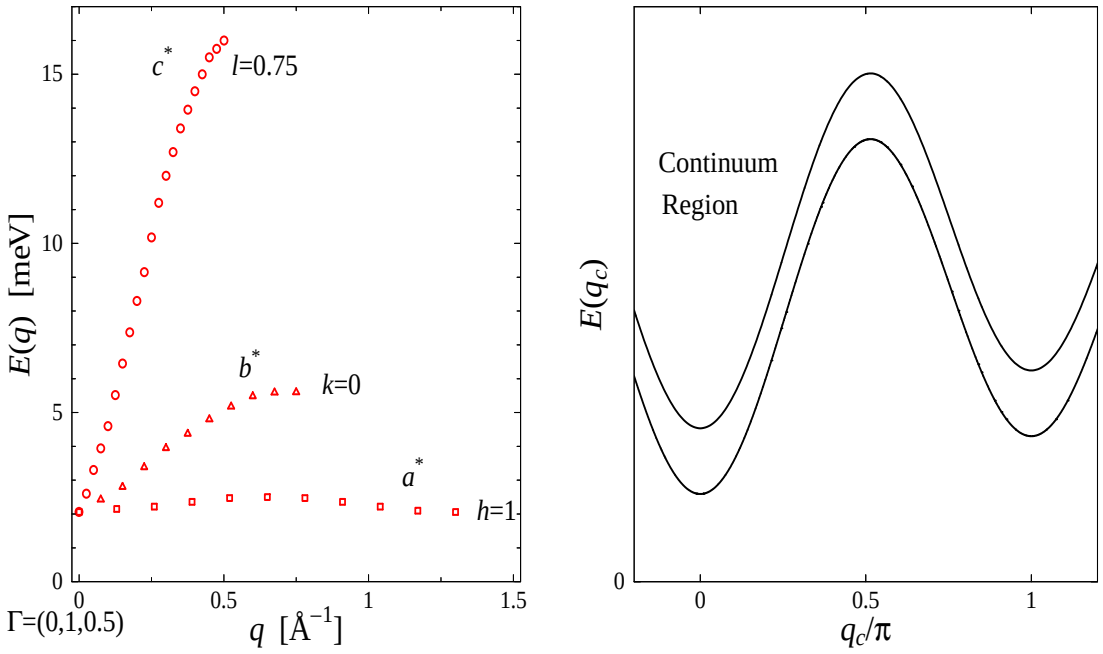

Figure 3.3: The left figure shows the dispersion curves of magnetic excitations in the SP phase of $CuGeO_3$ observed by inelastic neutron scattering measurements [12]. Schematic illustration of the second gap in the SP phase is shown in the right figure.

phase of $CuGeO_3$ there exists a gap above the lowest triplet excited states (the so-called "second gap") and continuum of excited states starts above the second gap. The right figure of Fig. 3.3 illustrates schematically the second gap.

3.2 Exchange Splitting of EPR Spectra in $CuGeO_3$ under Ultra-High Magnetic Fields – Theoretical Analysis

Recently EPR measurements have been performed under high magnetic fields up to 100 T in uniform phase of $CuGeO_3$, and the exchange splitting has been observed reflecting the different principal axes of the g-values of two adjacent Cu^{2+} ions [13]. We have analyzed the observed EPR spectra (peak position and intensity) by using the mean-field random-phase-approximation (MF–RPA), and evaluated the value of interchain exchange coupling J'. Further, to elucidate the nature of the respective EPR peak we solve the equation of motion for the spins with use of the MF–RPA Hamiltonian.

3.2.1 What Is Exchange Splitting of EPR Spectra

The $CuGeO_3$ is regarded as a pseudo-one dimensional system with non-negligible interchain coupling, judging from a couple of experimental results, and has received interest as it challenges the view that one-dimensional nature is very important for spin-Peierls system. In such a sense, it is significant to investigate in detail the interchain interaction of $CuGeO_3$. In the past, from the results of inelastic neutron scattering measurements, the interchain exchange coupling J' along the b-axis has been estimated to be -0.52 meV (antiferromagnetic), which is about one tenth of the intrachain exchange coupling J along the c-axis [12]. It is noted, however, that the estimation is rather crude since the usual spin-wave theory has been used to analyze the observations because of no available theory for the magnetic excitation in spin-Peierls systems with interchain coupling. Further, the neutron scattering results have been analyzed also by Pair-DCEFA (dynamical correlated-effective-field approximation) and the value of J' has been evaluated to be -0.37 meV. However the estimation on the basis of Pair-DCEFA is also insufficient from the quantitative view point because it cannot treat precisely the magnetic excitation of purely one-dimensional exchange alternating spin systems. Therefore, it is desired to make other experimental measurements which can give important information for the interchain exchange coupling.

In $CuGeO_3$ the CuO_6 octahedrons form zigzag chains along the b-axis and they lean

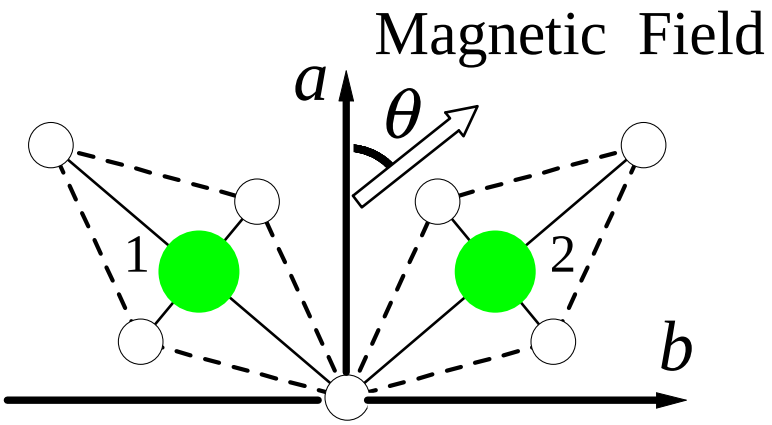

Figure 3.4: The crystal structure of $CuGeO_3$ in the ab-plane at T=300 K. The closed and the open circles represent copper and oxygen atoms, respectively. There are two types of CuO_6 octahedron: one leans by -56 deg from the a-axis and the other by $+56$ deg [37]. The open arrow denotes the direction of the applied magnetic field.

alternatively by −56 deg and +56 deg from the a-axis in the ab-plane, as shown in Fig. 3.4 [37]. This apparently indicates that the principal axes of the g-values of two adjacent Cu^{2+} ions along the b-axis, named as sublattice 1 and 2, respectively, are different. Then, interchain exchange coupling can be investigated by using the exchange splitting of the electron paramagnetic resonance (EPR) spectra. In fact, high-field EPR measurements have been done recently, and Fig. 3.5 shows the magnetic field dependence, up to 100 T, of EPR spectra [13] observed at T=300 K on condition that the wave length λ of photon is fixed at 119 μm. The spectra obtained at about 83 T show a single peak for θ=0 deg and

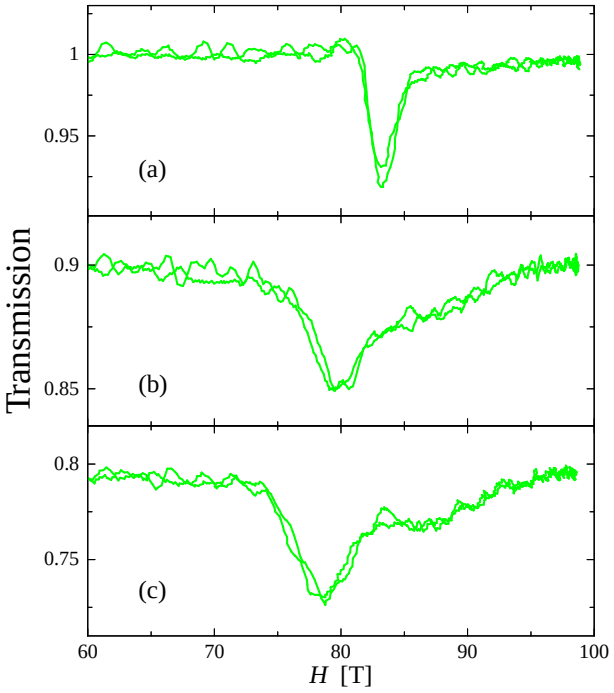

Figure 3.5: The observed EPR spectra observed at T=300 K and for λ = 119 μm: (a) θ=0 deg, (b) θ=30 deg and (c) θ=45 deg, where θ denotes the angle between the a-axis and the applied magnetic field. The overlapping jagged curves denote the experimental data observed for both the up and down magnetic fields.

two non-symmetrical peaks for θ=30 and 45 deg reflecting the different principal axes of g-values of two adjacent Cu^{2+} ions. Here, θ represents the direction of the magnetic fields applied in the ab-plane measured from the a-axis as shown in Fig. 3.4. This results apparently mean that the splitting of EPR spectra has been observed successfully by changing the direction of the magnetic fields. In this section, the interchain exchange integral J' along the b-axis has been estimated by analyzing the observed exchange splitting of EPR spectra.

3.2.2 Generalized Theory

Now, x, y, z are principal axis of g tensor, and X, Y, Z are axes associated with quantisation axis, in which the Zeeman interaction is diagonalised. The components of a spin in the (X, Y, Z) coordinate system are connected with those in the (x, y, z) coordinate system by the following transformation:

$$\begin{pmatrix} S^X \\ S^Y \\ S^Z \end{pmatrix} = \begin{pmatrix} \cos\psi\cos\phi & \cos\psi\sin\phi & -\sin\psi \\ -\sin\phi & \cos\phi & 0 \\ \sin\psi\cos\phi & \sin\psi\sin\phi & \cos\psi \end{pmatrix} \begin{pmatrix} S^x \\ S^y \\ S^z \end{pmatrix}, \tag{3.1}$$

where ψ is the angle between the z and Z axis and ϕ denotes the azimuthal angle of Z measured from the x axis.

For simplicity, we treat two spins system, in which two spins exist at respective site 1 and 2, and the principal axis of each spin are not coincident. As shown in Fig. 3.6, when

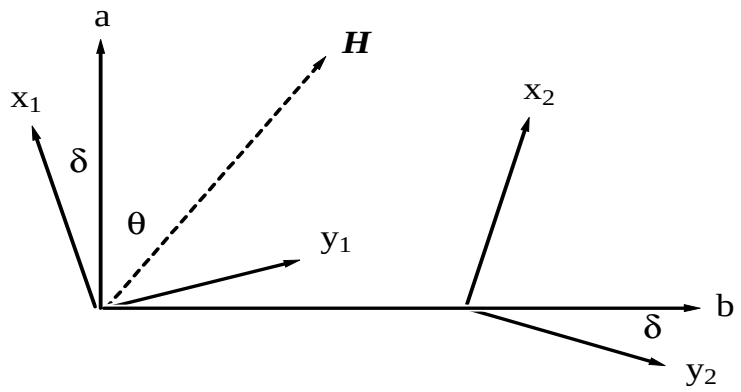

Figure 3.6: The magnetic field $\vec{H}$ is applied in the ab-plane of two spins system with different coordinate system which are shown by respective x_1y_1 and x_2y_2-axes. Here, we have assumed that two z-axes coincide with each other. The direction of magnetic fields are designated by azimuthal angle θ, and the angle between x_1 and x_2 axes is denoted by 2δ.

the magnetic fields $\vec{H}$ are applied in the ab-plane with an azimuthal angle θ measured from the a-axis, the Zeeman interaction at site 1 is written as,

$$\mathcal{H}_{\text{Zeeman}} = g_x\mu_{\text{B}}H_xS_1^x + g_y\mu_{\text{B}}H_yS_1^y, \tag{3.2}$$

with $H_x = H_0\cos(\theta+\delta)$, $H_y = H_0\sin(\theta+\delta)$. By using the relation (3.1) with $\psi = \pi/2$, the expression is transformed as follows:

$$\mathcal{H}_{\text{Zeeman}} = (-g_x\mu_{\text{B}}H_x\sin\phi + g_y\mu_{\text{B}}H_y\cos\phi)S_1^Y + (g_x\mu_{\text{B}}H_x\cos\phi + g_y\mu_{\text{B}}H_y\sin\phi)S_1^Z. \tag{3.3}$$

Here, we select the condition so that the coefficient of S_1^Y vanishes. Its condition is as follows:

$$\tan(\theta+\delta) = \frac{g_x}{g_y}\tan\phi. \tag{3.4}$$

By making use of $\cos\phi = g_x\cos(\theta+\delta)/[g_x^2\cos^2(\theta+\delta)+g_y^2\sin^2(\theta+\delta)]^{1/2}$ from eq. (3.4), the resultant Zeeman interaction is given as,

$$\mathcal{H}_{\rm Zeeman} = g_1\mu_{\rm B}H_0S_1^Z, \tag{3.5}$$

with

$$g_1 = [g_x^2\cos^2(\theta+\delta)+g_y^2\sin^2(\theta+\delta)]^{1/2},$$

where g_x, g_y, g_z are the principal value of g-tensor. By adopting the condition eq. (3.4), the relation between (S_1^X, S_1^Y, S_1^Z) and (S_1^x, S_1^y, S_1^z) is given newly as

$$\begin{pmatrix} S_1^X \\ S_1^Y \\ S_1^Z \end{pmatrix} = \frac{1}{g_1}\begin{pmatrix} 0 & 0 & -g_1 \\ -g_y\sin(\theta+\delta) & g_x\cos(\theta+\delta) & 0 \\ g_x\cos(\theta+\delta) & g_y\sin(\theta+\delta) & 0 \end{pmatrix}\begin{pmatrix} S_1^x \\ S_1^y \\ S_1^z \end{pmatrix}. \tag{3.6}$$

Since the x, y, z are the principal axis of g-tensor for $\vec{S}_1$, the following expression is obtained:

$$\begin{pmatrix} M_1^x \\ M_1^y \\ M_1^z \end{pmatrix} = -\mu_{\rm B}\begin{pmatrix} g^x & 0 & 0 \\ 0 & g^y & 0 \\ 0 & 0 & g^z \end{pmatrix}\begin{pmatrix} S_1^x \\ S_1^y \\ S_1^z \end{pmatrix}. \tag{3.7}$$

By considering eq. (3.1) and (3.6), the relation between $(M_1^X,\ M_1^Y,\ M_1^Z)$and $(S_1^X,\ S_1^Y,\ S_1^Z)$ are expressed as,

$$\begin{pmatrix} M_1^X \\ M_1^Y \\ M_1^Z \end{pmatrix} = -\mu_{\rm B}\begin{pmatrix} g_1^X & 0 & 0 \\ 0 & g_1^Y & g_1^{YZ} \\ 0 & g_1^{ZY} & g_1^Z \end{pmatrix}\begin{pmatrix} S_1^X \\ S_1^Y \\ S_1^Z \end{pmatrix}, \tag{3.8}$$

where the g-tensor in the (X, Y, Z) coordinate system is introduced by

$$\begin{aligned} g_1^X &= g_z, \\ g_1^Y &= (g_xg_y/g_1^2)[g_x\cos^2(\theta+\delta)+g_y\sin^2(\theta+\delta)], \\ g_1^Z &= (1/g_1^2)[g_x^3\cos^2(\theta+\delta)+g_y^3\sin^2(\theta+\delta)], \\ g_1^{YZ} &= g_1^{ZY} = -(g_xg_y/g_1^2)(g_x-g_y)\cos(\theta+\delta)\sin(\theta+\delta). \end{aligned}$$

And now we have put $g_1^{YZ} = g_1^{ZY} \sim 0$ by assuming $g_x \sim g_y$. Further the relation between M_2^X, M_2^Y, M_2^Z and S_2^X, S_2^Y, S_2^Z is obtained by replacing δ with $-\delta$.

For the purpose of investigating the intensity, we must find the expression of response function in this system. The interaction under the time dependent magnetic fields $H(t)$ is given by,

$$\mathcal{H}'(t) = -\vec{H}_1(t) \cdot (\vec{M}_1 + \vec{M}_2), \tag{3.9}$$

with

$$M_i^{\pm} = M_i^X \pm \mathrm{i} M_i^Y = -\frac{1}{2}\mu_{\mathrm{B}}(g_i^X + g_i^Y)S_i^{\pm} - \frac{1}{2}\mu_{\mathrm{B}}(g_i^X - g_i^Y)S_i^{\mp}, \tag{3.10}$$

$$M_i^Z = g_i^Z \mu_{\mathrm{B}} S_i^Z, \tag{3.11}$$

for i=1, 2. With use of $g_i^x \sim g_i^y$ which is reasonable assumption for the present system, we have $M_i^{\pm} \sim -\frac{1}{2}\mu_{\mathrm{B}}(g_i^X + g_i^Y)S_i^{\pm}$.

The response function $\chi(\omega)$ can be calculated immediately. When $\chi(\omega)$ is defined as,

$$\chi(\omega) = \frac{\mathrm{i}}{\hbar}\int_0^{\infty} \mathrm{d}t \mathrm{e}^{\mathrm{i}\omega t}\langle [M_1^+(t) + M_2^+(t), M_1^-(0) + M_2^-(0)]_- \rangle, \tag{3.12}$$

we obtain the following expression,

$$\begin{aligned}\chi(\omega) &= (g_1^X + g_1^Y)^2 \chi_{11}^{+-}(\omega) + (g_2^X + g_2^Y)^2 \chi_{22}^{+-}(\omega) \\ &\quad + (g_1^X + g_1^Y)(g_2^X + g_2^Y)\{\chi_{21}^{+-}(\omega) + \chi_{12}^{+-}(\omega)\},\end{aligned} \tag{3.13}$$

where $\chi_{ij}^{+-}(\omega) = \dfrac{\mathrm{i}}{\hbar}\displaystyle\int_0^{\infty} \mathrm{d}t \mathrm{e}^{\mathrm{i}\omega t}\langle [S_i^+(t), S_i^-(0)]_- \rangle$ (i, j=1 or 2). Further, the imaginary part of $\chi(\omega)$ corresponds to the intensity.

3.2.3 Investigation by Hamano-Shibata Theory

First we have used the theory of exchange splitting under high magnetic fields proposed by Hamano and Shibata [16]. Here the only outline of this theory is briefly described, because the calculational method itself are not so effective for the present system.

This theory uses the exchange-coupled two spins model and is effective even at low temperatures and also for ultra-high magnetic fields in comparison with the theory of Anderson [38] based on the high temperature approximation. The relevant Hamiltonian for our present analysis is expressed simply as follows:

$$\mathcal{H} = -2J'\vec{S}_1 \cdot \vec{S}_2 + \mu_{\mathrm{B}} H(g_1 S_1^Z + g_2 S_2^Z). \tag{3.14}$$

Here the direction of the applied magnetic field H is taken as the Z-axis, $\vec{S}_1$ and $\vec{S}_2$ denote S=1/2 spins in the sublattices 1 and 2, respectively, and g_1 and g_2 represent the respective effective g-value along the Z-axis which can be calculated by use of the g-tensors determined by Yamamoto *et al* [37]. The EPR spectra is determined by the imaginary part of the dynamical susceptibility, Im$\chi(\omega)$, and we use the expression of $\chi(\omega)$ obtained by Hamano and Shibata [16] in which the effect of damping is taken account through the relaxation times T_1 and T_2. By assuming $T_2 = 2T_1$ we have determined the values of J' and T_1 so as to reproduce as well as possible the EPR spectra for θ = 0, 30 and 45 deg observed at T=300 K with λ = 119 μm light. The determined values of J' and T_1 are -0.42 meV and 1.6×10^{-12} s. Further, the results of fitting are shown by the solid curve in Fig. 3.7.

It should be mentioned here that there is usually large inhomogeneity of H in case of ultra-high magnetic fields higher than 60 T. Therefore, the value of T_1 estimated above may not represent the intrinsic damping effect of the spin system. To obtain a more reliable value of T_1 we have performed fitting for an another experimental data of θ=0 deg at T=300 K with λ =513 μm light. As the result we have evaluated T_1 to be 1.0×10^{-11} s which is much longer than that evaluated previously. By using these parameters J' and T_1, the results become as shown by the dotted curves in Fig. 3.7. For θ=30 and 45 deg, the calculated spectra evidently consist of four peaks which corresponding to the transition of $|1) \leftrightarrow |4)$, $|1) \leftrightarrow |2)$, $|2) \leftrightarrow |3)$ and $|3) \leftrightarrow |4)$, in the order of increasing field. Here $|i)$ (i=1 $\sim$ 4) denote the four eigenstates of the spin pair Hamiltonian and explicitly written as $|1) = |1,1\rangle$, $|2) = a|1,0\rangle + b|0,0\rangle$ ($|a| > |b|$), $|3) = |1,-1\rangle$, $|4) = c|0,0\rangle + d|1,0\rangle$ ($|c| > |d|$) where $|S, M_Z\rangle$ (S=1 or 0) are the eigenstates of the total spin $\vec{S}_1 + \vec{S}_2$.

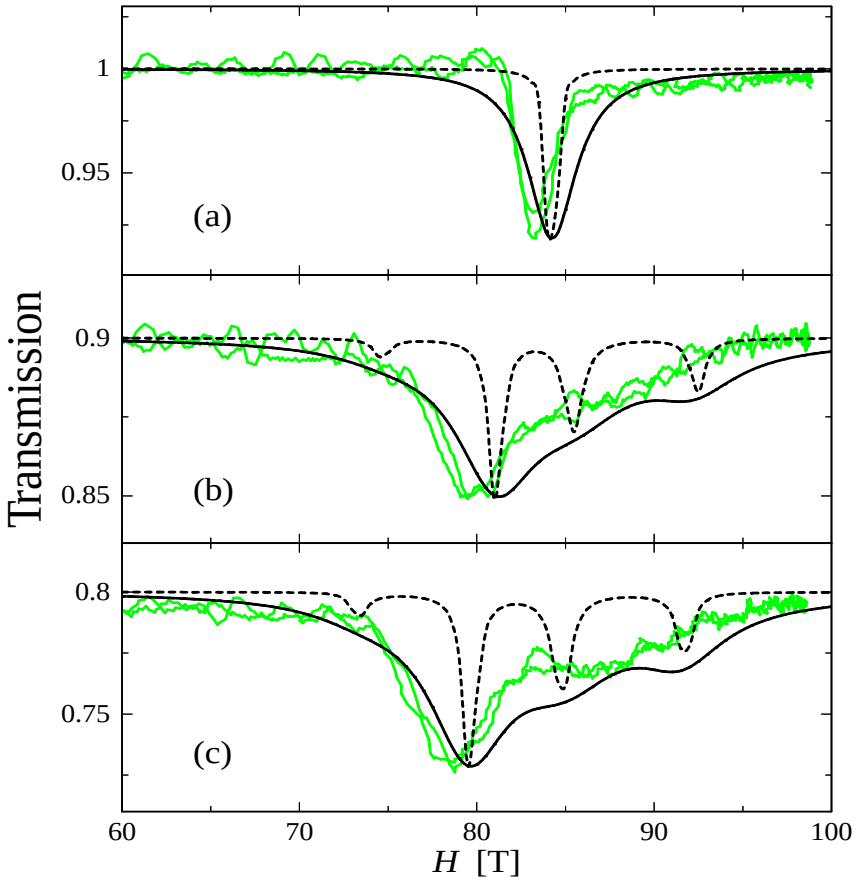

Figure 3.7: The EPR spectra calculated by using Hamano-Shibata theory at T=300 K and for λ = 119 μm: (a) θ=0 deg, (b) θ=30 deg and (c) θ=45 deg, where θ denotes the angle between the a-axis and the applied magnetic field. The full and the dotted curves represent the theoretical results calculated with use of T_1=1.6×10^{-12} s and 1.0×10^{-11} s, respectively. The overlapping jagged curves denote the experimental data observed for both the up and down magnetic fields.

3.2.4 Investigation by Molecular-Field Random-Phase Approximation

In the above theoretical analysis on the basis of Hamada-Shibata theory there are two problems. First, we have obtained four peaks in the case of θ=30 and 45 deg, which contradicts with the experimental data showing only two peaks. Secondly, in the analysis the intrachain exchange coupling J is completely neglected in spite of $J/J' \sim 10.0$ [12]. Therefore we have tried to analyze the observed EPR spectra by applying molecular-field random-phase approximation (MF–RPA) to the two-dimensional spin system (in the bc-plane) with the intrachain exchange coupling J along the c-axis and the interchain

exchange coupling J' along the b-axis. At high temperatures such as T=300 K, which is much larger than the magnitude of J, it is expected that MF–RPA gives reasonable results.

The Hamiltonian for the bc-plane in the uniform phase is written as,

$$\begin{aligned}\mathcal{H} &= \sum_{i,j}[\sum_{k=1,2} -2J\vec{S}_{i,j,k}\cdot\vec{S}_{i,j+1,k} - 2J'(\vec{S}_{i,j,1}\cdot\vec{S}_{i,j,2} + \vec{S}_{i,j,2}\cdot\vec{S}_{i+1,j,1}) \\ &\quad +\mu_{\rm B}H(g_1S^Z_{i,j,1} + g_2S^Z_{i,j,2})]. \end{aligned} \tag{3.15}$$

By using the mean field approximation (MFA), the effective Hamiltonian is obtained as follows:

$$\mathcal{H}^{\rm MFA}_{i,j} = A_{12}S^Z_{i,j,1} + A_{21}S^Z_{i,j,2} \equiv \mathcal{H}_1 + \mathcal{H}_2. \tag{3.16}$$

Here the effective fields are introduced by

$$A_{ij} = -4(J\langle S^Z_i\rangle + J'\langle S^Z_j\rangle) + g_i\mu_{\rm B}H. \tag{3.17}$$

The field-induced spin moments $\langle S^Z_1\rangle$ and $\langle S^Z_2\rangle$ are determined from the usual self-consistency eq.,

$$\langle S^Z_1\rangle = {\rm Tr}[S^Z_1{\rm e}^{-\beta\mathcal{H}_1}]/{\rm Tr}[{\rm e}^{-\beta\mathcal{H}_1}], \tag{3.18}$$

$$\langle S^Z_2\rangle = {\rm Tr}[S^Z_2{\rm e}^{-\beta\mathcal{H}_2}]/{\rm Tr}[{\rm e}^{-\beta\mathcal{H}_2}]. \tag{3.19}$$

The single-ion spin susceptibility $\phi(\omega)$ is obtained by using eq. (2.11), that is, $\phi^{+-}_{11}(\omega) = -\langle S^Z_1\rangle/2(\omega - A_{12})$ and $\phi^{+-}_{22}(\omega) = -\langle S^Z_2\rangle/2(\omega - A_{21})$.

From now on we think of the two-dimensional spin system in the bc-plane. When the fictitious rotating magnetic fields $h^+_{\vec{q},n}{\rm e}^{{\rm i}(\vec{q}\cdot\vec{R}_{in}-\omega t)}$ (n=1 or 2) are applied to respective sublattice, within the random-Phase Approximation we obtain the following relation:

$$\begin{pmatrix} h & k \\ l & m \end{pmatrix}\begin{pmatrix} \langle S^+_{\vec{q}1}\rangle \\ \langle S^+_{\vec{q}2}\rangle \end{pmatrix} = \begin{pmatrix} \phi^{+-}_{11}(\omega) & 0 \\ 0 & \phi^{+-}_{22}(\omega) \end{pmatrix}\begin{pmatrix} h^+_{\vec{q}1}{\rm e}^{-{\rm i}\omega t} \\ h^+_{\vec{q}2}{\rm e}^{-{\rm i}\omega t} \end{pmatrix}, \tag{3.20}$$

with

$$\begin{aligned} h &= 1 - 2J\phi^{+-}_{11}\cos(g_cc), \quad k = -2J'\phi^{+-}_{11}\cos(g_bb), \\ l &= -2J'\phi^{+-}_{22}\cos(g_bb), \quad m = 1 - 2J\phi^{+-}_{22}\cos(g_cc). \end{aligned}$$

And the susceptibility is obtained as follows:

$$\begin{aligned}\begin{pmatrix} \langle S^+_{\vec{q}1}\rangle \\ \langle S^+_{\vec{q}2}\rangle \end{pmatrix} &= \frac{1}{hm-kl}\begin{pmatrix} m\phi^{+-}_{11} & -k\phi^{+-}_{22} \\ -l\phi^{+-}_{11} & h\phi^{+-}_{22} \end{pmatrix}\begin{pmatrix} h^+_{\vec{q}1}{\rm e}^{-{\rm i}\omega t} \\ h^+_{\vec{q}2}{\rm e}^{-{\rm i}\omega t} \end{pmatrix} \\ &\equiv \begin{pmatrix} \chi^{+-}_{11}(\vec{q},\omega) & \chi^{+-}_{12}(\vec{q},\omega) \\ \chi^{+-}_{21}(\vec{q},\omega) & \chi^{+-}_{22}(\vec{q},\omega) \end{pmatrix}\begin{pmatrix} h^+_{\vec{q}1}{\rm e}^{-{\rm i}\omega t} \\ h^+_{\vec{q}2}{\rm e}^{-{\rm i}\omega t} \end{pmatrix}. \end{aligned} \tag{3.21}$$

The EPR spectra are determined by the imaginary part of the $\vec{q}$=0 component of the dynamical susceptibility $\chi(\vec{q}=0,\omega)$ which are given as eq. (3.13). Then we simply give the final expression of Im $\chi(\vec{q}=0,\omega)$:

$$\begin{aligned}
&\mathrm{Im}\chi(\vec{q}=0,\omega) \propto \frac{1}{\omega_+ - \omega_-} \times \\
&[\{U_{12}(\omega_+ - A_{21}) + U_{21}G^2(\omega_+ - A_{12}) + V\}\delta(\omega - \omega_+) \\
&+\{U_{12}(A_{21} - \omega_-) + U_{21}G^2(A_{12} - \omega_-) - V\}\delta(\omega - \omega_-)],
\end{aligned} \tag{3.22}$$

with

$$\begin{aligned}
&\omega_\pm = \frac{1}{2}\left[X_+ \pm \sqrt{X_-^2 + 16U_{12}U_{21}J'^2}\right], \\
&X_\pm = A_{12} \pm A_{21} - 2J(U_{12} \pm U_{21}), \\
&V = 2U_{12}U_{21}(J + JG^2 - 2J'G), \\
&U_{ij} = \tanh\left(\frac{\beta A_{ij}}{2}\right),\ A_{ij} = -4(J\langle S_i^Z\rangle + J'\langle S_j^Z\rangle) + g_i\mu_\mathrm{B}H, \\
&G = \frac{g_z + (g_x g_y/{g_2}^2)[g_x\cos^2(\theta-\delta) + g_y\sin^2(\theta-\delta)]}{g_z + (g_x g_y/{g_1}^2)[g_x\cos^2(\theta+\delta) + g_y\sin^2(\theta+\delta)]},
\end{aligned}$$

where $\omega_\pm$ are the quasi-particle energies with $\vec{q}$=0, and $\langle S_1^Z\rangle$ and $\langle S_2^Z\rangle$ represent the field-induced spin moments of the sublattices 1 and 2, respectively, which can be determined self-consistently, and $\beta = 1/k_\mathrm{B}T$. It is noted that the damping effect cannot be taken into account by MF–RPA and the EPR spectra are given by line spectra.

We have determined the values of J and J' so as to reproduce as well as possible the observed peak positions and the relative intensities. The evaluated values are J=−5.0 meV and J'=−0.41 meV. This value of J corresponds well to that estimated from the inelastic neutron scattering measurement [12]. The EPR spectra calculated by using these exchange parameters are shown by the vertical bars in Fig. 3.8. As seen from the figures agreement between the MF–RPA results and the observations is quite well. In particular MF–RPA predicts certainly two peaks for θ=30 and 45 deg. In a similar way, we have investigated by using the same exchange parameter also the case of further high fields, that is, the spectra for θ = 0, 30 and 45 deg observed at T=300 K with λ = 96.5 μm light. vertical bars. It is found that MF–RPA's EPR spectra explain fairly well also such a experimental result. Therefore, judging from the total view point MF–RPA method is more appropriate than the Hamano-Shibata theory to analyze the high-field EPR spectra at high temperatures, although both the methods have given almost the same value for the interchain exchange coupling of $CuGeO_3$.

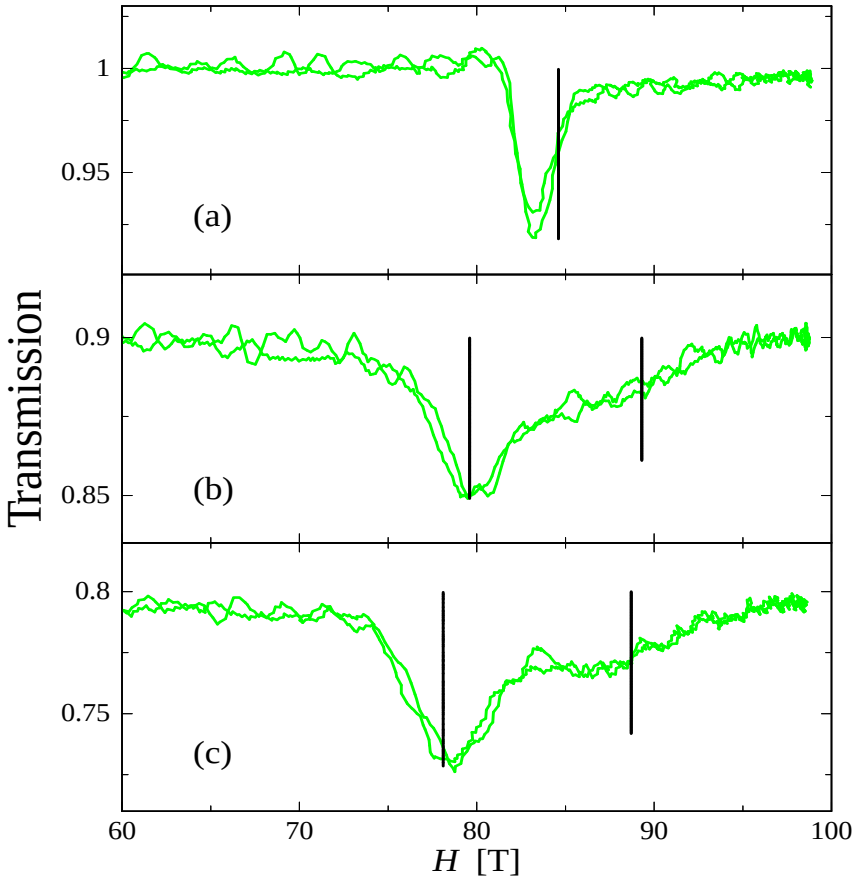

Figure 3.8: The EPR spectra calculated by MF–RPA (the vertical bars) at T=300 K and for $\lambda = 119$ μm: (a) θ=0 deg, (b) θ=30 deg and (c) θ=45 deg, where θ denotes the angle between the a-axis and the applied magnetic field. The overlapping jagged curves denote the experimental data observed for both the up and down magnetic fields.

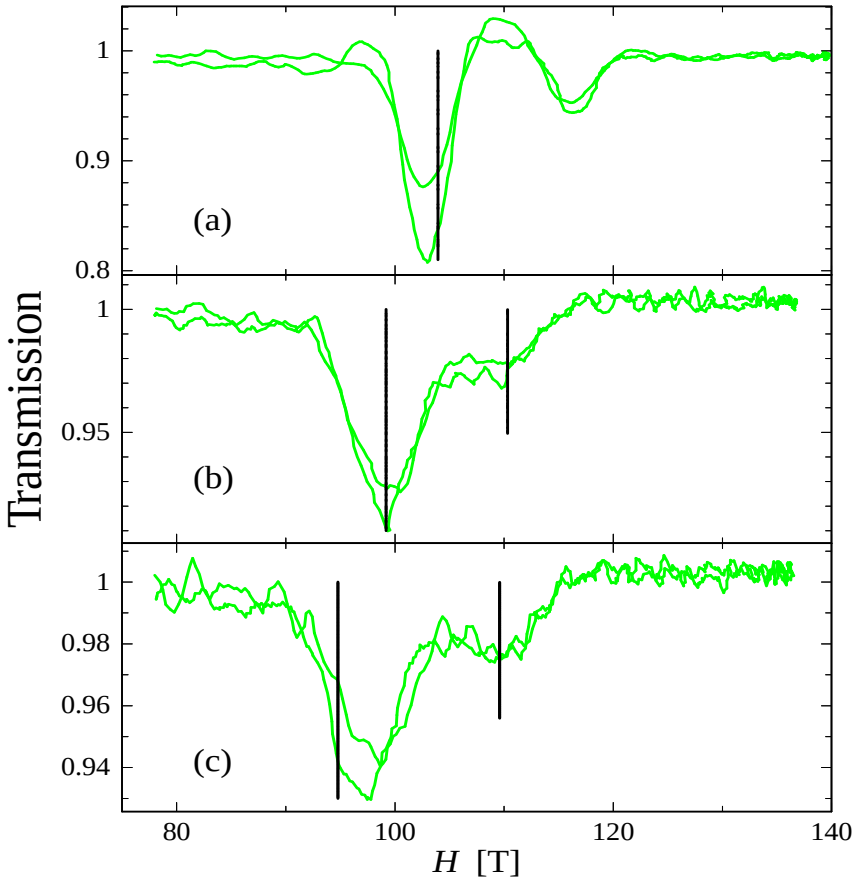

Figure 3.9: The EPR spectra calculated by MF–RPA (the vertical bars) at T=300 K and for $\lambda = 96.5$ μm: (a) θ=0 deg, (b) θ=30 deg and (c) θ=45 deg. The jagged curves denote the observed experimental data.

3.2.5 Analysis of Resonance Mode

Now the origin of two peaks is investigated by solving the equation of motions for spins of the sublattice i=1 and 2. Here, we think of the case that the uniform magnetic fields and the rotation magnetic fields in electromagnetic wave are applied to Z and XY direction, respectively. Then the motion of spin rotation is done on condition that Z-axis become the axis of rotation.

The equation of motion for spins are given by

$$\frac{\mathrm{d}S^{+}_{i,j,k}}{\mathrm{d}t} = \frac{1}{\mathrm{i}\hbar}[S^{+}_{i,j,k}, \mathcal{H}]. \tag{3.23}$$

The equations obtained by substituting the Hamiltonian (3.15) for eq. (3.23) are as follows:

$$\begin{aligned}\frac{\mathrm{d}}{\mathrm{d}t}S^+_{i,j,1} &= \frac{1}{\mathrm{i}\hbar}[-2J(S^Z_{i,j,1}S^+_{i,j+1,1} - S^+_{i,j,1}S^Z_{i,j+1,1} + S^+_{i,j-1,1}S^Z_{i,j,1} - S^Z_{i,j-1,1}S^+_{i,j,1}) \\ &\quad -2J'(S^Z_{i,j,1}S^+_{i,j,2} - S^+_{i,j,1}S^Z_{i,j,2} + S^+_{i-1,j,2}S^Z_{i,j,1} - S^Z_{i-1,j,2}S^+_{i,j,1}) \\ &\quad -g_1\mu_{\mathrm{B}}HS^+_{i,j,1}], \qquad (3.24) \\ \frac{\mathrm{d}}{\mathrm{d}t}S^+_{i,j,2} &= \frac{1}{\mathrm{i}\hbar}[-2J(S^Z_{i,j,2}S^+_{i,j+1,2} - S^+_{i,j,2}S^Z_{i,j+1,2} + S^+_{i,j-1,2}S^Z_{i,j,2} - S^Z_{i,j-1,2}S^+_{i,j,2}) \\ &\quad -2J'(S^+_{i,j,1}S^Z_{i,j,2} - S^Z_{i,j,1}S^+_{i,j,2} + S^Z_{i,j,2}S^+_{i+,j,1} - S^+_{i,j,2}S^Z_{i+1,j,1}) \\ &\quad -g_2\mu_{\mathrm{B}}HS^+_{i,j,2}]. \qquad (3.25)\end{aligned}$$

We now adopt the following approximation: the Z-components of spin moments is fixed and only its XY-components are fluctuating. As further calculational procedure, we first replace $S^Z_{i,j,k}$ with thermal average $\langle S^Z_n\rangle$ (n=1 or 2) on the assumption that Z components of spin moment are constant for the arbitrary lm. Secondly, the Fourier transform is performed only for the transverse component $S^{\pm}_{i,j,1}$, $S^{\pm}_{i,j,2}$. In short, the terms inclusive of Z component are those being obtained by MFA, while all the other represent the terms being treated by RPA. This procedure conforms just to the treatment of MF–RPA. The resultant equation is as follows:

$$\frac{\mathrm{d}}{\mathrm{d}t}S^+_{\vec{q}1} = \frac{1}{\mathrm{i}\hbar}\left[(4J\langle S^Z_1\rangle + 4J'\langle S^Z_2\rangle - g_1\mu_{\mathrm{B}}H - 4J\langle S^Z_1\rangle\cos(q_cc))S^+_{\vec{q}1} - 4J'\langle S^Z_1\rangle\cos(q_bb)S^+_{\vec{q}2}\right], \qquad (3.26)$$

$$\frac{\mathrm{d}}{\mathrm{d}t}S^+_{\vec{q}2} = \frac{1}{\mathrm{i}\hbar}\left[(4J\langle S^Z_2\rangle + 4J'\langle S^Z_1\rangle - g_2\mu_{\mathrm{B}}H - 4J\langle S^Z_2\rangle\cos(q_cc))S^+_{\vec{q}2} - 4J'\langle S^Z_2\rangle\cos(q_bb)S^+_{\vec{q}1}\right]. \qquad (3.27)$$

For the above equation, we think of the solutions of $c_1S^+_{\vec{q}1} + c_2S^+_{\vec{q}2}$, where $S^+_{\vec{q}1}$, $S^+_{\vec{q}2}$ are generally known to have time dependence $\mathrm{e}^{\mathrm{i}\omega t}$. Then the obtained determinant is given as,

$$\begin{vmatrix} u-\omega & w_1 \\ w_2 & v-\omega \end{vmatrix} = 0, \qquad (3.28)$$

with

$$\begin{aligned} u &= 4[J\langle S^Z_1\rangle(\cos(q_cc)-1) - J'\langle S^Z_2\rangle] + g_1\mu_{\mathrm{B}}H, \\ v &= 4[J\langle S^Z_2\rangle(\cos(q_cc)-1) - J'\langle S^Z_1\rangle] + g_2\mu_{\mathrm{B}}H, \\ w_1 &= 4J'\langle S^Z_1\rangle\cos(q_bb), \quad w_2 = 4J'\langle S^Z_2\rangle\cos(q_bb). \end{aligned}$$

Here, it should be noted that this equation corresponds clearly to the secular equation of matrix obtained by putting $h_{\vec{q}1}$, $h_{\vec{q}2}$=0 in eq. (3.20), that is, its right hand side is zero. The energy of quasi-particle are as follows:

$$\omega_{\pm} = \frac{1}{2}\left[u + v \pm \sqrt{(u+v)^2 - 4(uv - w_1 w_2)}\right]. \tag{3.29}$$

Putting $\vec{q}$=0 in the above expression, we obtain the peak position of EPR spectra,

$$\begin{aligned}\omega_{\pm} &= \frac{1}{2}[-4J'\langle S_2^Z\rangle - 4J'\langle S_1^Z\rangle + g_1\mu_{\rm B}H + g_2\mu_{\rm B}H \\ &\quad \pm\{(4J'\langle S_2^Z\rangle + 4J'\langle S_1^Z\rangle - g_1\mu_{\rm B}H - g_2\mu_{\rm B}H)^2 \\ &\quad +16J'\langle S_2^Z\rangle g_2\mu_{\rm B}H + 16J'\langle S_1^Z\rangle\mu_{\rm B}H - 4g_1g_2(\mu_{\rm B}H)^2\}^{1/2}].\end{aligned} \tag{3.30}$$

This is certainly equal to that of eq. (3.22). Also, the mode at $\vec{q}$=0 is writen as $c_1 S_{ij1}^{+} + c_2 S_{ij1}^{+}$ and then the relations between the coefficients c_1 and c_2 are given for $\omega = \omega_{\pm}$ as follows:

$$c_1/c_2 = 4J'\langle S_1^Z\rangle/[4J'\langle S_2^Z\rangle - g_1\mu_{\rm B}H + \omega_{\pm}]. \tag{3.31}$$

We consider about the motion of spin for respective $\omega_{\pm}$. In short, the values of c_1/c_2 for respective $\omega_{\pm}$ are discussed. At the present case, since the numerator of eq. (3.31), $4J'\langle S_1^Z\rangle$, has a plus values, we have investigated about its denominator,

$$\begin{aligned}&2J'(\langle S_2^Z\rangle - \langle S_1^Z\rangle) - \frac{\mu_{\rm B}H}{2}(g_2 - g_1) \pm \frac{1}{2}[\{4J'(\langle S_1^Z\rangle + \langle S_2^Z\rangle) - \mu_{\rm B}H(g_1+g_2)\}^2 \\ &+16\mu_{\rm B}HJ'(g_1\langle S_1^Z\rangle + g_2\langle S_2^Z\rangle) - 4g_1g_2(\mu_{\rm B}H)^2]^{1/2}.\end{aligned} \tag{3.32}$$

Now, we have $J'/J \ll 1$, $-0.5 < \langle S_1^Z\rangle, \langle S_2^Z\rangle < 0$, and $|J| < \Delta g\mu_{\rm B}H$ is realized under the high magnetic fields. Then the follwing transformation is performed, that is,

$$(3.32) \approx \frac{\mu_{\rm B}H}{2}(g_2 - g_1) \pm \left[\frac{\mu_{\rm B}H}{2}|g_1 - g_2| + \frac{4J'(\langle S_1^Z\rangle g_1 + \langle S_2^Z\rangle g_2)}{|g_1 - g_2|\mu_{\rm B}H}\right]. \tag{3.33}$$

For $g_1 > g_2$, eq. (3.33) is

$$\begin{cases} \dfrac{4J'(\langle S_1^Z\rangle g_1 + \langle S_2^Z\rangle g_2)}{|g_1 - g_2|\mu_{\rm B}H} > 0, & \text{for } \omega_{+}, \\ (g_2 - g_1)\mu_{\rm B}H - \dfrac{4J'(\langle S_1^Z\rangle g_1 + \langle S_2^Z\rangle g_2)}{|g_1 - g_2|\mu_{\rm B}H} < 0, & \text{for } \omega_{-}. \end{cases}$$

For $g_1 < g_2$, eq. (3.33) is,

$$\begin{cases} (g_2 - g_1)\mu_{\rm B}H + \dfrac{4J'(\langle S_1^Z\rangle g_1 + \langle S_2^Z\rangle g_2)}{|g_1 - g_2|\mu_{\rm B}H} > 0, & \text{for } \omega_{+}, \\ -\dfrac{4J'(\langle S_1^Z\rangle g_1 + \langle S_2^Z\rangle g_2)}{|g_1 - g_2|\mu_{\rm B}H} < 0, & \text{for } \omega_{-}. \end{cases}$$

Here the relation of $\frac{4J'(\langle S_1^Z\rangle g_1+\langle S_2^Z\rangle g_2)}{|g_1-g_2|\mu_B H} > 0$ have been taken into account. Anyway, it is found that the spin at sublattice 1 and 2 perform the motion with coupling each other and the obtained modes correspond to the motion of the respective in phase and out of phase. These are often understood as the mode such as ferromagnetic and antiferromagnetic resonance. Now the relation of $g_1 > g_2$ is found in the case of θ=30, 45 degree by using g [37] values of $CuGeO_3$. In Fig. 3.10(a) we show the magnetic fields dependencies of $\omega_\pm$

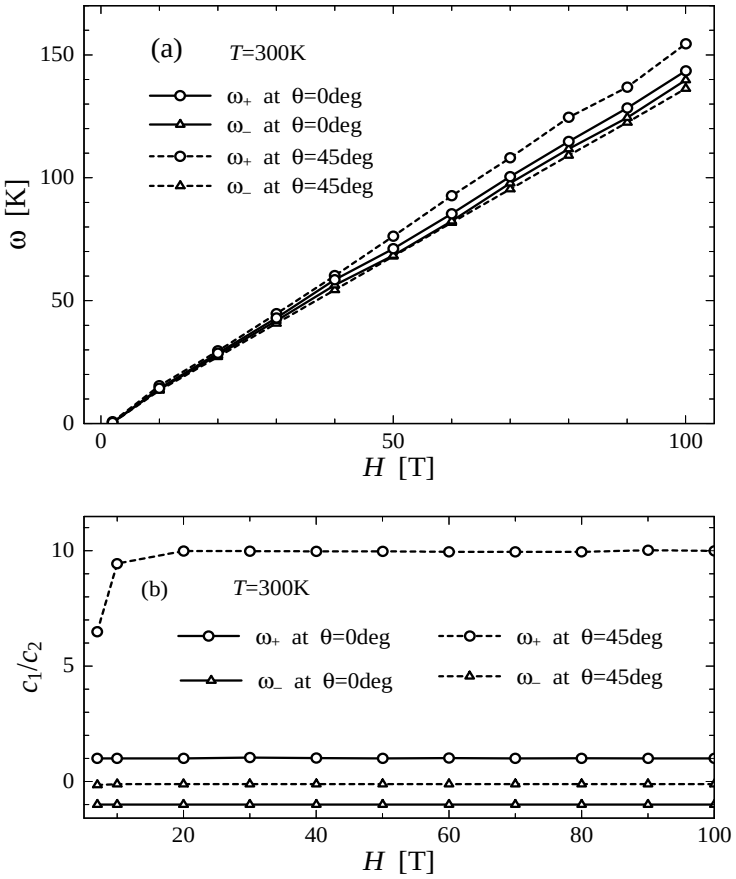

Figure 3.10: (a) The magnetic fields dependence of quasi-particle energy ω_+ and ω_- at T=300 K are shown by the circle and triangle, respectively. Further the solid and dotted lines represent the case of magnetic fields with θ=0 and 45 degree, respectively. (b) The magnetic fields dependence of c_1/c_2 for ω_+ and ω_- at T=300 K are shown by the circle and triangle, respectively. Further the solid and dotted lines represent the case of magnetic fields with θ=0 and 45 degree, respectively.

for θ=0, 45 degree at T=300 K. The solid and dotted lines represent the quasi-particle energy for θ=0 and 45 degree, respectively. And the circle and triangle on lines denote ω_+ and ω_-, respectively. As seen from figure, the magnitude of ω_- associated with the

Table 3.1: The estimated exchange integral J' (interchain) and J (intrachain) are summarized, respectively.

	Hamano-Shibata theory	MF–RPA
J' (interchain)	–0.42 meV	–0.41 meV
J (intrachain)	——	–5.00 meV

antiferromagnetic resonance is obviously smaller than that of ω_+ of the ferromagnetic resonance at each magnetic fields. It is thought to be a reasonable results by considering that the interchain coupling is now antiferromagnetic interaction. For the same case, the magnetic fields dependencies of c_1/c_2 in $CuGeO_3$ are shown in Fig. 3.10(b). The solid and dotted lines represent c_2/c_1 for θ=0 and 45 degree, respectively. The circle and triangle on lines are c_2/c_1 for ω_+ and ω_-, respectively. The characteristic behavior on c_1/c_2, in which the c_1/c_2 for ω_+ have the magnitude larger than that for ω_-, is originated from the relation $g_1 > g_2$ in $CuGeO_3$.

3.2.6 Conclusion

In conclusion the interchain exchange integral J' along the b-axis of $CuGeO_3$ has been evaluated to be about -0.4 meV by analyzing the exchange splitting of EPR spectra observed at T=300 K under ultra-high magnetic fields on the basis of the two methods, Hamada-Shibata theory and MF–RPA. This value of J' is smaller than that estimated from the inelastic neutron scattering measurement [12]. Here, to be remarkable, the MF–RPA method is quite effective to treat high-field EPR spectra at high temperatures. In order to elucidate the nature of the respective EPR peak we have solved the equation of motion for the spins with use of the MF–RPA Hamiltonian. It has been clarified that the spins at sublattices 1 and 2 make correlated motion and the observed two peaks correspond to the respective ferromagnetic and antiferromagnetic resonance.

3.3 ESR spectra in SP phase

In the spin-Peierls phase (SP phase) of $CuGeO_3$ the transitions [13, 41, 15] from the singlet ground state to two kinds of triplet excited states, which lie respectively at 2 meV and 5 meV above the ground state, have been observed by ESR measurements. To be more precise, the observed transitions correspond to those from the ground state to the

$M = \pm 1$ states in respective triplet excited states. From now on these observed two transitions are named respectively as the transition 1 (2 meV) and the transition 2 (5 meV). It should be emphasized here that these transitions between the singlet and triplet states are usually forbidden because the total spin is conserved in the isotropic Heisenberg systems. Therefore, in order to understand the observed ESR spectra we have to seek for mechanisms which destroy the conservation of the total spin.

3.3.1 Outline about Mechanism of Transition

Judging from the magnitude of the transition energy, it is most probable that the transition 1 corresponds to transition from the ground state to the lowest triplet state with q=0 (see Fig. 3.11). As a mechanism which makes this transition allowed, we may think of the Dzyaloshinsky-Moriya (D–M) interaction. In fact, from EPR measurements at room temperature it is suggested the D–M interaction certainly exists for the nearest-neighboring (n.n.) Cu pair along the c-axis and the so-called $\vec{d}$ vector is perpendicular to the c-axis, i.e. $\vec{d} \perp c$ [39]. According to the Moriya rule [40], the condition $\vec{d} \perp c$ restricts the crystal symmetry, namely the crystal symmetry should satisfy at least one of the following rules for the Cu pair along the c-axis.

(i) There should be mirror plane which is perpendicular to the Cu-Cu bonding line and which bisects this bonding line.

(ii) There should be a mirror plane including the Cu-Cu bonding line.

(iii) There should be a twofold rotation axis which is perpendicular to the Cu-Cu bonding line and which passes through the midpoint of the bonding line.

As to the crystal structure in the SP phase at low temperatures there is no definite conclusion at present, but there are a couple of proposals. One is the model structure proposed by Hidaka *et al* (see Fig. 3.2), and the symmetry of this structure satisfies the above condition (iii). If we adopt this crystal structure, the D–M interaction exists between the two Cu ions in the dimer along the c-axis. Furthermore, the two Cu ions in the dimer may have the different effective g-values. In the following we assume the D–M interaction and the different g-values for the Cu dimer along the c-axis, and it will be shown later that the transition 1 is successfully explained by this assumption.

Now we turn to the origin for the transition 2. Judging from the magnitude of the transition energy one possibility is that the transition 2 corresponds to the transition from

the ground state to the triplet excited state with $q = \pi$ (see Fig. 3.11). In this case we must find out a mechanism of the zone folding of the $q = \pi$ triplet state because the ground state has the crystal momentum $q = 0$ and in the ESR measurements the crystal momentum have to be conserved. As an origin of the zone folding we may consider the staggered field induced along the b-direction which is caused by the zigzag chain structure of CuO_6 octahedron along the b-axis as described in the previous section. Another possibility we propose here is that the transition 2 may correspond to the transition from the ground state to the continuum state above the second gap (see Fig. 3.11).

In the following subsections we carry out analysis of the ESR spectra (both the transitions 1 and 2) on the basis of two kinds of models. One is the zone folding model which takes account of the zigzag chain structure of CuO_6 octahedron along the b-axis. Another takes into account the transition to the continuum state with $q = 0$ above the second gap. Since there is no simple theory for the continuum state, we adopt a quite simple model in which triplet states with $q = 0$ above the second gap is approximated by the product of two triplet states of n.n. dimers. This model will be called the 2 triplet model. In both the models the D–M interaction and the different g-values for the Cu dimer along the c-axis are assumed, and we carry out the detailed analysis of ESR spectra such as the dependence on the light polarization and the magnitude and direction of the magnetic fields.

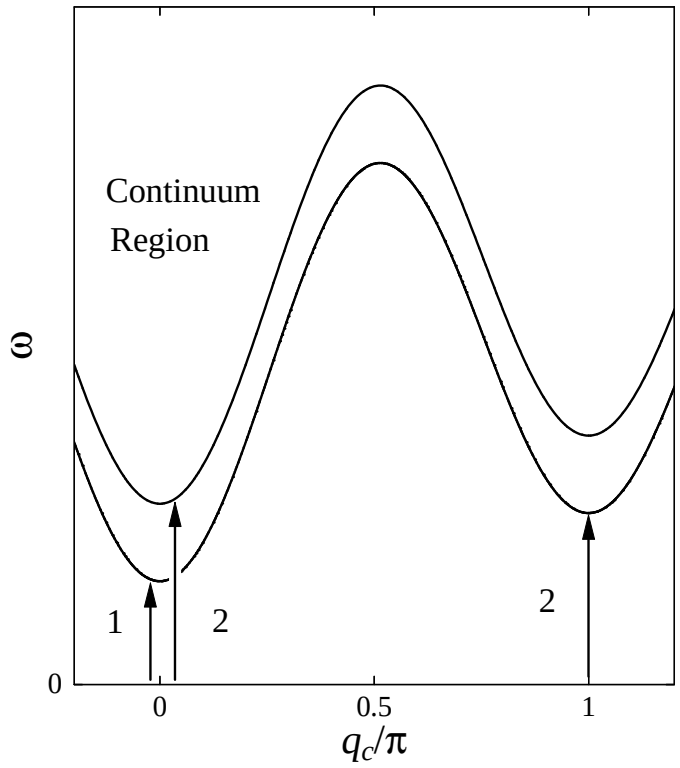

Figure 3.11: Schematic illustration of magnon dispersion in the SP phase. The arrows named as 1 and 2 mean the transition 1 and 2.

3.3.2 Zone Folding Model

Crystal structure and effective Hamiltonian

The structures of the *bc*-plane and the *ab* plane in the SP phase are shown in Figs. 3.1 and 3.2, respectively. Here it should be noted that the structure of the *bc*-plane is that suggested from the analysis of EPR spectra. If the structure as shown in Fig. 3.2 is adopted, the effective *g*-values, g_1 and g_2, of Cu ions at site 1 and 2 in the dimer, can have different values according to the distortion of crystal structure.

The principal axis vectors, $\vec{\beta}$ and $\vec{\gamma}$, of the primitive cell and the reciprocal lattice vectors, $\vec{\beta}^*$ and $\vec{\gamma}^*$, are given as,

$$\vec{\beta} = \frac{b}{2}\vec{e}_b + \frac{c+c'}{2}\vec{e}_c, \qquad \vec{\gamma} = (c+c')\vec{e}_c,$$
$$\vec{\beta}^* = \frac{4\pi}{b}\vec{e}_b, \qquad \vec{\gamma}^* = 2\pi\left(\frac{-1}{b}\vec{e}_b + \frac{1}{c+c'}\vec{e}_c\right),$$

respectively. Here $\vec{e}_b$ and $\vec{e}_c$ denote the unit vector of the *b*-axis and the *c*-axis, respectively. Fig. 3.12(a) represents the $q_b q_c$-plane in the *q*-space, and the circles represent the reciprocal

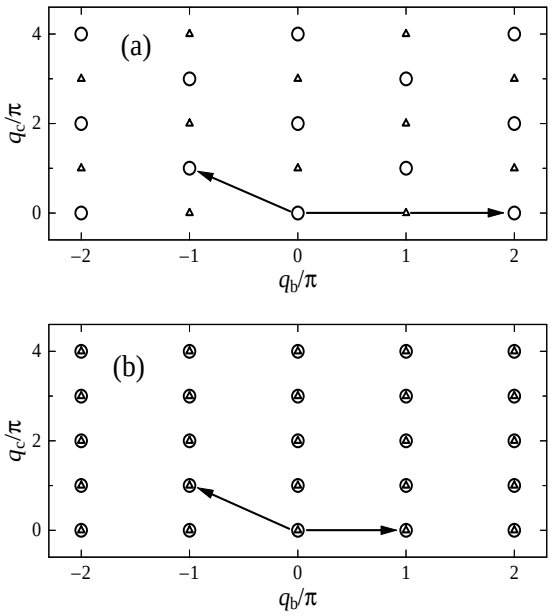

Figure 3.12: The q-space of $CuGeO_3$: (a) q_bq_c-plane, (b) one folded by making $\vec{\beta}$ twice. The circles and triangles represent the respective equivalent reciprocal lattice points, and the arrows are the reciprocal lattice vectors. The unit of q_b/π and q_c/π are $2/(c+c')$ and $2/b$, respectively.

lattice points and the triangles the points equivalent to $(q_b,\ q_c) = (0,\ \pi)$. Since the observable mode in the ESR measurement is only the $\vec{q} = 0$ mode, the zone folding as shown in Fig. 3.13 is necessary to observe the excitation at $(q_b,\ q_c) = (0,\ \pi)$, and it can be accomplished if the period along the b-direction becomes the double. Now, we think of the case of making $\vec{\beta}$ twice. Then the reciprocal lattice vectors are obtained as follows:

$$\vec{\beta}^* = \frac{2\pi}{b}\vec{e}_b, \qquad \vec{\gamma}^* = 2\pi\left(\frac{-1}{b}\vec{e}_b + \frac{1}{c+c'}\vec{e}_c\right).$$

In this case, it is found that the circles are coincident with the triangles as shown in Fig. 3.12(b), that is, the necessary zone folding is certainly realized.

As shown in Fig. 3.2(b), the CuO_6 octahedrons form zigzag chains along the b-axis and they lean alternatively by -56 deg and $+56$ deg from the a-axis in the ab-plane. This apparently indicates that the principal axes of the g-tensor of two adjacent Cu ions along the b-axis, named respectively as sublattice #1 and #2, are different. When the magnetic fields are applied in the direction of the a-axis, the slight magnetic fields are induced perpendicular to the direction of the applied magnetic fields and alternative along the b-axis, namely the staggered field is induced. As shown in Fig. 3.2(b), abc (or xyz) are the coordinate system of the crystal, respectively, and also XYZ is defined as the

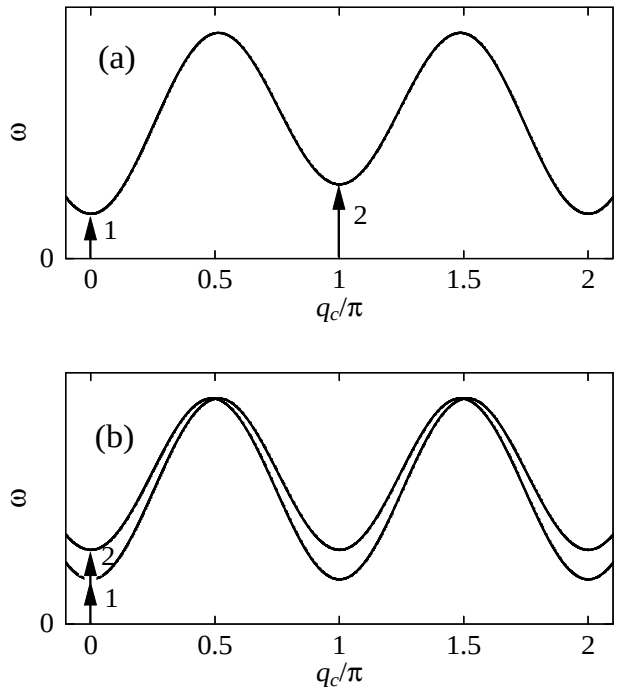

Figure 3.13: The magnon dispersion $\omega(q_b = 0, q_c)$ for bc-plane in $CuGeO_3$: (a) the zero field and (b) the non-zero field. The arrows named as 1 and 2 mean the transition 1 and 2, respectively. Under the magnetic field, the zone folded dispersion is obtained. Since the observable mode in the ESR measurement is $\vec{q} = 0$ mode, we regard the transition 2 as that from zone folded mode. The unit of q_c/π is $2/(c + c')$, where c and c' denote the distance between two Cu ions of intra-dimer and inter-dimer along c-axis, respectively, as shown in Fig. 3.1(a).

principal axis of the g-tensor for CuO_6. The g-tensor at site 1 is expressed in the xyz coordinate system as follows:

$$\begin{pmatrix} g_X \cos^2\theta + g_Z \sin^2\theta & 0 & (g_Z - g_X)\sin\theta\cos\theta \\ 0 & g_Y & 0 \\ (g_Z - g_X)\sin\theta\cos\theta & 0 & g_X \sin^2\theta + g_Z \cos^2\theta \end{pmatrix}, \tag{3.34}$$

where g_X, g_Y, g_Z are the principal values of the g-tensor, and θ shows the angle between the a-axis and one of the principal axis. For site 2 we need to put $\theta \to -\theta$. By using these g-tensors, the total Zeeman interactions at site 1 and 2 under the magnetic fields along the a-axis is written down as,

$$\begin{aligned} \mathcal{H}_{\rm Zeeman} &= \mu_{\rm B} H[(g_X \sin^2\theta + g_Z \cos^2\theta)S_1^z + (g_Z - g_Y)\sin\theta\cos\theta)S_1^x \\ &\quad +(g_X \sin^2\theta + g_Z \cos^2\theta)S_2^z - (g_Z - g_X)\sin\theta\cos\theta)S_2^x], \end{aligned} \tag{3.35}$$

where H is the magnetic field and S_1^x, S_1^z (S_2^x, S_2^z) denote the x and z components of the spin at site1 (site2), respectively. The second and forth terms turn out to be the Zeeman interactions due to the staggered field. By using g_Y=2.049, g_Z=2.336, θ =56 deg [19] we obtain

$$(g_Z - g_Y)\sin\theta\cos\theta \sim 0.13. \tag{3.36}$$

And, if this is divided by $(g_X\cos^2\theta + g_Z\sin^2\theta)$, the effective staggered field $H_{\rm st}^x$ is obtained finally as,

$$H_{\rm st}^x \sim 0.06H. \tag{3.37}$$

This staggered field makes $\vec{\beta}$ twice and it causes the zone folding.

On the basis of the above discussion, we propose the following model Hamiltonian under the magnetic field parallel to the a-axis (z-axis), for the Cu^{2+} spins in the bc-plane of $CuGeO_3$:

$$\begin{aligned}\mathcal{H} &= \sum_{i,j}[-2J_1\vec{S}_{i,j,1}\cdot\vec{S}_{i,j,2} - 2J_2\vec{S}_{i,j,2}\cdot\vec{S}_{i,j+1,1} - 2J_3(\vec{S}_{i,j,1}\cdot\vec{S}_{i+1,j-1,2} + \vec{S}_{i,j,2}\cdot\vec{S}_{i+1,j,1}) \\ &\quad +\mu_{\rm B}H(g_{1z}S_{i,j,1}^z + g_{2z}S_{i,j,2}^z) + \vec{d}\cdot(\vec{S}_{i,1}\times\vec{S}_{i,2}) + {\rm e}^{{\rm i}\vec{Q}\cdot\vec{r}_{i,j}}\mu_{\rm B}H_{\rm st}^x(g_{1x}S_{i,j,1}^x + g_{2x}S_{i,j,2}^x)],\end{aligned} \tag{3.38}$$

with $\vec{r}_{ij} = [i(b/2), j(c+c')/2]$, $\vec{Q} = (2\pi/b, 0)$. J_1, J_2 and J_3 denote the antiferromagnetic exchange integral of the intra-dimer, inter-dimer and interchain, respectively, and the last term represents the Zeeman interaction due to the induced staggered field. It is noted that we have assumed that the g-values of site 1 and 2 are generally different. Further, in this subsection we assume that the $\vec{d}$ lies in the ab-plane (xz-plane), *i.e.* $\vec{d} = (d_x, 0, d_z)$, which is suggested from the EPR measurements at room temperature [39].

Singlet-triplet dimer model

Now, to discuss qualitatively the intensity of ESR spectra at T=0 K we use the singlet-triplet dimer model, whose framework is described as follows. First, as the picture of triplet excited states in the SP phase, we simply think that a triplet pair formed within a dimer is traveling in the singlet sea, that is, the direct products of singlet pairs. Then, the triplet excited states propagating with wave vector $\vec{k}$ is described explicitly as

$$|{\rm es}, \vec{k}, M_z\rangle = \frac{1}{\sqrt{N}}\sum_{l,m}{\rm e}^{{\rm i}\vec{k}\cdot\vec{r}_{l,m}}|{\rm triplet}, M_Z\rangle_{l,m}\prod_{u,v(\neq l,m)}|{\rm singlet}\rangle_{u,v}, \tag{3.39}$$

with

$$|\text{singlet}\rangle_{u,v} = \frac{1}{\sqrt{2}}(\alpha_1\beta_2 - \beta_1\alpha_2)_{u,v},$$

$$|\text{triplet}, M_z\rangle_{l,m} = \begin{cases} (\alpha_1\alpha_2)_{l,m} & \text{for } M_z = 1, \\ \frac{1}{\sqrt{2}}(\alpha_1\beta_2 + \beta_1\alpha_2)_{l,m} & \text{for } M_z = 0, \\ (\beta_1\beta_2)_{l,m} & \text{for } M_z = -1, \end{cases}$$

where α_i, β_j (i, j=1 or 2) show the up spin at site i and the down spin at site j in the dimer, respectively, M_z denote the magnetic quantum number, and l, m (or u, v) are the coordinate for the dimers in the bc-plane. As the singlet ground state we may choose the following wave function

$$|\text{gs}\rangle = \prod_{l,m} |\text{singlet}\rangle_{l,m}. \tag{3.40}$$

In the present study we treat, as the excited states, only the lowest triplet excited states. Therefore, the other excited states such as plural triplet pairs traveling in the singlet sea are completely excluded.

By using the above bases, the diagonal elements are easily calculated, and the magnon dispersion of the triplet exited states under the zero field and without the D–M interaction is given by

$$\omega(q_b, q_c) \;=\; 2|J_1| - |J_2|\cos q_c(c+c') - 2|J_3|\cos\frac{q_b b}{2}\cos\frac{q_c(c+c')}{2}. \tag{3.41}$$

This dispersion is shown in Fig. 3.13(a). If this singlet-triplet model is applied to purely one-dimensional case, the results do not show a good agreement with the magnon dispersion obtained by the exact diagonalization method. However, we believe that this model will make a sense for qualitative discussion. If we take into account the D–M interaction and the magnetic field along the a-axis, the singlet ground state $|\text{gs}\rangle$ hybridizes with the triplet states $|\text{es}, 0, M_z\rangle$ and $|\text{es}, \pi, M_z\rangle$ where 0 denotes $\vec{k} = (0, 0)$ and π represents $\vec{k} = (0, \pi)$. The Hamiltonian matrix in the subspace of $|\text{gs}\rangle$, $|\text{es}, 0, -1\rangle$, $|\text{es}, 0, 0\rangle$, $|\text{es}, 0, 1\rangle$, $|\text{es}, \pi, -1\rangle$, $|\text{es}, \pi, 0\rangle$, $|\text{es}, \pi, 1\rangle$ is expressed explicitly as follows:

$$\mathcal{H} = \begin{pmatrix} 0 & \frac{\mathrm{i}d_x}{2\sqrt{2}} & \frac{\Delta g_z H - \mathrm{i}d_z}{2} & \frac{-\mathrm{i}d_x}{2\sqrt{2}} & \frac{\Delta g_x h^x_{st}}{2\sqrt{2}} & 0 & \frac{-\Delta g_x h^x_{st}}{2\sqrt{2}} \\ \frac{-\mathrm{i}d_x}{2\sqrt{2}} & \omega(0) - \frac{g_z h}{2} & 0 & 0 & 0 & \frac{g_x h^x_{st}}{2\sqrt{2}} & 0 \\ \frac{\Delta g h + \mathrm{i}d_z}{2} & 0 & \omega(0) & 0 & \frac{g_x h^x_{st}}{2\sqrt{2}} & 0 & \frac{g_x h^x_{st}}{2\sqrt{2}} \\ \frac{\mathrm{i}d_x}{2\sqrt{2}} & 0 & 0 & \omega(0) + \frac{g_z h}{2} & 0 & \frac{g_x h^x_{st}}{2\sqrt{2}} & 0 \\ \frac{\Delta g_x h^x_{st}}{2\sqrt{2}} & 0 & \frac{g_x h^x_{st}}{2\sqrt{2}} & 0 & \omega(\pi) - \frac{g_z h}{2} & 0 & 0 \\ 0 & \frac{g_x h^x_{st}}{2\sqrt{2}} & 0 & \frac{g_x h^x_{st}}{2\sqrt{2}} & 0 & \omega(\pi) & \frac{g_x h^x_{st}}{2\sqrt{2}} \\ -\frac{\Delta g_x h^x_{st}}{2\sqrt{2}} & 0 & \frac{g_x h^x_{st}}{2\sqrt{2}} & 0 & 0 & \frac{g_x h^x_{st}}{2\sqrt{2}} & \omega(\pi) + \frac{g_z h}{2} \end{pmatrix}, \tag{3.42}$$

with $\Delta g_z = g_{1z} - g_{2z}$, $\Delta g_x = g_{1x} - g_{2x}$, $g_x = g_{1x} + g_{2x}$, $g_z = g_{1z} + g_{2z}$, $\mu_B H \to h$, $\mu_B H^x_{st} \to h^x_{st}$, and $\omega(0)$ and $\omega(\pi)$ denote magnon energy for $\vec{k} = (0,0)$ and $\vec{k} = (0,\pi)$, respectively. The eigenstates $|n)$ are given by,

$$\begin{aligned} |n) &= C^n_1|\mathrm{gs}\rangle + C^n_2|\mathrm{es},0,-1\rangle + C^n_3|\mathrm{es},0,0\rangle + C^n_4|\mathrm{es},0,1\rangle \\ &\quad + C^n_5|\mathrm{es},\pi,-1\rangle + C^n_6|\mathrm{es},\pi,0\rangle + C^n_7|\mathrm{es},\pi,1\rangle. \end{aligned} \tag{3.43}$$

Calculation of ESR spectra

In investigating the intensity of ESR spectra, it is noted first that the selection rules based on the relations between the direction of propagating vector of light and that of the magnetic field are associated with S^z_{total} and $S^{\pm}_{\mathrm{total}}(=\sum_{i,j}(S^{\pm}_{ij1} + S^{\pm}_{ij2}))$. The respective intensity of ESR spectra, I_z for S^z_{total} and $I_{\pm}$ for $S^{\pm}_{\mathrm{total}}$ at T=0 K, are given explicitly as,

$$\begin{aligned} I_z &= |(n' \mid \sum_{i,j}(S^z_{ij1} + S^z_{ij2}) \mid \mathrm{gs})|^2 \\ &= |{C^4_{n'}}^* C^{\mathrm{gs}}_4 - {C^{n'}_2}^* C^{\mathrm{gs}}_2 + {C^{n'}_7}^* C^{\mathrm{gs}}_7 - {C^{n'}_5}^* C^{\mathrm{gs}}_5|^2, \end{aligned} \tag{3.44}$$

$$\begin{aligned} I_{\perp,+} &= |(n' \mid \sum_{i,j}(S^+_{ij1} + S^+_{ij2}) \mid \mathrm{gs})|^2 \\ &= |\frac{1}{\sqrt{2}}({C^{n'}_3}^* C^{\mathrm{gs}}_2 + 2{C^{n'}_4}^* C^{\mathrm{gs}}_3 + {C^{n'}_6}^* C^{\mathrm{gs}}_5 + 2{C^{n'}_7}^* C^{\mathrm{gs}}_6)|^2, \end{aligned} \tag{3.45}$$

$$\begin{aligned} I_{\perp,-} &= |(n' \mid \sum_{i,j}(S^-_{ij1} + S^-_{ij2}) \mid \mathrm{gs})|^2 \\ &= |\frac{1}{\sqrt{2}}({C^{n'}_3}^* C^{\mathrm{gs}}_4 + 2{C^{n'}_2}^* C^{\mathrm{gs}}_3 + {C^{n'}_6}^* C^{\mathrm{gs}}_7 + 2{C^{n'}_5}^* C^{\mathrm{gs}}_6)|^2. \end{aligned} \tag{3.46}$$

It is noted here that $I_{\pm}$ represents the intensity in the Faraday configuration.

In the following we use the notations $|\mathrm{es1}, M_{\mathrm{z}})$ and $|\mathrm{es2}, M_{\mathrm{z}})$. Here es1 (es2) denotes the triplet excited state with q=(0,0) (q=(0,π)), and M_{z} represents the main component of the triplet in the hybridized states. Further we use the abbreviation $I_z(|\mathrm{gs}) \to |\mathrm{es1}, \pm 1))$ for $|(\mathrm{es1}, \pm 1 \mid \sum_{i,j}(S^z_{ij1} + S^z_{ij2}) \mid \mathrm{gs})|^2$. As an example we show in Fug. 4 the calculational results which are obtained by using the following parameters: $|J_1| = 50.0$ K, $|J_2/J_1| = 0.9$, $J_3/J_1 = 0.08$, $g_{1z} = 2.0$, $g_{2z} = 2.0$, $g_{1x} = 2.2$, $g_{2x} = 2.0$ and $d_x = d_z(\sim \Delta g|J_1|/g)$=0.1$|J_1|$ K. It is noted that $I_z(|\mathrm{gs}) \to |\mathrm{es1}, 0))$, $I_z(|\mathrm{gs}) \to |\mathrm{es2}, \pm 1))$, $I_-(|\mathrm{gs}) \to |\mathrm{es1}, -1))$, $I_{\pm}(|\mathrm{gs}) \to |\mathrm{es1}, 1))$, $I_{\pm}(|\mathrm{gs}) \to |\mathrm{es2}, 0))$ have finite values and the other combinations become almost zero.

In Fig. 3.14(a) we show the magnetic field dependence of the intensity $I_{\pm}(|\mathrm{gs}) \to |n))$ which does not take zero. The circle and triangles denote the $I_-(|\mathrm{gs}) \to |\mathrm{es1}, -1))$ and $I_+(|\mathrm{gs}) \to |\mathrm{es2}, 0))$, respectively, and the square represents the other intensities. It is

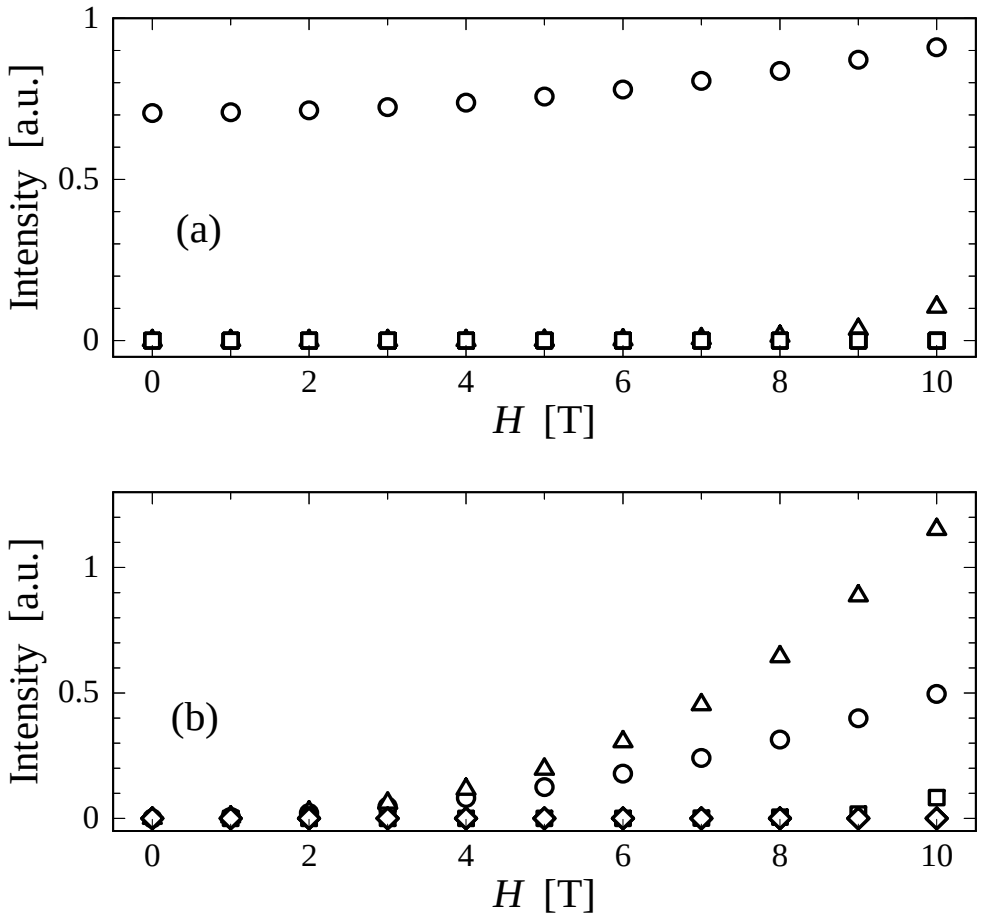

Figure 3.14: The magnetic field dependencies of intensity obtained by considering the zone-folding model are shown. In (a), the circle and triangle denote the respective $I_{-}(|\mathrm{gs}) \rightarrow |\mathrm{es1}, -1))$ and $I_{+}(|\mathrm{gs}) \rightarrow |\mathrm{es2}, 0))$, and the square represents the other intensities. In (b), the circle, triangle and square denote $I_z(|\mathrm{gs}) \rightarrow |\mathrm{es2},\ 1))$, $I_z(|\mathrm{gs}) \rightarrow |\mathrm{es2},\ -1))$ and $I_z(|\mathrm{gs}) \rightarrow |\mathrm{es1},\ 0))$.

found that $I_{-}(|\mathrm{gs}) \rightarrow |\mathrm{es1}, -1))$ and $I_{+}(|\mathrm{gs}) \rightarrow |\mathrm{es2}, 0))$ increase with increasing the magnetic fields. In particular, $I_{-}(|\mathrm{gs}) \rightarrow |\mathrm{es1}, -1))$ has a finite value under zero magnetic fields, which is due to the D–M interaction. Further the magnitude of $I_{-}(|\mathrm{gs}) \rightarrow |\mathrm{es1},\ -1))$ are larger than that of $I_{+}(|\mathrm{gs}) \rightarrow |\mathrm{es2},\ 0))$ for the whole ranges. In Fig. 3.14(b) the magnetic field dependencies of $I_z(|\mathrm{gs}) \rightarrow |n))$ are shown. The circles, triangles and squares denote $I_z(|\mathrm{gs}) \rightarrow |\ \mathrm{es}\ 2,\ 1\ ))$, $I_z(|\mathrm{gs}) \rightarrow |\mathrm{es}\ 2,\ -1\ ))$ and $I_z(|\mathrm{gs}) \rightarrow |\mathrm{es}\ 1,\ 0\ ))$, respectively. The $I_z(|\mathrm{gs}) \rightarrow |\ \mathrm{es2},\ 1))$ and $I_z(|\mathrm{gs}) \rightarrow |\mathrm{es2},\ -1))$ exhibit the monotonous increase with increasing H, reflecting the increase of the staggered field when the magnetic field increases. The $I_z(|\mathrm{gs}) \rightarrow |\mathrm{es1},\ 0))$ also show the same dependence on the magnetic

fields. It originates from the Zeeman interaction with the different g values in the dimer.

Quite recently the transition 2 has been observed by the far-infrared-absorption spectroscopy under zero magnetic field. Also it was shown by the new ESR measurements that the intensities of the transition 2 are little dependent on the magnetic fields. Further, a series of transitions have been observed under the magnetic fields parallel to the b- and c-axis as well as along the a-axis. Then, judging from the above results it is difficult to explain the observed ESR spectra by means of using the zone folding which is brought about by the staggered field when the magnetic field is applied parallel to the a-axis.

3.3.3 Two Triplet Model

Recently, the complete structure of the double gap in the spin Peierls system $CuGeO_3$ has been observed by the neutron scattering experiment [14]. Namely, there are the usual first gap between the singlet ground state and the triplet excited states and also the second gap between the triplet excited states and the continuum regions. These phenomenon represents the characteristic nature in the S=1/2 AF–AF alternating chain. In this subsection, we assume that the triplet excited states and the excited states in the continuum regions, both of which have the crystal momentum q=0, exist respectively at 2 meV and 5 meV above the ground state. Namely, the transition 1 and 2 are interpreted as those from the ground state to the usual triplet excited states and the excited states in the continuum regions, respectively. The subspace of only k=0 in Hamiltonian of the pure one-dimensional system is now just used.

The Hamiltonian of pure one-dimensional system is written as,

$$\mathcal{H} = \sum_i [-2J_1 \vec{S}_{i,1} \cdot \vec{S}_{i,2} - 2J_2 \vec{S}_{i,2} \cdot \vec{S}_{i+1,1} + \mu_{\rm B} H (g_1 S^Z_{i,1} + g_2 S^Z_{i,2}) + \vec{d} \cdot (\vec{S}_{i,1} \times \vec{S}_{i,2})], \tag{3.47}$$

with $\vec{r}_i = [i(c+c')]$. And $\vec{d}$ is now given as (d_a, d_b, d_c), where a, b, c represent the principal axes of crystal. In this subsection we consider a general $\vec{d}$ vector and do not confine $\vec{d}$ in the ab-plane. As will be shown later, d_a, d_b and d_c play an important role in discussing the configuration dependence of intensity.

Now, we think about the excited states in the continuum regions. A couple of the interpretation such as two unbound spin have been previously suggested to understand the nature of this excited states. However, there is no definite model at present. We assume that two triplet excited states traveling in the direct product of singlet pair are considered to be one of the states above the second gap. For two triplet states, the value of total spin

S allows 0, 1, 2 from the composition of two spins with S=1. Here, for S=1, by using the bases being mentioned below it is shown that the off diagonal elements and intensity become zero. This explanations is described in Appendix A. After all, as regards two triplet states, the subspaces of S=0 and 2 are adopted. Since the observed transition 2 are the transitions to $M = \pm 1$ states, at the present model $M = \pm 1$ states of S=2 is thought be the transitional states. Further, in order to make the smallest subspace enough to explain the phenomena, the adjacent triplet pairs are used. Its states are written explicitly as follows by making use of the notation $|S, M_z\rangle_i$ on the i-dimer,

$$|0,0\rangle_{i,i+1} = \frac{1}{\sqrt{3}}(-|1,-1\rangle_i|1,1\rangle_{i+1} + |1,0\rangle_i|1,0\rangle_{i+1} - |1,1\rangle_i|1,-1\rangle_{i+1}) \quad (3.48)$$

$$|2,2\rangle_{i,i+1} = |1,1\rangle_i|1,1\rangle_{i+1}, \quad (3.49)$$

$$|2,1\rangle_{i,i+1} = \frac{1}{\sqrt{2}}(|1,1\rangle_i|1,0\rangle_{i+1} + |1,0\rangle_i|1,1\rangle_{i+1}), \quad (3.50)$$

$$|2,0\rangle_{i,i+1} = \frac{1}{\sqrt{6}}(|1,-1\rangle_i|1,1\rangle_{i+1} + 2|1,0\rangle_i|1,0\rangle_{i+1} + |1,1\rangle_i|1,-1\rangle_{i+1}), \quad (3.51)$$

$$|2,-1\rangle_{i,i+1} = \frac{1}{\sqrt{2}}(|1,-1\rangle_i|1,0\rangle_{i+1} + |1,0\rangle_i|1,-1\rangle_{i+1}), \quad (3.52)$$

$$|2,2\rangle_{i,i+1} = |1,-1\rangle_i|1,-1\rangle_{i+1}. \quad (3.53)$$

From now on the triplet excited states of eq. (3.39) and this two triplet excited states are named as 1 triplet and 2 triplet states, respectively. By using these states $|S, M_z\rangle_{i,i+1}$, we define the bases of 2 triplet states at k=0 as,

$$|2\mathrm{tr}, S, M_z\rangle = \frac{1}{\sqrt{N}}\sum_i |S, M_z\rangle_{i,i+1} \prod_{j(\neq i,i+1)} |\mathrm{singlet}\rangle_j. \quad (3.54)$$

The diagonal elements of 2 triplet states under the zero magnetic fields are obtained as $2|J_1|$ from the ground state. Also it is found that a few off-diagonal elements between 2 triplet states and the other states become non-zero due to the D–M interaction and the Zeeman interaction with different g values.

We now discuss the subspace of S=0, 1, 2, 0, where the first 0 is the singlet ground state and the last 0 corresponds to the state obtained from 2 triplet states. By making use of these bases the 10×10 Hamiltonian matrix under the magnetic fields parallel to the a-, b- and c-axes are easily obtained. To be important, the D–M interaction and the Zeeman interaction with the different g-values contribute to the hybridization between the states with different total S.

For various configurations, the intensities of ESR spectra at T=0 K in this system

are given as,

$$I_x = |(n \mid \sum_i (S_i^x + aS_{i2}^x) \mid \mathrm{gs})|^2, \tag{3.55}$$

$$I_y = |(n \mid \sum_i (S_i^y + aS_{i2}^y) \mid \mathrm{gs})|^2, \tag{3.56}$$

$$I_z = |(n \mid \sum_i (S_i^z + aS_{i2}^z) \mid \mathrm{gs})|^2, \tag{3.57}$$

where |gs) and |n) represents the resultant ground state and excited states of $\mathcal{H}$ and $S_i^\alpha \equiv S_{i1}^\alpha + S_{i2}^\alpha$ (α=x, y, z). Further a is $(g_2 - g_1)/g_1$, and its introduction represents that the differences of g value have been taken in account also for the selection rules. Here we find that the transition 2 become possible by its introduction as well as the resultant ground state with 2 triplet states under the hybridization. Further, in the selection rules there are non-zero elements between 2 triplet states and 1 triplet states whose components exist in the ground state.

Now the intensity of ESR spectra under the magnetic fields along the a-, b- and c-axis have been calculated by using the parameter values as $|J_1|$=50.0 K, $|J_2/J_1|$=0.9, g_1=2.2, g_2=2.0, d_a=0.1 $|J|$, d_b=0.05 $|J|$ and d_c=0.2 $|J|$, as an example. Here the values of d_a, d_b and d_c are selected so as to reproduce the experimental results which will be touched upon later. We show in Figs. 3.15∼3.17 the magnetic fields dependence of intensities of transition 1 in the respective configuration. The Figs. 3.15, 3.16 and 3.17 show the intensities under the magnetic fields H parallel to a, b and c-axis, respectively. And (a), (b) and (c) in these figures represent the intensity of transition from the |gs) to |1tr, -1), |1tr, 0) and |1tr, 1), respectively. Here the used notation |1tr, M_z) means 1 triplet states with M_z as a main component in the hybridized states. Further, the circles, triangles and squares in these figures denote the intensity on the basis of I_x, I_y and I_z, respectively. In a similar way, |2tr, M_z) is the state with the main component M_z in 2 triplet states. As seen from these figures, the intensities are not so greatly dependent on the magnetic fields. However, among them the intensity of transitions from |gs) to |1tr, -1) and |1tr, 1) show a slight magnetic fields dependence in comparison with that from |gs) to |1tr, 0). This difference is thought to be originated from degree of magnetic fields dependence in transitional states.

We show in Figs. 3.18 and 3.19 the magnetic fields dependence of intensity for transition 2 in the respective configuration. Here we show only the transitions to the $M = \pm 1$ states which have been practically observed, and the relatively strong intensities among them are picked up. Figures 3.18(a), (b) and (c) show the intensities in low intensity region under the magnetic fields H parallel to the a-, b- and c-axis, respectively.

Table 3.2: The degree of intensities for transition 2 is shown in the various configuration. These are investigated by considering 2 triplet states. Further h_{rf} is the rotational magnetic fields in electromagnetic wave. The S, M and W mean strong, medium and weak, respectively.

	$H//a$	$H//b$	$H//c$
$h_{rf}//$a	S	W	S
$h_{rf}//$b	M	S	S
$h_{rf}//$c	W	W	S

Table 3.3: The degree of intensities for transition 2 is investigated experimentally in the various configuration [17]. The notation is the same as that of Table. 3.2.

	$H//a$	$H//b$	$H//c$
$h_{rf}//$a	S	W	S
$h_{rf}//$b	S	M	S
$h_{rf}//$c	M	M	S

In a similar way, the intensities in high intensity region, that is, the intensity of transition from |gs) to |2tr, 2, 1), is shown in Fig. 3.19. As seen from these figures, in regard to the number of observable spectra, the case of $H//$c becomes maximum. These are merely due to the condition $d_c > d_a$, d_b. Also, as seen from these figures, a couple of intensities depend on the magnetic fields in low fields regions, but they show little dependence in high fields regions. In particular, Figs. 3.18(c) and 3.19 obviously shows such behaviors. It is associated with the Zeeman splitting, namely in the low fields a few states hybridize with respective large probability, while the high fields lead to a slight hybridization between our focusing state and the other states. The behaviors in low field regions can be changed considerably by the selection of parameter values. Therefore we do not pay much attention to this regions, and assert that the behaviors in the high field regions are essential.

In order to see the differences clearly, the degree of intensities calculated in each configuration are shown in Table. 3.2. By comparing these results with the experimental data in Table. 3.3 [17], we find that the agreements between the calculated results and observations are quite well. It should be emphasized that the direction of $\vec{d}$ plays an important role in the configuration dependence of intensity and the relation of $d_c > d_a, d_b$ is necessary to explain the observations.

Indeed, the magnitude of intensity for transition 2 is much smaller than that for 1 triplet states. However, we consider that the magnitude itself does not have significant meaning at present because the present model takes into account only the restricted 2 triplet states of eq. (3.54). As the additional remarks, the transitions to $M_z = \pm 2$ are possible under both zero and finite magnetic fields, at present model, though the magnitude of intensity is very small.

In summary, we recognize that the magnitude of intensity for the transition 1 is lager than that for the transition 2, and most of the intensities are not so greatly dependent on the magnetic fields. Also, by considering 2 triplet states, it can be obviously shown that transition 1 and 2 under zero magnetic fields are possible for the whole configurations. As a matter of fact, the experimental results show that the intensities for its transitions are little dependent on the magnetic fields [17]. And a couple of experiments under zero magnetic fields have been performed and transition 2 have been observed [18, 42, 43].

Thus, the model with use of 2 triplet states is thought to be suitable for explaining the observed phenomena. However, there are a couple of problems left for the study in future. In this model the 2 triplet states are treated as S=2 states with five degeneracy, nevertheless the experimental suggestion for S=2 states are not reported so far. We hope that the transition to $M = \pm 2$ will be observed by ESR measurement in future, The further detailed experiments are desired also in order to confirm the effectiveness of the model with use of 2 triplet states. Theoretically it will be useful to calculate the ESR intensities by using the exact diagonalization method for finite spin chains to obtain more quantitative understanding.

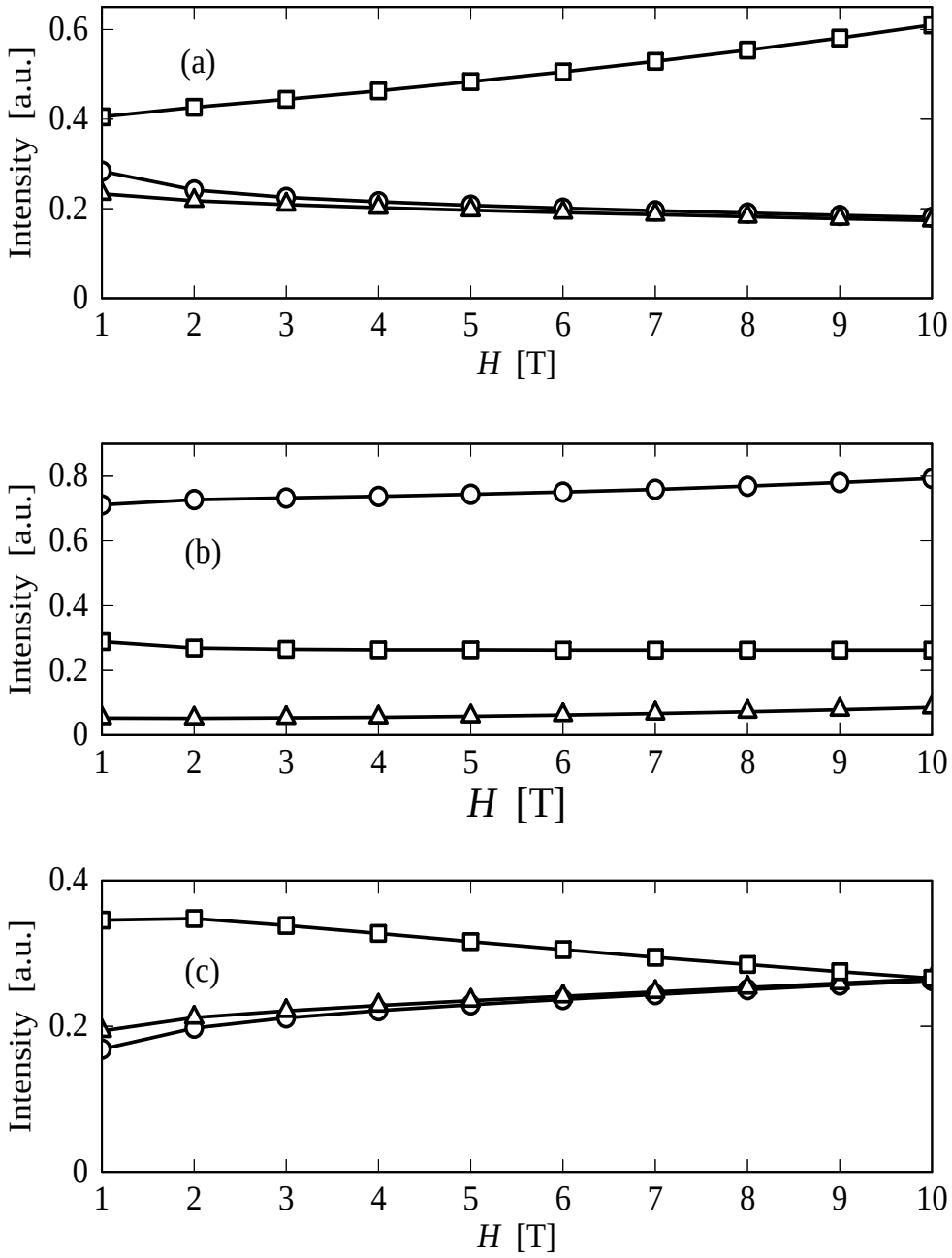

Figure 3.15: The magnetic fields dependencies of intensity of transition to the 1 triplet states are shown, in which the magnetic fields are applied parallel to a. Then (a), (b) and (c) represent the intensity of transition from the |gs) to |1tr, -1), |1tr, 0) and |1tr, 1), respectively. The circle, triangle and square in these figures denote the intensity on the basis of I_x, I_y and I_z, respectively.

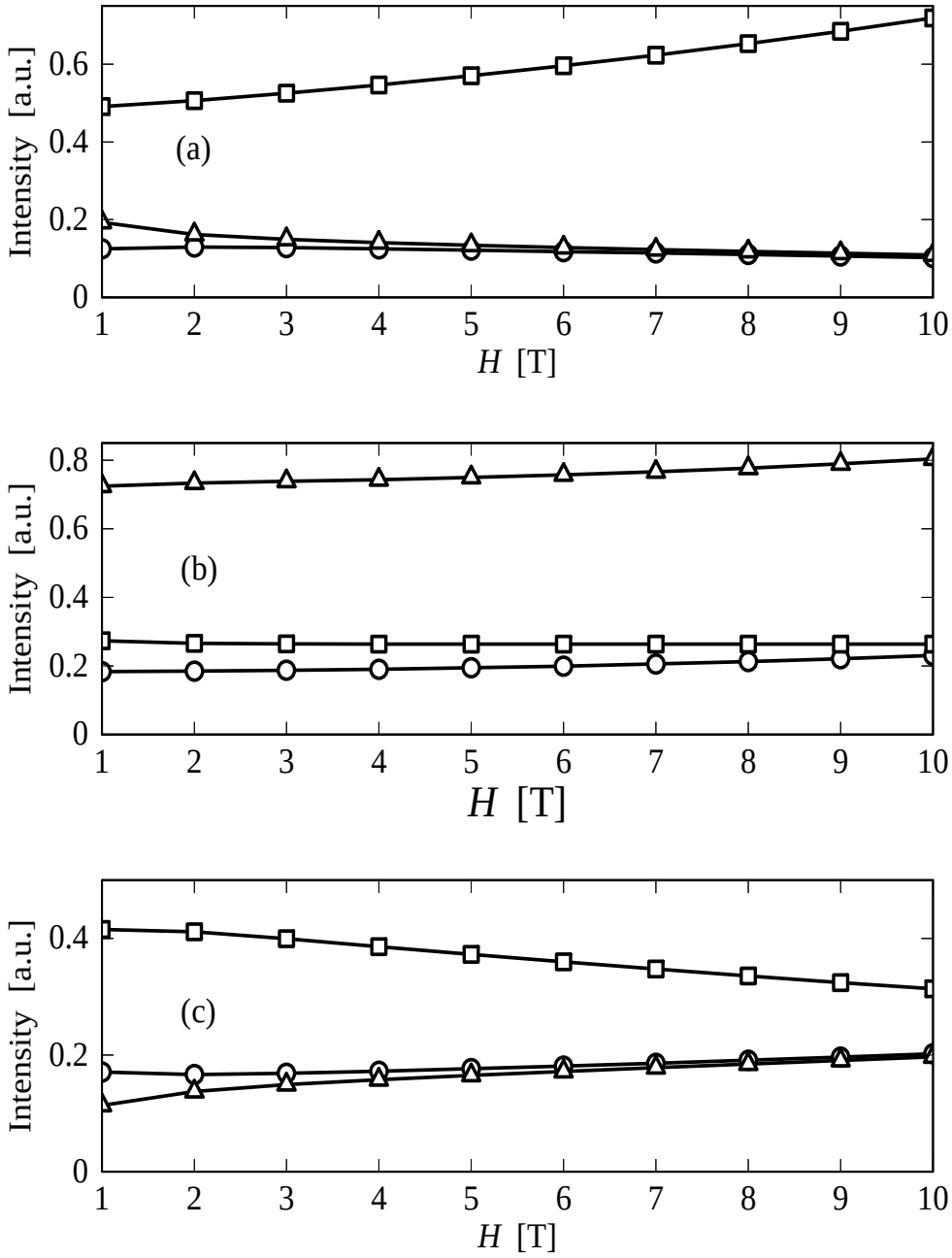

Figure 3.16: The magnetic fields dependencies of intensity of transition to the 1 triplet states are shown, in which the magnetic fields are applied parallel to b. The notation of line and point is the same as that of Fig. 3.15.

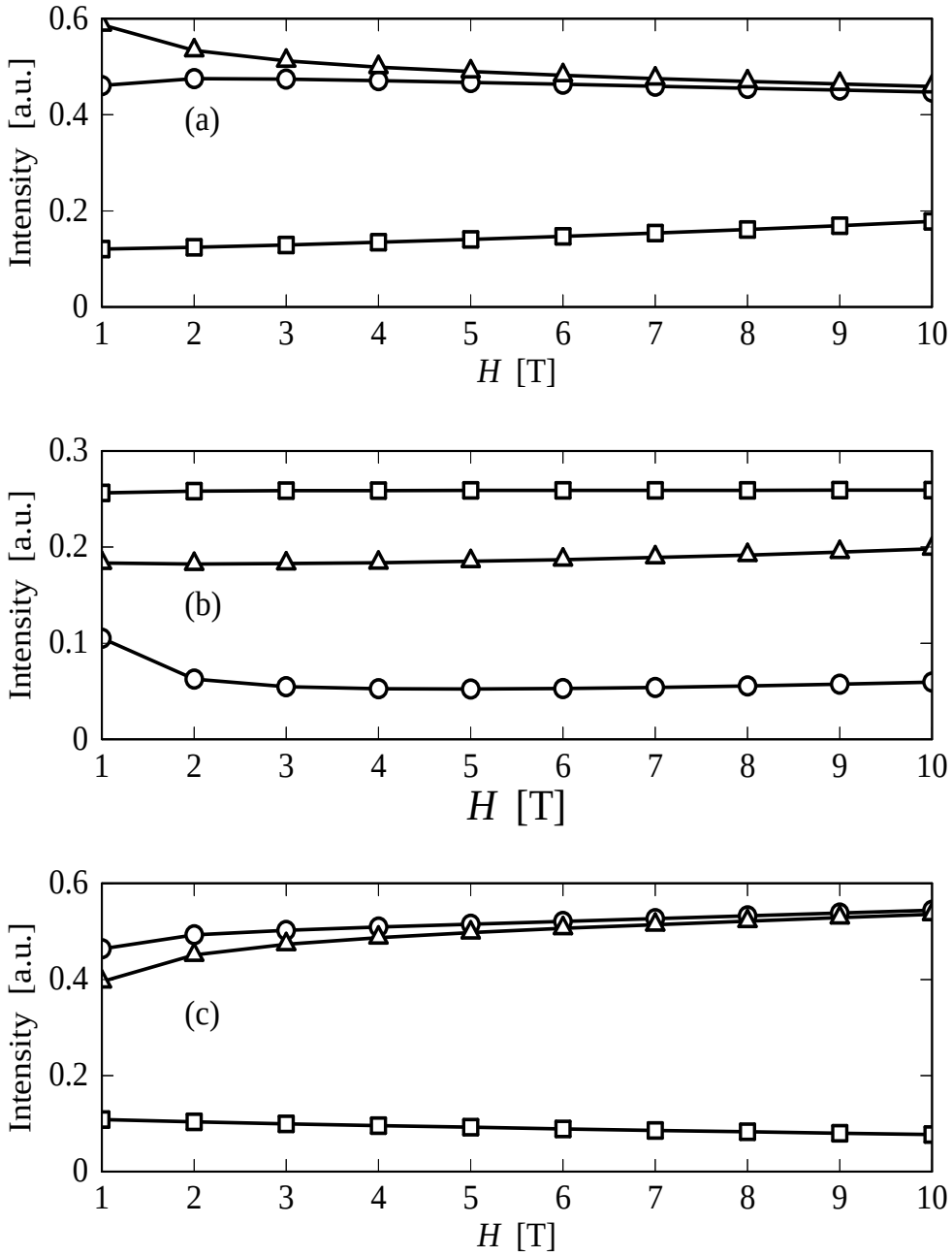

Figure 3.17: The magnetic fields dependencies of intensity of transition to the 1 triplet states are shown, in which the magnetic fields are applied parallel to c. The notation of line and point is the same as that of Fig. 3.15.

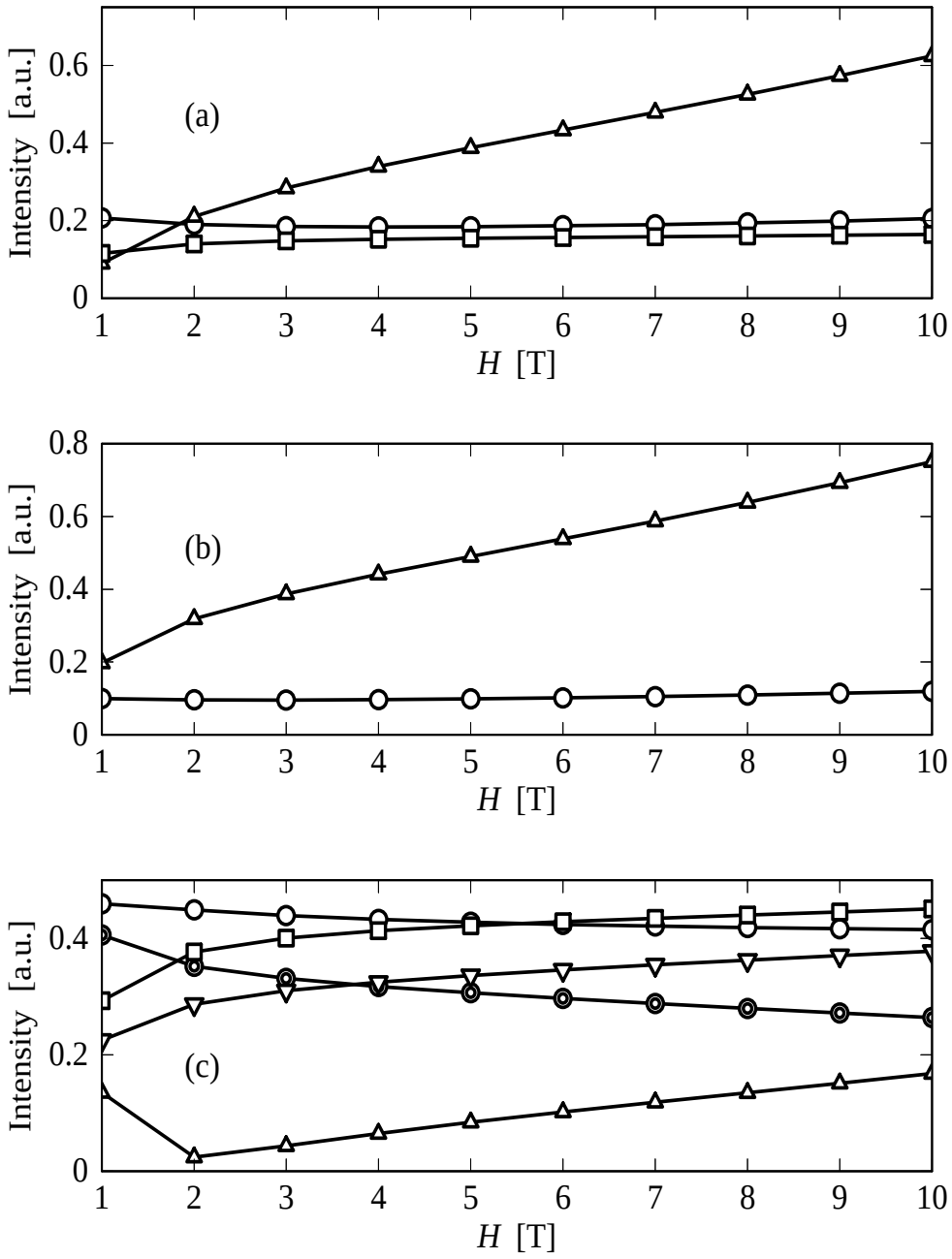

Figure 3.18: The magnetic fields dependence of intensity in low intensity region for the 2 triplet states. We focus on the only transitions to $M = \pm 1$ states. And among them, the relative strong intensities are shown. The (a), (b) and (c) show the intensity under the magnetic fields H parallel to a, b and c-axis, respectively. For the whole figures, the circle, triangle and square represent the intensity of transition from the $I_x(|\mathrm{gs}) \rightarrow |2tr, -1))$, $I_z(|\mathrm{gs}) \rightarrow |2tr, -1)$ and $I_x(|\mathrm{gs}) \rightarrow |2tr, 1)$, respectively. Here, as example $I_x(|\mathrm{gs}) \rightarrow |2tr, -1))$ denote the intensity I_x for the transition from |gs) to |2tr, -1). In (c) $I_y(|\mathrm{gs}) \rightarrow |2tr, 1)$ and $I_y(|\mathrm{gs}) \rightarrow |2tr, -1)$ are shown by the inverse triangle and double circle, respectively.

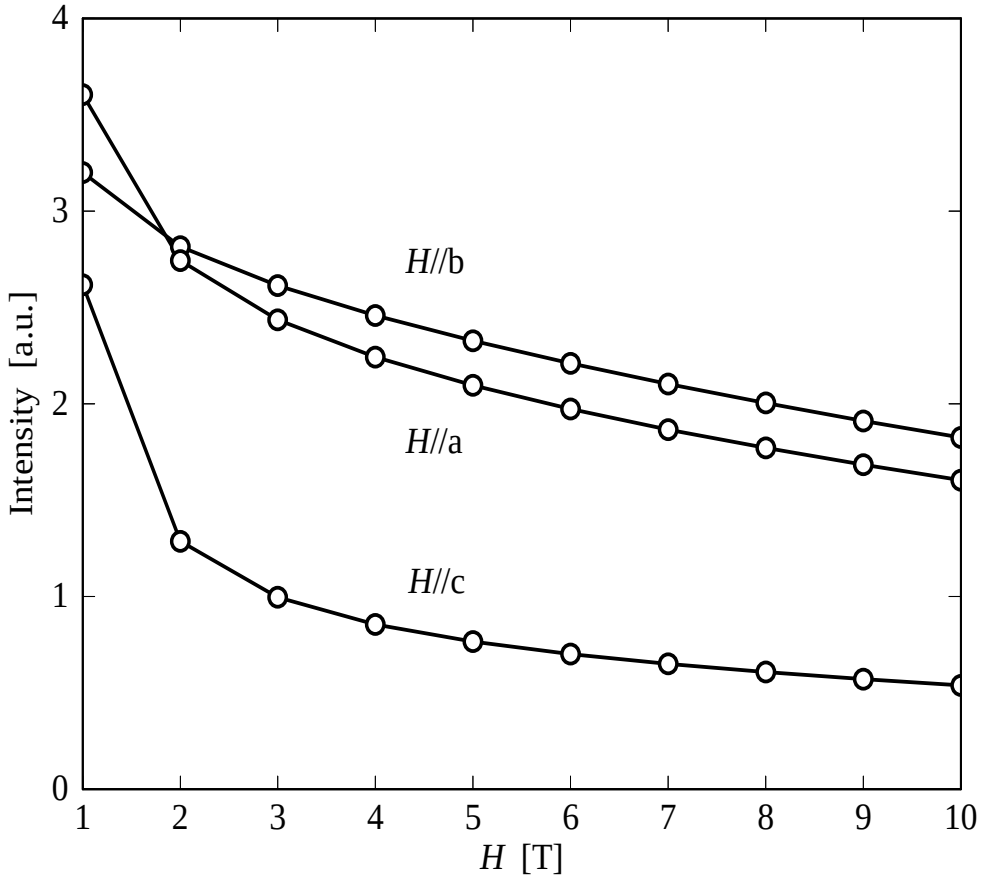

Figure 3.19: The magnetic fields dependence of intensity in high intensity region for the 2 triplet states. Figure shows the intensity $I_z(|\mathrm{gs}) \rightarrow |2tr, 1))$ under the magnetic fields H parallel to a, b and c-axis, respectively.

Chapter 4

Summary

In this thesis we have performed theoretical studies on the magnetic properties of pseudo-one-dimensional quantum spin systems. In particular, by paying particular attention to role of interchain coupling we have developed the useful theoretical methods and analyzed a couple of magnetic phenomena in which interchain coupling plays an important role. The main results are summarized as follows:

Magnetic Properties in Pseudo-One-Dimensional Exchange-Alternating Systems

We first have developed a new method called Pair-DCEFA by extending DCEFA originally proposed by Suzuki to the pair-approximation. By applying Pair-DCEFA to S=1/2 chains with alternating exchange coupling J_1 and J_2 it has been shown that Pair-DCEFA is practically useful for a fairly wide range of $a = J_2/J_1$, particularly for $a < 0$ with $J_1 < 0$. Then, the effect of interchain coupling in pseudo-1D S=1/2 exchange-alternating systems has been investigated by using the combined method in which the intrachain and interchain couplings are treated by Pair-DCEFA and MFA, respectively. In practice we have estimated the intrachain and the interchain exchange integrals of real pseudo-1D AF–F alternating systems, Cu(TIM)$CuCl_4$, (4-BzpipdH)$CuCl_3$ and MeNN.

We have extended the combined method of Pair-DCEFA and MFA to the case under magnetic fields in order to investigate the magnetic phase transition under magnetic fields in pseudo-1D exchange-alternating systems. By applying the method to real pseudo-1D S=1/2 AF–F alternating system $(CH_3)_2CHNH_3CuCl_3$ whose magnetic phase transition is observed only under magnetic fields, the interchain exchange coupling as well as intrachain exchange coupling have been evaluated, and magnetic field dependence of T_N has been determined. Further, the temperature dependence of nuclear spin-lattice relaxation rate of this system has been also analyzed by Pair-DCEFA.

The q-dependent staggered susceptibilities at finite temperature of S=1/2 exchange alternating chains have been calculated for the first time by using the EDM for finite chains. Then, we have shown that interchain coupling can be evaluated more quantitatively with use of the staggered susceptibilities obtained by the EDM and by applying the MFA to interchain interaction.

Finally, we have calculated intensities of inelastic neutron scattering of pure-1D S=1/2 AF–F alternating chains by numerical calculations based on the exact diagonalization method. We have found that the so-called second gap exists always and the lowest energy in the continuum region above the second gap takes maximum value at $q = \pi/2$. Further, the magnitude of the second gap at q=0 decreases with increasing the magnitude of the ferromagnetic coupling. The intensities due to the continuum state above the second gap are weak in general, but it was pointed out that the continuum states may be observable at large q. Finally the intensities due to the lowest triplet states take the maximum value at $q = \pi/2$ for the whole range of exchange ratio.

Magnetic Resonance in spin Peierls System $CuGeO_3$

The interchain exchange integral J' along the b-axis of $CuGeO_3$ has been evaluated by analyzing the exchange splitting of EPR spectra observed at T=300 K under ultra-high magnetic fields on the basis of the two methods, Hamada-Shibata theory and MF–RPA. In particular, the two peak structure of the observed ESR spectra and its dependence on the field direction are well explained by the MF–RPA method. By solving the equation of motion for the spins with use of the MF–RPA Hamiltonian, it was clarified that the observed two peaks correspond to the ferromagnetic and antiferromagnetic resonance, respectively.

We have investigated also the direct transitions from the singlet ground state to two kinds of triplet excited states lying respectively at 2 meV and 5 meV above the ground state, which have been observed by ESR measurements. By assuming the Dzyaloshinsky-Moriya interaction and the different g values for spin pairs of the Cu dimer, which can be expected reasonably from the supposed crystal structure, we have shown first that the 2 meV line is ascribed to the transition to the lowest triplet state at q=0. Since the 5 meV line cannot be understood simply by taking into account the Dzyaloshinsky-Moriya interaction and the different g values, as possible mechanisms of the transition to 5 meV states we considered the following two cases: the 5 meV state is regarded as, (1) the zone folded triplet states brought about by the staggered field induced along the direction of

interchain, or (2) the two triplet excited states above the so-called second gap. We have shown that the model (2) is a promising mechanism for the 5 meV line, because it can explain well the configuration dependence of the observed ESR spectra and also the recent experimental findings such as the observation under zero magnetic field.

Appendix A

S=1 States in Two Triplet Model

For the two triplet states, the allowed values of the total spin S are 0, 1 and 2. Among these three total S states, the state of S=1 has not been considered in §3-3. In this Appendix we explain why we could neglect safely the S=1 state, namely we show here that the off diagonal elements of the Hamiltonian or the ESR transition, which are associated with this S=1 state, are vanishing in our present model.

The eigenvectors of S=1 formed from two triplet states are expressed as follows:

$$|1,1\rangle_{i,i+1} = \frac{1}{\sqrt{2}}(|1,1\rangle_i|1,0\rangle_{i+1} - |1,0\rangle_i|1,1\rangle_{i+1}), \tag{A.1}$$

$$|1,0\rangle_{i,i+1} = \frac{1}{\sqrt{2}}(|1,1\rangle_i|1,-1\rangle_{i+1} - |1,-1\rangle_i|1,1\rangle_{i+1}), \tag{A.2}$$

$$|1,-1\rangle_{i,i+1} = \frac{1}{\sqrt{2}}(|1,0\rangle_i|1,-1\rangle_{i+1} - |1,-1\rangle_i|1,0\rangle_{i+1}), \tag{A.3}$$

with

$$|1,M_z\rangle_i = \begin{cases} (\alpha_1\alpha_2)_i & \text{for } M_z = 1, \\ \frac{1}{\sqrt{2}}(\alpha_1\beta_2 + \beta_1\alpha_2)_i & \text{for } M_z = 0, \\ (\beta_1\beta_2)_i & \text{for } M_z = -1. \end{cases}$$

By using the above states, two triplet states $|2\mathrm{tr},S,M_z\rangle$ with S=1 are defined as,

$$|2\mathrm{tr},1,M_z\rangle = \frac{1}{\sqrt{N}}\sum_i |1,M_z\rangle_{i,i+1} \prod_{j(\neq i,i+1)} |\mathrm{singlet}\rangle_j, \tag{A.4}$$

with

$$|\mathrm{singlet}\rangle_j = \frac{1}{\sqrt{2}}(\alpha_1\beta_2 - \beta_1\alpha_2)_j,$$

for $M_z = -1, 0, 1$. Now, by making use of these states as the bases we calculate the matrix elements of the Hamiltonian or the ESR transition. Here it is noted that in our present

model only the subspace of wave vector k=0 is considered and further the other excited states such as three or more triplet pairs and also two triplet pairs separated from nearest neighbors are completely excluded.

For example, suppose to operate the D–M interaction $\sum_i \vec{d}\cdot[\vec{S}_{i,1}\times\vec{S}_{i,2}]$ and the Zeeman interaction with different g-values $\sum_i H(g_{1z}S^z_{i,1}+g_{2z}S^z_{i,2})$ on the S=1 states, It is easily understood that the resultant states turn into those obtained by changing one of the two triplet states into the singlet state in eq.(A.4). On the basis of this fact and the anti-bonding nature of $|1,M_z\rangle_{i,i+1}$, we can show that there are no off-diagonal matrix elements. For example,

$$\begin{aligned}
&\langle 1\mathrm{tr},M_z|\sum_i \vec{d}\cdot[\vec{S}_{i,1}\times\vec{S}_{i,2}]|2\mathrm{tr},1,1\rangle \\
&= \langle 1\mathrm{tr},M_z|\frac{d_y-\mathrm{i}d_x}{2\sqrt{2}}\frac{1}{\sqrt{N}}\sum_i(|\mathrm{singlet}\rangle_i|1,0\rangle_{i+1}-|1,0\rangle_i|\mathrm{singlet}\rangle_{i+1})\prod_{j(\neq i,i+1)}|\mathrm{singlet}\rangle_j \\
&\quad -\langle 1\mathrm{tr},M_z|\frac{\mathrm{i}d_z}{2}\frac{1}{\sqrt{N}}\sum_i(|1,1\rangle_i|\mathrm{singlet}\rangle_{i+1}-|\mathrm{singlet}\rangle_i|1,1\rangle_{i+1})\prod_{j(\neq i,i+1)}|\mathrm{singlet}\rangle_j \\
&= 0, \qquad\qquad (A.5)
\end{aligned}$$

where

$$|1\mathrm{tr},M_z\rangle=\frac{1}{\sqrt{N}}\sum_i|1,M_z\rangle_i\prod_{j(\neq i)}|\mathrm{singlet}\rangle_j,\qquad (M_z\ =\ -1,\ 0,\ 1)$$

represents the 1 triplet state with k=0. Proofs for other cases are given in the similar way.

Bibliography

[1] M. Hagiwara, Y. Narumi, K. Kindo, T. C. Kobayashi, H. Yamakage, K. Amaya and G. Schumauch: J. Phys. Soc. Jpn. **66** (1997) 1792.

[2] M. Takahashi, Y. Hosokoshi, H. Nakano, T. Goto, M. Takahashi and M. Kinoshita: Mol. Cryst. Liq. Cryst. **306** (1997) 111.

[3] H. Manaka, I. Yamada and K. Yamaguchi: J. Phys. Soc. Jpn. **66** (1997) 564.

[4] M. Hase, I. Terasaki and K. Uchinokura: Phys. Rev. Lett. **70** (1993) 3651.

[5] F. D. M. Haldane: Phys. Lett. **93** A (1983) 464; Phys. Rev. Lett. **50** (1983) 1153.

[6] H. Tanaka, T. Takatsu, W. Shiramura and T. Ono: J. Phys. Soc. Jpn. **65** (1996) 1945.

[7] W. Duffy, Jr. and K. P. Barr: Phys. Rev. **165** (1968) 165.

[8] K. Hida: Phys. Rev. B **45** (1992) 2207.

[9] J. J. Borrás-Almenar, E. Coronado, J. Curely, R. Georges and J. C. Gianduzzo: Inorg. Chem. **33** (1994) 5171.

[10] H. Manaka, I. Yamada, Z. Honda, H. A. Katori and K. Katsumata: J. Phys. Soc. Jpn. **67** (1998) 3913.

[11] T. Kubo and T. Waketa: private communications.

[12] M. Nishi, O. Fujita, J. Akimitsu: Phys. Rev. Lett. **50** (1994) 6508.

[13] H. Nojiri, H. Ohta, N. Miura and M. Motokawa: Physica B **246-247** (1998) 16.

[14] M. Aïn, J. E. Lorenzo, L. P. Regnault, G. Dhalenne, A. Revcolevschi, B. Hennion and Th. Jolicoeur: Phys. Rev. Lett. **78** (1997) 1560.

[15] T. M. Brill, J. P. Boucher, J. Voiron, A. Revcolevschi and J. P. Renard: Phys. Rev. Lett. **73** (1994) 1545.

[16] Y. Hamano and F. Shibata: J. Phys. C: Solid State Phys. **17** (1984) 4843.

[17] H. Nojiri: private communications.

[18] K. Takehana: private communications.

[19] N. Suzuki: J. Phys. Soc. Jpn., **45** (1978) 1791.

[20] H. Takeuchi, N. Suzuki and K. Motizuki: J. Phys. Soc. Jpn. **49** (1980) 1283.

[21] N. Suzuki: J. Phys. Soc. Jpn. **50** (1981) 2931.

[22] N. Suzuki: J. Phys. Soc. Jpn. **52** (1983) 1002.

[23] N. Suzuki: J. Phys. Soc. Jpn. **52** (1983) 1009.

[24] N. Suzuki and K. Motizuki: J. Phys. C **16** (1983) 2133.

[25] Y. Matsumoto, M. Otani, H. Miyagi and N. Suzuki: Mol. Cryst. Liq. Cryst. **306** (1997) 339.

[26] J. des Cloizeaux and J. J. Pearson: Phys. Rev. **128** (1962) 2131.

[27] S. Eggert, I. Affleck and M. Takahashi: Phys. Rev. Lett. **73** (1994) 332.

[28] T. Moriya: Prog. Theor. Phys. **28** (1962) 371.

[29] D. Hone, C. Scherer and F. Borsa: Phys. Rev. B **9** (1974) 965.

[30] T. Goto, S. Maegawa and T. Kawai: J. Phys. Soc. Jpn. **55** (1986) 1066.

[31] T. Moriya: *Spin Fluctuations in Itinerant Electron Magnetism*, Springer Series in Solid State Sciences 56 (Springer, Berlin, 1985).

[32] S. A. Roberts, D. R. Bloomquist, R. D. Willett and H. W. Dodgen: J. Am. Chem. Soc. **103** (1981) 2603.

[33] K. Hida: J. Phys. Soc. Jpn. **63** (1994) 2514.

[34] K. Hirota, D. E. Cox, J. E. Lorenzo, G. Shirane, J. M. Tranquada, M. Hase, K. Uchinokura, H. Kojima, Y. Shibuya and I. Tanaka: Phys. Rev. Lett. **73** (1994) 736.

[35] M. Hidaka, M. Hatae, I. Yamada, M. Nishi and J. Akimitsu: J. Phys. Condense. Matter **9** (1997) 809.

[36] M. Arai, M. Fujita, M. Motokawa, J. Akimitsu and S. M. Bennington: Phys. Rev. Lett. **77** (1996) 3649.

[37] Y. Yamamoto, H. Ohta, M. Motokawa, O. Fujita and J. Akimitsu: J. Phys. Soc. Jpn. **66** (1997) 1115.

[38] P. W. Anderson, J. Phys. Soc. Jpn. **9** (1954) 316.

[39] I. Yamada, M. Nishi and J. Akimitsu: J. Phys. Condense. Matter **8** (1996) 2625.

[40] T. Moriya: Phys. Rev. **120** (1960) 91.

[41] H. Nojiri, N. Miura, M. Hase, K. Uchinokura, H. Kojima, I. Tanaka, Y. Shibuya, S. Luther and M. von Ortenberg : preprint.

[42] P. H. M. van Loosdrecht, S. Huant and G. Martinez: Phys. Rev. B **54** (1996) 3730.

[43] G. Li, J. L. Musfeldt, W. J. Wang, S. Jandl, M. Poirier, A. Revcolevshi and G. Dhalenne: Phys. Rev. B **54** (1996) 15633.

List of Publications

- S. Kokado and N. Suzuki:
  Magnetic Properties of Organic AF–F Alternating Chains.
  Mol. Cryst. Liq. Cryst. **306** (1997, Oct.) 487-493.

- S. Kokado and N. Suzuki:
  Pair Dynamical Correlated-Effective-Field Approximation.
  J. Phys. Soc. Jpn. **66**, No.11 (1997, Nov.) 3605-3610.

- S. Kokado and N. Suzuki:
  Magnetic Properties of S=1/2 AF–F Alternating Chains —Effect of Interchain Coupling.
  J. Magn. & Magn. Mater. **177-181** (1998, Feb.) 677-678.

- S. Kokado, H. Nojiri, N. Miura and N. Suzuki:
  Exchange Splitting of EPR Spectra in $CuGeO_3$ under Ultra-High Magnetic Fields —Theoretical Analysis.
  Physica B **246-247** (1998, Jul.) 238-241.

- S. Kokado and N. Suzuki:
  Staggered Susceptibility of S=1/2 Exchange-Alternating Chains Studied by Exact Diagonalization Method.
  J. Magn. & Magn. Mater. (1999) in press.

- S. Kokado and N. Suzuki:
  Magnetic Properties of Pseudo-1D S=1/2 AF–F Alternating Chains under Magnetic Fields.
  Mol. Cryst. Liq. Cryst. (1999) in press.

- S. Kokado and N. Suzuki:
  Theoretical Study on EPR and ESR Spectra in $CuGeO_3$.
  Proceeding of the 4th International Symposium on Advanced Physical Fields (1999, Mar.) in press.